THE INFLUENCE OF COPPER ADDITION ON THE CORROSION BEHAVIOUR OF LOW NICKEL AUSTENITIC STAINLESS STEELS

by

Suzanne Lisa Vismer

A thesis submitted to the Faculty of Engineering, University of Cape Town in fulfilment of the degree of Master of Science in Engineering

Department of Materials Engineering
University of Cape Town
February 1997

ABSTRACT

The influence of copper and nitrogen as partial substitutes for nickel on the corrosion performance of three metastable austenitic stainless steels, in various microstructural conditions, has been investigated. These alloys (based on AISI 301), which are to be used essentially in forming applications, were developed to counteract the increasing cost of nickel. Copper and nitrogen are both cheap and readily available alternative alloying additions. While nitrogen has been found to enhance the mechanical properties of austenitic stainless steels, copper is said to prevent delayed cracking after deep drawing.

The experimental alloys contain nominal amounts of 17Cr-5.4Ni-0.25N (wt%) with copper additions ranging from 0 to 3.3 wt%. Characterisation of the corrosion performance of these alloys involved testing in the solution treated, solution treated and aged, solution treated and deformed and the solution treated, deformed and aged conditions. These tests included potentiodynamic scans, polarisation resistance measurements and Tafel plots conducted in 5 volume % de-aerated sulphuric acid solution at 30°C as well as pitting tests in NaCl solutions.

The results showed that all three alloys displayed the lowest corrosion rates in the solution treated condition. The corrosion rates of the alloys in the solution treated and aged condition did not vary significantly with ageing time. Microscopy, however, revealed an increase in intergranular corrosion attack with ageing time. Thus, potentiodynamic tests did not seem a suitable method for quantifying the influence of copper on the sensitisation of these alloys. During deformation at room temperature, copper was found to stabilise the austenite resulting in more martensite being formed in the copper-free alloy. This martensite is expected to decrease corrosion resistance which could account for the copper-free alloy's relatively high corrosion rates in the solution treated and deformed condition. Deformation carried out at different temperatures, but to equivalent strains, allowed equal amounts of martensite to be achieved amongst the alloys. In this way, corrosion tests revealed that copper was found to reduce the dissolution rate of martensite. Following deformation (at controlled temperatures) and ageing, copper did not appear to influence the precipitation kinetics leading to sensitisation of the martensite. For all microstructural conditions, the copper-containing alloys consistently exhibited the highest corrosion resistance.

Comparisons with the standard AISI 301 and 304L alloys showed that the copper-containing novel alloys showed superior corrosion resistance. The corrosion characterisation conducted in this thesis of these novel copper-containing alloys, proves that these alloys look promising as substitutes for the conventional alloys presently used in forming applications.

TABLE OF CONTENTS

CHAPTER 1
INTRODUCTION

1.1 PROJECT MOTIVATION

The austenitic grades of stainless steel make up the largest category of stainless steels manufactured on an international basis. These grades contain a nominal amount of 8 wt% nickel and are used for their very good deep drawing abilities as well as for their excellent corrosion properties. Although nickel is used as one of the most important alloying elements in that it controls the austenite stability, it is becoming increasingly expensive which necessitates the consideration of alternative alloying additions.

Work has been carried out by Sibanda[1], amongst others, on alloys in which nickel has been reduced as an alloying element while the nitrogen levels have been increased in order to retain the austenite stability. Nitrogen is a very cheap substitute and is readily available. But, how does nitrogen affect the deep drawing ability of this alloy?

The work carried out by Sibanda on alloys with low nickel contents (5.4 wt%) and nitrogen additions between 0.2-0.25 wt%[1] showed that these alloys maintained their good deep drawability despite their reduction in nickel content. These alloys also formed a desirable amount of martensite during deformation. This deformation-induced martensite transformation results in a higher work hardening rate (WHR) which leads to transformation induced plasticity (TRIP). However, the drawn components were found to crack after a delay of a few hours. This was found to be due to the nitrogen having an embrittling effect on the martensite.

The same work showed that when copper is added to these alloys, the austenite stability is increased although there is a slight reduction in deep drawability due to the reduced TRIP effect. Since delayed cracking is deleterious to formability properties, there are two possible solutions which can be considered to prevent delayed cracking after deep drawing. These are as follows:

a. Perform a post-forming stress relief heat treatment on the nitrogen containing alloys, OR
b. Introduce copper to reduce the amount of embrittled martensite formed during deformation.

Both solutions mean further costs but surely not as much as those incurred from the use of nickel.

In view of the necessity to maintain a good level of corrosion resistance, the following questions need to be considered:

1. What are the effects of tempering the nitrogen containing alloys on corrosion resistance?
2. What are the effects of copper additions on the corrosion resistance?

Preliminary work was carried out on three alloys with similar compositions to those used in the present study i.e. nominally 17Cr-5.4Ni-0.25N (wt%) with copper additions ranging from 0-3.3 wt%[(2)]. Corrosion tests in de-aerated 5 volume % sulphuric acid showed that when the alloys were tested in the solution treated condition, corrosion rates decreased with an increase in copper content. Following deformation and ageing, the relatively poor corrosion properties of the alloy containing no copper was exacerbated.

These findings cannot be fully explained because, in the first instance, the relatively poor corrosion properties of the copper free alloy in the solution treated condition could be attributed to one or both of the following: (i) there is no copper in this alloy to improve the corrosion performance and/or (ii) the microstructure is more unstable in this alloy. Secondly, the role of copper on the dissolution properties after deformation and ageing is not clear since there is an additional variant in the form of martensite volume fraction. The following questions are posed regarding the relatively poor corrosion performance after deformation and ageing of the alloy containing no copper:

i. Is this because the martensite formed during deformation results in more rapid precipitation (and hence sensitisation) due to more nucleation sites, OR
ii. The martensite itself leads to preferential attack due to its high energy state, OR
iii. The copper additions in the other alloys could markedly retard the precipitation kinetics due to its stabilising effect on the austenite and therefore hinder the sensitisation phenomenon.

Of course, all possibilities are likely, but the relative contributions need to be ascertained.

1.2 PROJECT OBJECTIVES

The following issues shall be addressed in the experimental programme and form the objectives for the present study:

a. Corrosion tests shall first be carried out on the alloys in the solution treated and aged condition. Given the range in copper additions (0-3.3 wt%) amongst the experimental alloys, this is an attempt to establish the influence of copper on the precipitation kinetics, and hence sensitisation, during ageing.

b. The alloys shall be subjected to corrosion in the solution treated and deformed condition. Deformation (which is carried out at room temperature) results in the formation of martensite in these metastable alloys. The influence of martensite on the dissolution properties of the alloys and more particularly, the influence of copper on the stability of the austenite during deformation shall thus be established.

c. The influence of copper on the dissolution rate of martensite needs to be determined. This means that the amount of martensite needs to be equal (thereby eliminating this variable) amongst all three alloys. Since all the alloys have different austenite stabilities, deformation needs to be carried out (to equivalent strains) at different temperatures in order to achieve equal martensite levels.

d. Finally, corrosion tests will be conducted on the alloys in the deformed and aged condition in order to determine whether copper has any effect on the precipitation kinetics (leading to sensitisation) of martensite during ageing. Equal martensite levels will be achieved by deforming the alloys at various temperatures (as carried out in (c) above), to equivalent strains and then subjecting the deformed alloys to ageing.

CHAPTER 2
LITERATURE REVIEW

2.1 AUSTENITIC STAINLESS STEELS

The 18Cr-8Ni composition of austenitic stainless steels and their modified versions have become the most widely used of the stainless steels because of their ease of fabrication, good weldability and a good "all round" resistance to corrosion[3]. Common uses and applications include holoware, builders hardware, architectural applications, abattoir, beer and beverage production and food processing equipment to name just a few[4].

The most common austenite alloys are iron-chromium-nickel steels and are widely known as the AISI 300 series. Because of their high chromium and nickel content, this series of stainless steels are the most corrosion resistant[5]. The alloys within this series are very different from one another (see Table 2.1). The AISI 200 series of steels contain lower nickel contents which are compensated by the addition of the austenite-forming elements, manganese and nitrogen. These alloys were developed to conserve nickel and are less expensive than the AISI 300 series[6].

	Composition (wt%)						
AISI Type	C	Mn	Cr	Ni	Mo	Si	N_2
201	0.15 max	5.5-7.5	16-18	3.5-5.5	-	1.0 max	0.25 max
301	0.15 max	2.0 max	16-18	6-8	-	1.0 max	0.03
302	0.15 max	2.0 max	17-19	8-10	-	1.0 max	0.03
304	0.08 max	2.0 max	18-20	8-12	-	1.0 max	0.03
310	0.25 max	2.0 max	24-26	19-22	-	1.5 max	0.03
316	0.08 max	2.0 max	16-18	10-14	2-3	1.0 max	0.03

Table 2.1 Nominal compositions of the standard AISI 201 alloy and AISI 300 series of Cr-Ni steels[4,5,6]

A brief review of the range of alloys begins with Type 301, which is employed in applications requiring formability especially where stretching is involved. It is described as the leanest of the AISI 300 series as it has a minimum amount of austenite stabilising alloying elements to make it fully austenitic. Type 301, which has a lowered chromium and nickel content to increase work hardening, is confined primarily to use at ambient temperatures. Types 302 and 304 have greater stability and improved corrosion resistance, Type 304 being the most widely produced stainless steel. Type 304 is used considerably at elevated temperatures. The addition of molybdenum to an essentially Type 304 base, represented by Type 316, imparts greater corrosion resistance and significantly enhanced elevated temperature strength. Alloys with greatly increased alloy contents such as Type 310 find their use primarily in elevated temperature applications. The low-carbon or "L" grades e.g. 304L have a minimum carbon content of 0.03 wt% in order to avoid sensitisation during welding[4,5].

2.1.1 THE ALLOYING ELEMENTS

Austenitic stainless steels are formed by adding a face-centred cubic (FCC) element to the iron-chromium system shown in Figure 2.1[7].

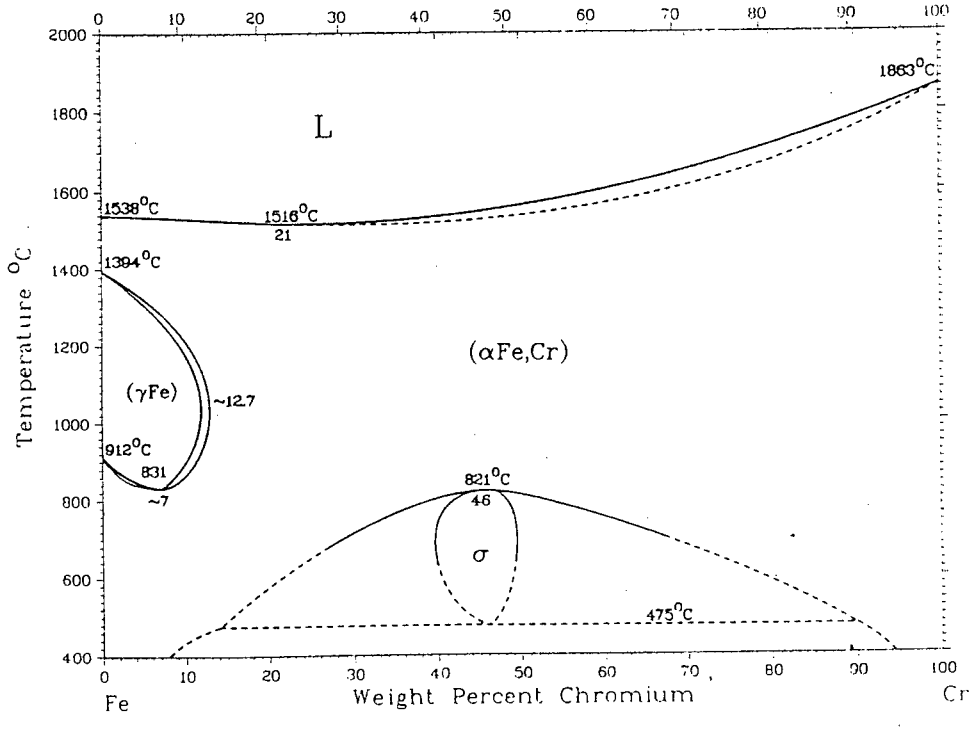

Figure 2.1 Section of the iron-chromium (Fe-Cr) equilibrium diagram[7]

Since the chromium content of austenitic stainless steels exceeds 16 wt%, Figure 2.1 implies that these steels should have a ferritic crystal structure. Therefore, alloying elements which shift the gamma loop have to be used, both to expand the austenitic crystal structure into the ferritic regions of higher chromium content, and to retain it at the lower temperatures. Nickel and manganese are the most commonly used alloying elements in the austenitic grades of stainless steel. Both elements are substitutional alloying elements which take the place of an iron atom in the crystal structure. They are large atoms and diffuse slowly in iron and therefore stabilise the austenite structure down to temperatures below that at which the atoms have sufficient mobility for a crystal structure change to occur[4].

In addition to nickel and manganese, other alloying elements are used depending on their austenite forming and/or austenite stabilising abilities:

a. Austenite formers

Depending on whether the alloying elements are austenite- or ferrite-forming elements, they will decrease or increase the tendency for delta-ferrite formation at the solution treatment temperature. The effect of alloying elements on the constitution of austenitic stainless steels can be considered by using chromium and nickel equivalent compositions in terms of the alloying additions[6].

The following values for the nickel and chromium equivalents for 12 wt% chromium steels are applied to a wide range of austenitic steels:

Chromium equivalent (Cr') = (Cr) + 2(Si) + 1.5(Mo) + 5(V) + 5.5(Al) + 1.75(Nb) + 1.5(Ti) + 0.75(W)

Nickel equivalent (Ni') = (Ni) + (Co) + 0.5(Mn) + 0.3(Cu) + 30(C) + 25(N)

where ( ) is the weight percent of the alloying addition[6].

The austenite forming elements contribute towards increasing the nickel equivalent and the ferrite forming elements contribute towards increasing the chromium equivalent. The significant contribution of carbon and nitrogen as austenite formers can be seen in the magnitude of their coefficients in the Ni′ equation. It is possible to make adjustments for the effect of any undissolved carbide, particularly in steels containing titanium or niobium[6].

b. Austenite stabilisers

In some of the less highly alloyed austenitic stainless steels, the austenite may be transformed to martensite (α′). This can occur in unstable alloys in the solution treated condition by quenching to below the $M_{s(\alpha')}$ (martensite start) temperature or by deformation at temperatures below $M_{d(\alpha')}$ (temperature below which martensite forms as a result of plastic deformation). This martensite transformation may also occur during refrigeration in more stable alloys in which $M_{s(\alpha')}$ is below room temperature. The ability of elements to depress the $M_{s(\alpha')}$ and $M_{d(\alpha')}$ temperatures is what is generally meant by austenite stabilising. Apart from cobalt, almost all alloying elements depress the $M_{s(\alpha')}$ temperature. $M_{s(\alpha')}$ is related to composition by the following empirical equation for austenitic stainless steels:

$$M_{s(\alpha')}\ (°C) = 502 - 810(C) - 1230(N) - 13(Mn) - 30(Ni) - 12(Cr) - 54(Cu) - 46(Mo)$$

where ( ) is the weight percent alloy addition[6].

Nitrogen and carbon reduce $M_{s(\alpha')}$ significantly as can be seen by the magnitude of their coefficients and are 30 - 40 times more effective in doing so than nickel. Even copper is a more effective stabiliser than nickel.

2.1.2 COPPER AS AN AUSTENITISING ADDITION TO STAINLESS STEEL

The effect of copper as an austenitising addition to stainless steel has been reported by numerous authors[5,8-17]. Copper has the ability to suppress the $M_{s(\alpha')}$ and $M_{d(\alpha')}$ temperatures of austenite[8]. In this way, copper is an effective stabiliser of austenite once it has been formed (sometimes as much as twice as effective as nickel[9]). Copper additions to suitable base compositions can suppress the transformation of austenite to martensite during plastic deformation at room temperatures[8,10]. The various expressions for nickel equivalent (Ni') generally give copper a coefficient of between 0.3 and 0.5[9,11,12], implying that it is about half as effective as nickel when it comes to preventing ferrite formation in a stainless steel (i.e. it is not as potent an austenite former as nickel).

Copper is also one of the few elements whose addition to austenite will raise the stacking fault energy (SFE) of the austenite[5,9,13]. An increased SFE promotes cross-slip of dislocations and reduces the resistance of the material to strain[14]. This, along with its stabilising effect on austenite, results in a lowering of the tensile strength and rate of work hardening[5,8,13,15].

It is acknowledged that the additions of copper to austenitic stainless steels improve the formability of the alloys[14]. Components which have been deep drawn from some austenitic stainless steels are known to exhibit cracking after a delay varying from an hour to several months[1,10]. The mechanism of cracking is connected with the presence of martensite in the drawn components, although the composition of the martensite appears more critical than the amount. Copper additions of 1.3 wt% were found to prevent delayed cracking in 5.5 wt% nickel alloys[1]. Copper additions inhibit the delayed cracking that may occur by moving the position of maximum rate of martensite formation with respect to applied strain up to higher strains, and can suppress it completely, thus improving drawability.

The only significant metallurgical disadvantage of copper is that additions of more than about 3 wt% can cause hot cracking during rolling[10,16,17]. Copper in the range 2 to 3 wt% represents a compromise and it is believed that such alloys offer a real prospect for future general purpose low-nickel stainless steel that could compete with AISI 304[10].

2.1.3 NITROGEN AS AN AUSTENITISING ADDITION TO STAINLESS STEEL

It is generally found that nitrogen is a convenient and cheap austenitising alloying element[5,8,18]. Nitrogen has a high coefficient in the nickel equivalent (Ni′) equation. It is therefore an effective austenite former and enlarges the gamma phase field. Nitrogen is also an important austenite stabiliser; it lowers both the $M_{s(\alpha')}$ and $M_{d(\alpha')}$ temperatures[5,8,19,20]. Recent realisation of the shortage of precious alloying elements has renewed the interest to develop nitrogen alloyed austenitic stainless steels. Increasing the nitrogen content from 0 to 0.25 wt% brings the stable austenite region at an 18 wt% chromium level from about 7 wt% nickel down to 4.5 wt% nickel[21]. As little as 0.07 wt% nitrogen has also been found to make a large difference to the austenite stability[20].

Tensile properties of high nitrogen stable austenitic stainless steels also generally improve with increasing nitrogen concentration as long as the nitrogen remains in interstitial solution. Both yield strength and tensile strength generally increase in proportion to the square root of the interstitial nitrogen content[22-25]. This, however, was not found for a 17Cr metastable austenitic alloy containing 7Mn-4Ni-0.04C-0.5Cu. Instead, nitrogen additions of up to 0.28 wt% lowered the UTS by about 30MPa per 0.1 wt% nitrogen added in these alloys. The proof stress did, however, increase by 20MPa per 0.1 wt% nitrogen added to these metastable alloys[8].

Nitrogen additions to certain austenitic base alloys also improve the elongation to fracture, apparently because nitrogen raises the rate of work hardening[26]. The work hardening rate can be controlled by the stacking fault energy (SFE). A higher SFE is associated with lower rates of work hardening. Additions of chromium, manganese, niobium, carbon and nitrogen, among others, are generally believed to lower the SFE[26-29]. The effect of nitrogen on the SFE, however, appears to depend on the amount in solution, with little change until at least 0.2 wt% is present[30]. The net effect of nitrogen on SFE is not entirely resolved.

Unfortunately, there are practical difficulties involved in adding large amounts of nitrogen. These are the results of the limited solubility of nitrogen in liquid and solid iron alloys. In order to obtain high nitrogen contents the solubility has to be increased by manganese, chromium and molybdenum additions. Additions of nickel, silicon and carbon, however, reduce the nitrogen solubility[31]. It has been shown that the nitrogen concentration in stainless steels can be further increased by melting under elevated nitrogen pressures[22,32].

Sibanda[1] showed that metastable austenitic stainless steels containing at least 0.22 wt% nitrogen exhibited delayed cracking after deep drawing. However, the additions of copper to these steels reduced the propensity for delayed fracture.

2.2 CORROSION

Corrosion is essentially a process involving two electrochemical reactions:

Oxidation: $M \rightarrow M^{+} + e^{-}$ (anodic)

Reduction: $M^{+} + e^{-} \rightarrow M$ (cathodic)

It therefore makes sense that electrochemical methods can be used to study and measure corroding systems.

2.2.1 MIXED POTENTIAL THEORY

The mixed potential theory proposes that all the electrons generated by the anodic reactions are consumed by corresponding reduction reactions. The mixed potential itself, which is commonly referred to as the corrosion potential, E_{corr}, is the potential at which the total rates of all the anodic reactions are equal to the total rates of all the cathodic reactions. The current density at E_{corr} is called the corrosion current density, I_{corr}, and is a measure of the corrosion rate[12].

2.2.2 CURRENT DENSITY MEASUREMENT

The corrosion current density, I_{corr}, cannot be measured directly since the current involved is one that flows between numerous microscopic anodic and cathodic sites on the surface of the corroding metal. However, it is possible to measure this current indirectly with the use of a counter electrode as well as a potentiostat which is employed in conjunction with a reference electrode (often a saturated calomel electrode). The metal sample is termed the working electrode and cathodic current is supplied to it by means of the counter electrode composed of some inert material such as graphite. In turn, the anodic current is supplied by the working electrode to the counter electrode. Current is essentially measured by means of an ammeter and the potential of the working electrode is measured with respect to the reference electrode by a potentiometer-electrometer circuit. This circuit together with the ammeter form the potentiostat. The potential and current are simultaneously measured[33]. Once the results are plotted in the form of a potentiodynamic scan or polarisation curve (graph of applied potential vs. measured current density), I_{corr} can be measured by one of two techniques[12]:

a. Tafel plot linear extrapolation
b. Linear polarisation resistance

2.2.3 THE POLARISATION CURVE

A convenient way to obtain an understanding of the passivity of stainless steels is by considering the polarisation curve. Figure 2.2 shows a typical polarisation curve for stainless steel in a sulphuric acid solution[12].

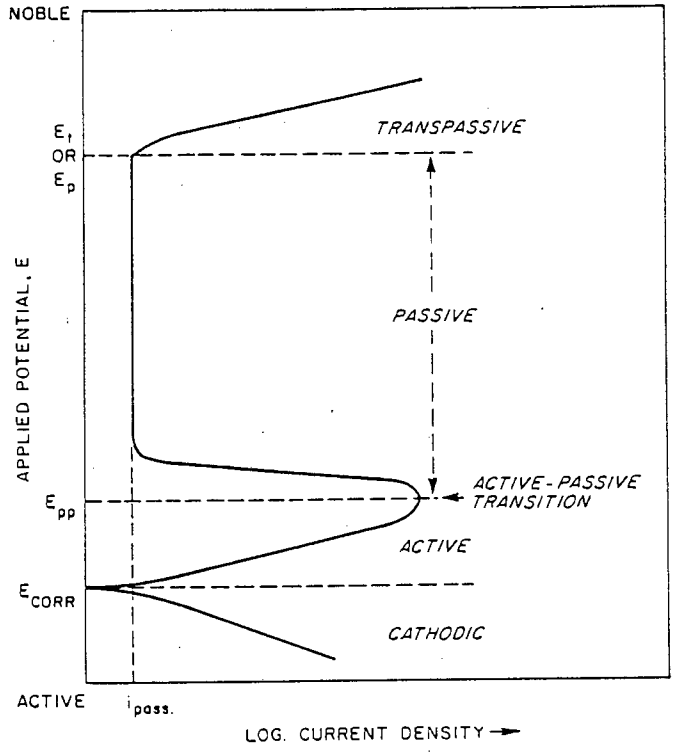

Figure 2.2 A schematic polarisation curve for a stainless steel in a sulphuric acid solution[12]

By increasing the applied potential, from E_{corr}, in the noble (positive) direction and measuring the resultant current density yields a somewhat unexpected potential/current density variation. First, the measured current ceases to increase with applied potential and at the primary passivating potential, E_{pp}, it begins to decrease. The point of maximum current density is termed the critical current density, I_{crit}, and represents the point of maximum anodic dissolution. The beginning of the decrease is known as the active-passive transition. Above this potential, the current drops to a very low value, I_{pass} (passive current density), and remains at a low value over a wide range of potentials. It is in this region that a protective Cr_2O_3 layer forms over the metal substrate, thereby lowering the corrosion rates of the substrate.

As the applied potential increases, another potential will be reached at which the measured current will again begin to increase. The potential at which this current increase takes place is critically dependent on the corrodent. For example, in a chloride free aqueous sulphuric acid solution this potential represents the onset of the evolution of oxygen by the electrolysis of water, and is known as E_t, the potential representing the onset of transpassive behaviour.

However, in chloride containing solutions, the current "breaks" at lower (more active) potentials. This "break" is accompanied by the breakdown of the passive film by the formation of localised pits and occurs at the pitting potential, E_{pit}[12].

2.3 GENERAL CORROSION OF AUSTENITIC STAINLESS STEEL

The conventional austenitic stainless alloys are considered to be the steels most resistant to industrial atmospheres and acid media. As conditions become more severe (higher temperatures, stronger acids, etc.), more alloying content (over that of AISI 304 stainless steel) is required[5].

2.3.1 EFFECT OF ALLOYING ELEMENTS ON ANODIC AND CATHODIC PROCESSES

Increasing the chromium content beyond 12-13 wt% will yield steels which can be passivated in more aggressive electrolytes. Alloying the steel with both chromium and nickel will markedly facilitate passivation by lowering I_{crit} and hence reducing the active range. E_{pp} is also shifted slightly towards the more electropositive (noble) direction (see Figure 2.3)[5].

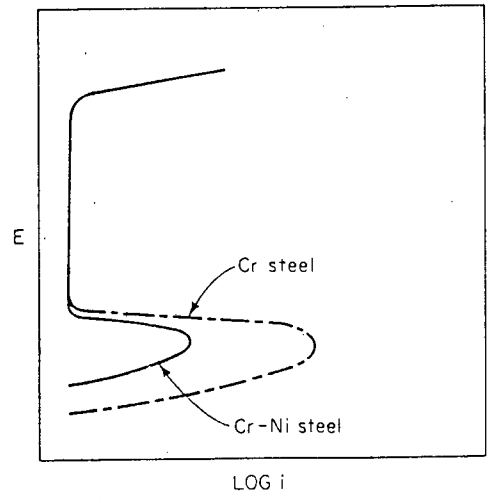

Figure 2.3 Relationship between corrosion rate and the electrode potential of a chromium steel and a Cr-Ni steel[5]

Alloying the austenitic Cr-Ni steels with very small amounts of molybdenum will further reduce I_{crit} but these steels have poor properties in the transpassive range and are therefore not suitable for highly oxidising electrolytes. Replacing molybdenum with silicon in Cr-Ni steels will improve their properties in the transpassive range[5].

a. Copper additions

Adding small amounts of copper will not appreciably affect the polarisation curve in the same way as the other elements mentioned thus far. Instead copper facilitates the cathodic process i.e. the reduction of the oxidising agent. Figure 2.4 shows how the addition of copper reduces the polarisation of the cathodic reaction so that the steel can be passivated instead of corroding in the active state[5].

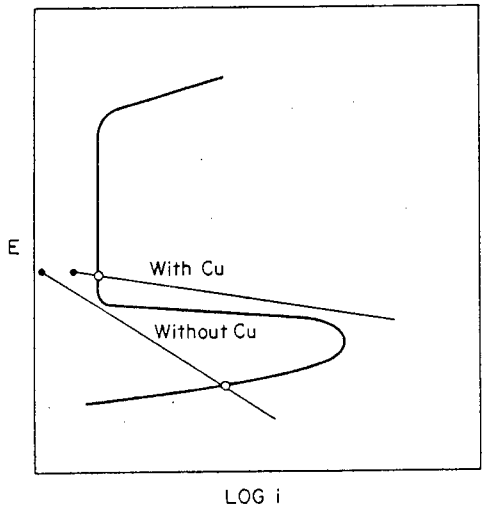

Figure 2.4 Importance of the cathodic process for the corrosion rate of a metal capable of being passivated[5]

Murase[34] found that the general corrosion resistance in sulphuric acid media showed improvements for both austenitic and ferritic stainless steels with copper additions. This work also revealed that the potentiodynamic scans showed a decrease in I_{crit} and corrosion rate values (Figure 2.5) with copper additions. The immersion tests showed similar trends. This observation, however, was reversed in nitric acid i.e. copper additions showed detrimental effects. Copper was also reported to have a detrimental effect on the passivity of ferritic stainless steels[34].

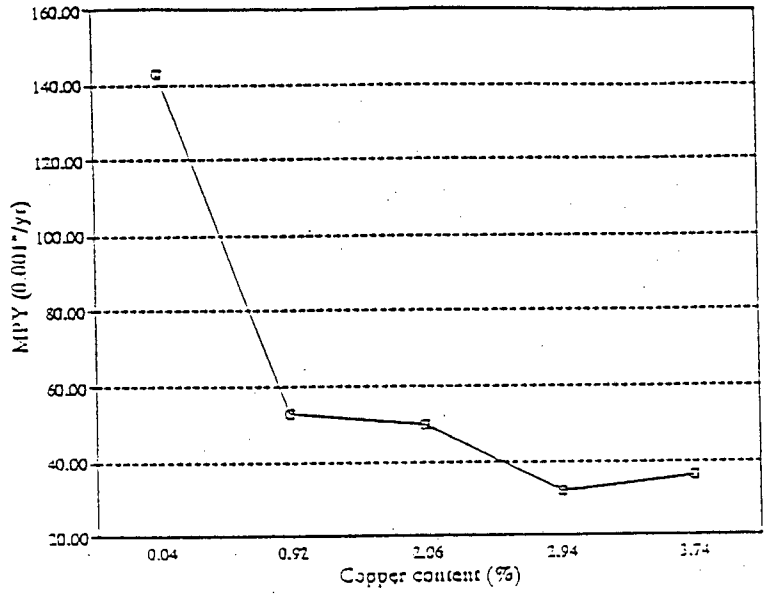

Figure 2.5 Influence of copper content on corrosion resistance of austenitic stainless steels in 1N sulphuric acid[34]

Yamamoto *et al*[35] also confirmed the reduction of corrosion rates with an increase in copper content in a sulphuric acid environment. With the addition of copper, the natural potentials of copper and niobium added 19Cr ferritic stainless steels shift to the noble side as corrosion proceeds. The corrosion potential is just below -500mV$_{SCE}$ after initial immersion and slowly increases with time to more noble potentials and finally levels off just below -400mV$_{SCE}$ (see Figure 2.6). This phenomenon seems to be attributable to the fact that smut, or corrosion product (see Section 2.4), formed on the steel surface decreases the anodic area and that the cathodic reaction is accelerated with the progress of corrosion.

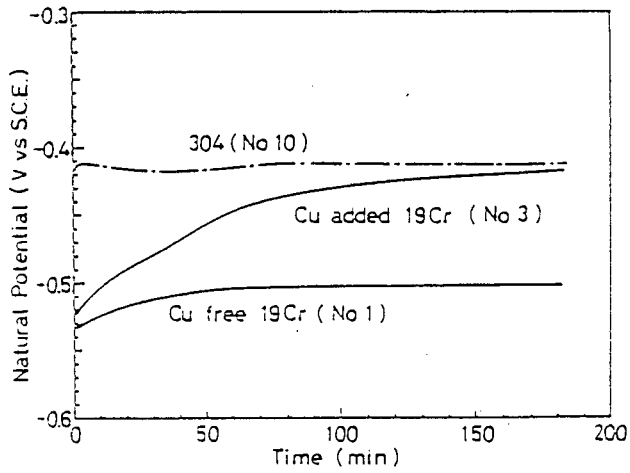

Figure 2.6 Changes in natural potentials of specimens with time in a 5% H_2SO_4 solution at 25°C[35]

The most important effect of copper additions (to ferritic stainless steels) on the anodic reaction is that it lowers the critical current density and shifts the passivation potential to the base (active) side. That is, with the addition of as low as 0.4 wt% Cu, the passivation potentials are shifted to approximately -500mV_{SCE}, nearly the same as the corrosion potential at the initial stage of immersion (see Figure 2.7).

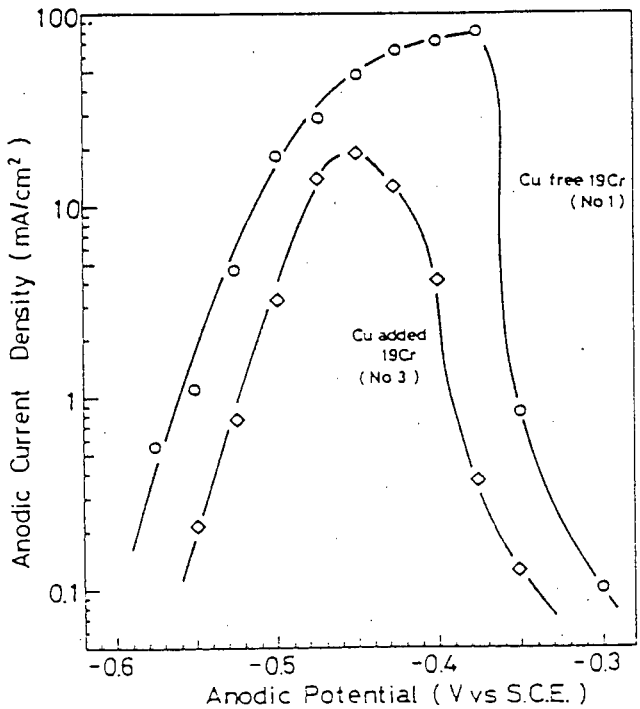

Figure 2.7 Real Anodic polarisation curves calculated from weight losses in 5% H_2SO_4 solution at 50°C[35]

In another study involving the electrochemical and corrosion behaviour of 18-8 austenitic stainless steel containing copper, it was found that the addition of copper enhanced the passivation in aerated 0.1M sulphuric acid.[36] This is probably due to the affinity of copper for oxygen and it is speculated that copper may assist the adsorption of oxygen. In the absence of dissolved oxygen (i.e. de-aerated), the passive current density increased with increasing amounts of copper in the stainless steel (see Figure 2.8).

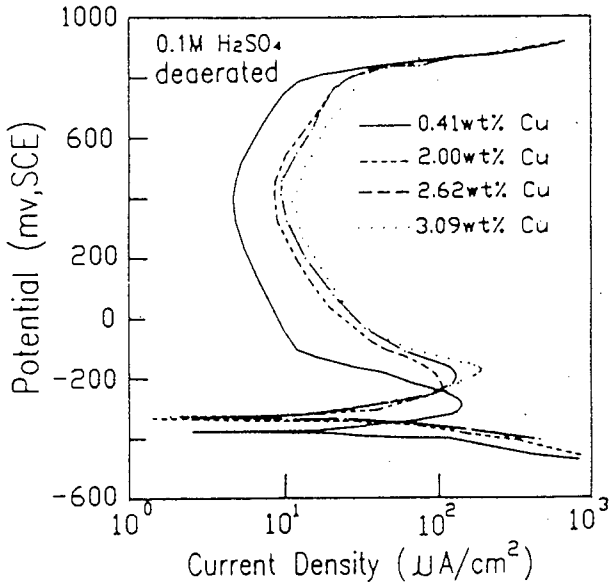

Figure 2.8 Potentiodynamic polarisation curves of Cu-containing stainless steels in de-aerated 0.1M sulphuric acid solution[36]

Furthermore, this study showed that the passive film formed on the high copper content stainless steel was less stable than that formed on the low copper content steel in de-aerated 0.1M sulphuric acid solution[36].

In a paper reporting the effects of molybdenum, copper, silicon and phosphorous on the anodic behaviour of 17Cr steels in sulphuric acid, Lislovs[37] found that the addition of 2 wt% copper to a 17Cr-1Mo-1Si-0.05P steel significantly decreased the value for I_{crit} (with respect to the same alloy without copper additions), but was detrimental to the stability of the passive film. On the other hand, the addition of 2 wt% copper to a 17Cr-3Mo steel (without additions of phosphorous and silicon) produced only a small decrease in the value for I_{crit} (with respect to the copper-free version of this steel), but greatly enhanced the passivity of the steel.

In acidic chloride solutions (3.5% NaCl), copper additions to austenitic stainless steel has been found to result in a decrease of active dissolution at 80°C. Copper shifts the passivation potential in the anodic direction and the pitting potential in the cathodic direction in this media, as illustrated in Figure 2.9[38].

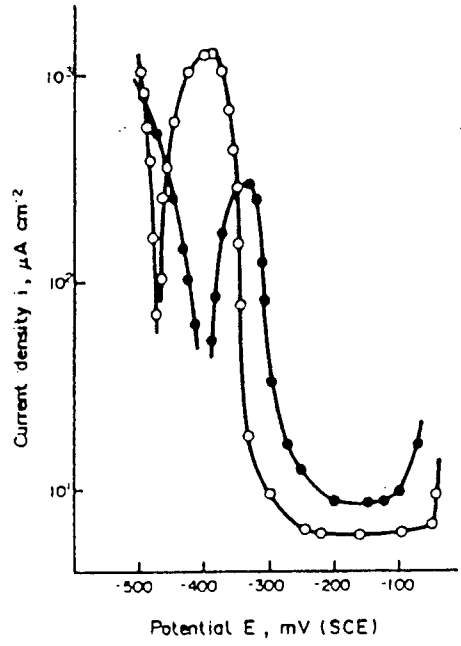

Figure 2.9 The polarisation curves of 18Cr-10Ni (O) and 18Cr-10Ni-2Cu (●) in 3.5% NaCl solution at 80°C[38]

This study also found that copper reduces the stability of the passive film by changing the passivation kinetics during the growth of this film[38]. Composition depth profiles of the passive film of two steels grown at -300mV$_{SCE}$ in 3.5% NaCl for 5 seconds were conducted (see Figure 2.10).

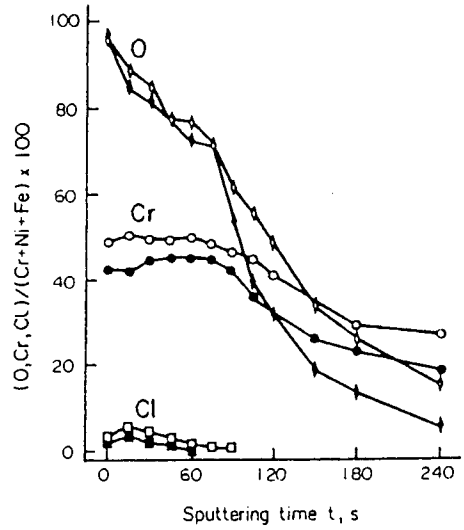

Figure 2.10 Depth profiles of 18Cr-10Ni (◊,○,□) and 18Cr-10Ni-2Cu (♦,●,■) after passivation at -300mV_{SCE} for 5 seconds[38]

These profiles showed that the specimen surfaces were enriched with chromium and oxygen. Throughout the depth profiles, the chromium enrichment on the surface of the 18Cr-10Ni steel was higher than that of the 18Cr-10Ni-2Cu steel. It can be concluded that copper retards the enrichment of chromium and oxygen on the surface of stainless steel during the passivation process[38].

The effects of copper, molybdenum and carbon on the rate and type of corrosion of 18Cr-8Ni stainless steels after deformation into U-shaped specimens have been investigated in 5N H_2SO_4 solutions containing up to 0.4M NaCl at 40°C[39]. Steels containing less than 0.1 wt% Mo exhibited general corrosion independent of copper content (0.1-1.04 wt%). In steels containing 0.1-1 wt% Mo, the type of corrosion changes with increasing copper content in the following way: firstly, at low copper content, general corrosion with grain boundary initiation, then intergranular corrosion and finally stress-corrosion cracking, as the copper content increases. For steels which exhibit intergranular corrosion, the depth of intergranular corrosion increases with increasing molybdenum content and decreases with increasing copper content.

In summary, it appears that the effect of copper on the corrosion behaviour of austenitic stainless steel is quite varied and complicated. However, it is the general trend that copper additions to austenitic stainless steel result in improvements to the corrosion performance in sulphuric acid media. This is noted essentially by the decrease in both I_{crit} values and corrosion rate values. It seems also that copper additions generally have a detrimental effect on the stability of the passive film in de-aerated sulphuric acid media. This is shown by the increase in passive current densities with increasing copper content. The effect of copper on corrosion performance is, however, largely dependent on the type of environment, whether or not oxygen is present and the presence of other alloying elements.

b. Nitrogen additions

Cortie studied the effect of nitrogen additions on metastable Fe-17Cr-7Mn-4Ni-0.04C-0.5Cu (wt%) austenitic stainless steel[10]. Potentiodynamic scans of the alloys in 10% sulphuric acid showed typical active-passive behaviour. The voltages E_{corr} and E_{pp} did not show any particular trends when plotted against nitrogen content. However, nitrogen additions from 0-0.3 wt% had a significant effect on I_{crit}, reducing it from 2.4 to 0.5mA/cm^2. This is regarded as a beneficial variation and makes it easier for the alloy to passivate in this particular environment. Beneficial effects of nitrogen were also recorded in the general corrosion rates[10]. Pickering[26] also found nitrogen to be beneficial in promoting passivity.

The values for I_{crit} and I_{pass} were also found to decrease with increasing nitrogen content when virtually nickel free Fe-Cr-Mn alloys were tested in 5% sulphuric acid (Figure 2.11). The passivation potential also moved to less noble values with increasing nitrogen content making the active region narrow[40].

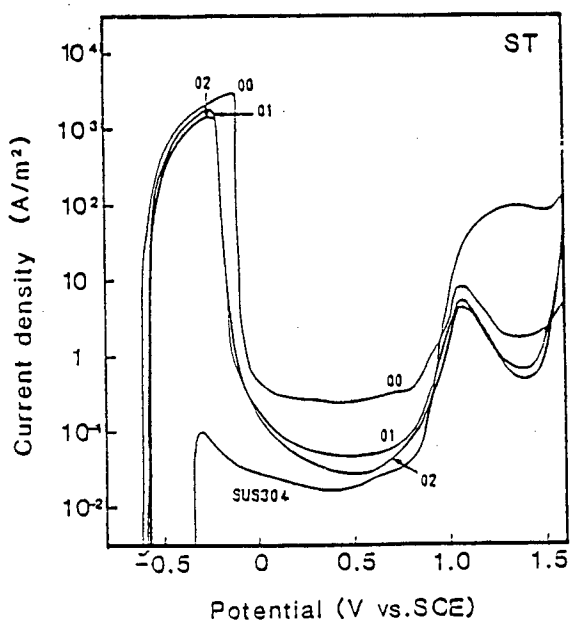

Figure 2.11 Effect of nitrogen content on anodic polarisation of solution treated Fe-12Cr-15Mn steels in 5% sulphuric acid at 30°C (00, 01, 02 = 0, 0.1, 0.2 wt% N respectively)[40]

2.4 METALLIC COPPER DEPOSITION AND THE SECOND ANODIC PEAK PHENOMENON

Yamamoto, *et al*[35] found metallic copper in the smut (mentioned in Section 2.3.1(a)) of 0.4 wt% copper added 19Cr ferritic stainless steels. It was decided that this copper was not the result of being left behind during the preferential attack of iron and other alloying elements, but rather that the metallic copper may have been the cathodic precipitate from the ions which were oxidised as Cu^{2+} and Cu^{+} into the electrolyte and then reduced. The equilibrium potentials of Cu/Cu^{2+} and Cu/Cu^{+} are $99mV_{SCE}$ and $279mV_{SCE}$, lying on the considerably nobler side compared with the anodic active potential region of stainless steels. Consequently, it is quite possible that, if the copper contained in steel dissolved as ions into solution, it is immediately reduced and cathodically precipitated. Thus, it may be thought that with the copper added stainless steels, the anodic reaction is inhibited not only by the anodic area being reduced by smuts, but also by the cathodic precipitation of metallic copper at anodic active sites.

Lizlovs[37] also found that the evaluation of the corrosion results for copper added 17Cr ferritic stainless steels is complicated by the simultaneous deposition of dissolved copper on the corroding specimen. This effect is expected to be the largest at potentials near E_{pp} (primary passivation potential), where the corrosion rates are at maximum values. This deposition of copper contributes a negative current of unknown and varying magnitude. The deposited copper is then anodically dissolved ($Cu \rightarrow Cu^{2+} + 2e$) resulting in an increase in anodic current. It was suggested by Lislovs[37], Seo[41] as well as Murase[34] that the small positive current "hump" or second anodic peak (Figure 2.12) seen in the potentiodynamic scans of stainless steels could be attributed to this dissolution of copper.

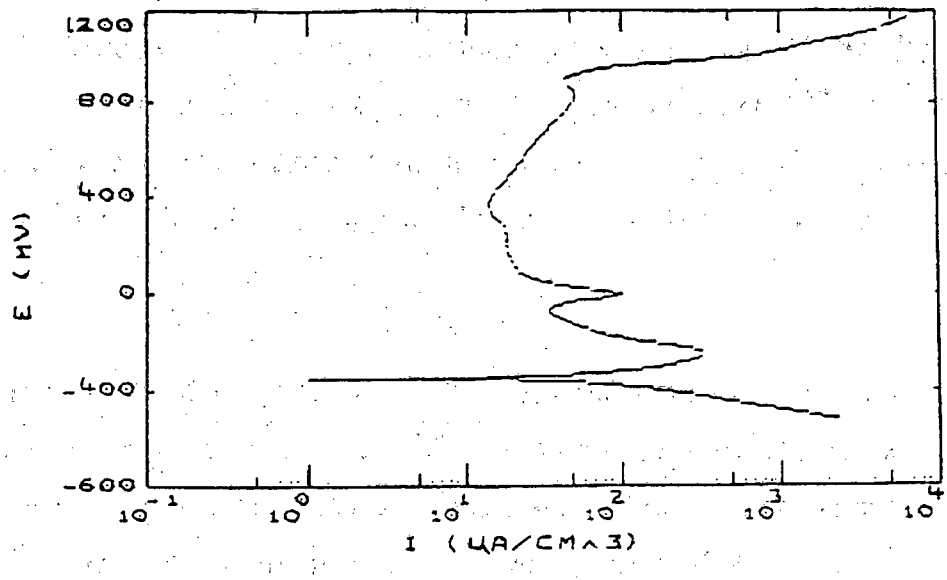

Figure 2.12 Potentiodynamic curve of 2.06 wt% Cu added austenitic stainless steel in 1 *N* H_2SO_4 at 30°C showing second anodic peak[34]

2.5 PITTING IN AUSTENITIC STAINLESS STEELS

Pitting is a form of localised corrosion in environments containing very aggressive ions such as chlorides. These aggressive ions penetrate the passive film at a certain potential and destroy it at weak points. The corrosion pits tend to develop at microstructural features such as grain boundaries and oxide inclusions[6]. Chromium, nickel and molybdenum additions have the effect of increasing the steels resistance to pitting[5,12].

The pitting corrosion resistance of austenitic stainless steels is known to improve with an increase in copper content in chloride containing media[34,36]. The increase in pitting potential with the increase in copper content shows that susceptibility of the alloys to pit initiation decreases with an increase in copper content[34]. Moskowitz *et al*[42], however, summarised the effect of copper on resistance of stainless steels to pitting in chloride solutions as variable. Copper has no effect in the absence of molybdenum, but a slightly detrimental effect in the presence of molybdenum[42].

The effect of nitrogen content on the pitting tendencies of austenitic stainless steel has been well reported and proven to be beneficial[26,42-45]. This effect is shown by the extension of the passive range when the pitting potential, E_{pit}, is increased towards the transpassive range[46]. Nitrogen is also the main factor in the pitting resistance equivalent (PRE) equation which is used as an empirical indicator for pitting resistance[47].

$$PRE = (\%Cr + 3.3\ \%Mo + 16\ \%N)$$

2.6 PRECIPITATION DURING AGEING

Precipitation reactions in austenitic stainless steels at elevated temperatures are complex and only general guidance to the precipitates formed can be gained by reference to constitutive diagrams[48].

When austenitic stainless steels are rapidly cooled from the solution treatment temperature, the dissolved carbide remains in solution. However, when supersaturated steels are thermally aged, carbide precipitation then occurs. In the absence of stabilising elements, $M_{23}C_6$ is the predominant carbide formed in the AISI 300 series austenitic stainless steel. $M_{23}C_6$ is mainly composed of chromium carbide, so the designation $Cr_{23}C_6$ is used frequently. Precipitation occurs very rapidly on the ferrite-austenite interfaces, followed by precipitation on other non-coherent boundaries including inclusions, grain and twin boundaries (Figure 2.13). The principal practical consequences of $M_{23}C_6$ precipitation are degradation of intergranular corrosion resistance and reduction in tensile properties, especially ductility and toughness[48].

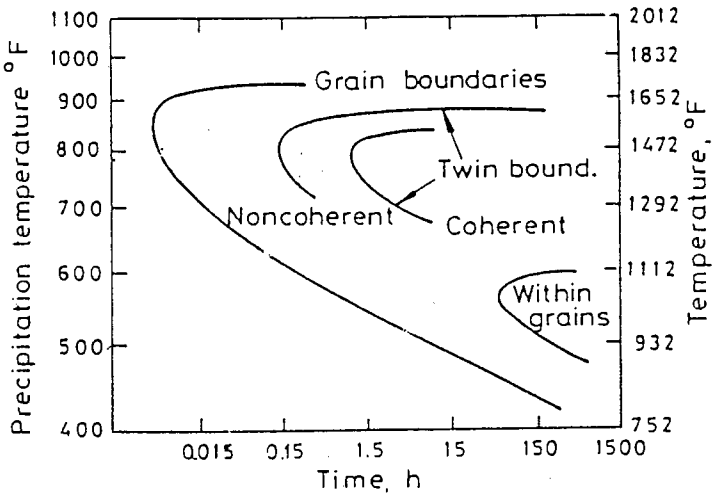

Figure 2.13 Precipitation kinetics of $M_{23}C_6$ carbide in 18Cr-9Ni AISI 304 stainless steel containing 0.05 wt% C[48]

2.6.1 NITRIDE PRECIPITATION

Many nitrides precipitate in the austenitic steels, the predominant one being Cr_2N. The solubility of Cr_2N, which has a hexagonal structure, is lower in the higher chromium and nickel AISI 310 than in AISI 304, probably because of the much higher nickel content. Both Cr_2N and $M_{23}C_6$ precipitate within the matrix, often on dislocations and also as grain boundary cellular precipitates. The higher the nitrogen content, the lower the ageing temperature at which cellular precipitation occurs[49].

Ageing of annealed high nitrogen (0.7 wt%) materials at 700°C produced only grain boundary Cr_2N precipitation. Faster precipitation kinetics at 900°C resulted in grain boundary, transgranular and cellular nitride precipitation as shown in Figure 2.14. Complete grain boundary nitride coverage occurred after 0.1 hours of ageing at 900°C but required about 1 hour at 700°C[49].

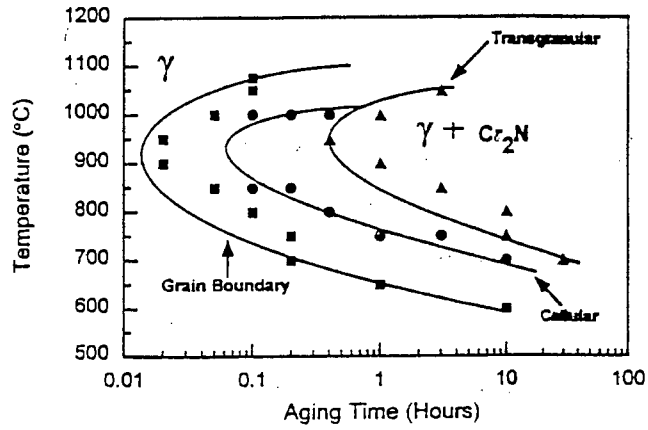

Figure 2.14 TTP diagram for grain boundary, cellular and transgranular nitride precipitation in annealed high nitrogen stainless steel[49]

Nitrogen has a high solubility in austenitic steels - in excess of 0.1 wt% at temperatures above 550°C. Owing to this solubility, only a small amount of nitrogen is found replacing carbon in $M_{23}C_6$ to form $M_{23}(CN)_6$, but in the presence of stronger carbide forming elements, such as niobium and titanium, nitrides are readily precipitated at high temperatures[26].

The precipitation of secondary phases has also been examined for a 20Cr-25Ni-4.5Mo-0.21N steel at 850°C, the temperature of most rapid precipitation. The precipitation sequence was found to be complex and involves several intermetallic carbide and nitride phases. Initial precipitation examined after 10 minutes is however dominated by Cr_2N[50].

Miyahara *et al*[40] showed that Fe-12Cr-15Mn containing 0.1-0.2 wt% nitrogen formed grain boundary precipitates after ageing at 700°C for 10 hours. Grain boundary nitrides were identified as Cr_2N by x-ray diffraction analysis. Carbide formation at grain boundaries introduced deep grain boundary corrosion in the active region and increased I_{pass} in the measurement of anodic polarisation. However, nitride formation showed shallow grain boundary corrosion and no change of the value for I_{pass}[40].

2.6.2 INFLUENCE OF PRIOR DEFORMATION ON PRECIPITATION KINETICS

The effect of cold work on ageing is to shift the time-temperature-precipitation diagram to shorter times and lower temperatures. The formation of $M_{23}C_6$ is markedly accelerated[48]. Simmons[49] investigated the effects of nitride (Cr_2N) precipitation of a typical high nitrogen, low carbon austenitic stainless steel, nominally Fe-19Cr-5Mn-5Ni-3Mo-0.024C-0.69N. His work showed that prior deformation increased precipitation kinetics and had a controlling influence on nitride morphology, enhancing grain boundary and transgranular Cr_2N, and retarding cellular precipitation. Prior deformation by cold rolling accelerated grain boundary Cr_2N precipitation kinetics (700°C and 900°C), retarded cellular precipitation (900°C) and caused the deformation-induced precipitation of needlelike transgranular nitride precipitates (700°C and 900°C) which were associated with periodic defect structures (deformation twins and concentrated slip bands).

This work also showed that precipitate structures can be altered by thermomechanical processing and, therefore, can be controlled to some degree by the type and magnitude of strain applied to the system. However, overall precipitation kinetics cannot be reduced by thermomechanical processing since it increases the volume of defect structures and the total energy of the material. Precipitation kinetics can only be retarded through the chemical driving force (i.e. composition changes).

2.7 SENSITISATION

Sensitisation is the process whereby precipitates of $Cr_{23}C_6$ form preferentially at grain boundaries. A small amount of carbon combines with a large amount of chromium, and thus depletes the surrounding grain boundary area of chromium. Since a chromium content of at least 12 wt% is needed for the formation of a protective passive film and hence prevention of extensive corrosion, the area around the grain boundaries are subject to higher corrosion rates. This results in intergranular corrosion taking place.

Carbon content should be kept below 0.03 wt% as higher volumes will favour formation of chromium carbides at the grain boundaries leading to sensitisation (if exposed to temperatures between 538 - 815°C)[5]. Titanium and niobium are used to reduce carbon solubility at the annealing temperature. This in turn helps prevent the process of sensitisation (they are strong carbide formers)[3].

2.7.1 INFLUENCE OF NITROGEN ON SENSITISATION

Briant *et al*[51] studied the sensitisation of high purity austenitic stainless steels and found that nitrogen retards nucleation and/or growth of carbides at grain boundaries and hence increases the time necessary for sensitisation (see Figure 2.15). For such a mechanism to be operative, nitrogen must diffuse to the grain boundaries and be present there during carbide nucleation and growth. Additions of manganese and molybdenum also help nitrogen retard the nucleation and growth of the carbides by stabilising the nitrogen in the grain boundaries through attractive chemical interactions. Nitrogen has a chemical attraction to both molybdenum and manganese, i.e. there will be a tendency for them to form a compound.

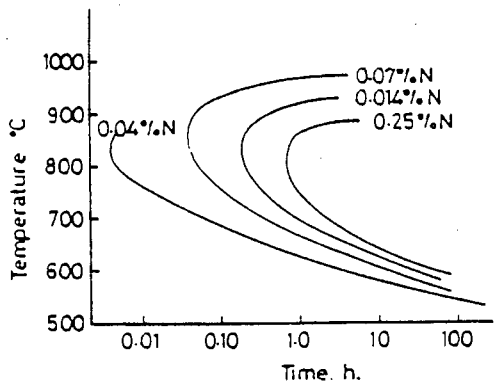

Figure 2.15 Effect of nitrogen on kinetics of $M_{23}C_6$ precipitation[26]

Similar trends were observed in an investigation on commercial purity alloys but are modified by the presence of impurities[52]. The discovery of a multiplicity of phases which occur at grain boundaries in sensitised AISI 316L stainless steel, containing more than 0.15 wt% nitrogen is interesting since this does not affect the sensitisation behaviour of this material. These phases which do not cause sensitisation serve to increase the distance between $M_{23}C_6$ precipitates and also may occupy grain boundary sites which would otherwise be available for carbide nucleation.

The addition of nitrogen contents varying from 0.029 to 0.123 wt% to a low carbon austenitic stainless steel containing 2.3 wt% molybdenum also showed that nitrogen improves the sensitisation resistance over the range of critical temperatures (600-850°C)[53]. During sensitisation by heat treatment in the temperature range 600-700°C, nitrogen segregates at the grain boundaries of austenitic stainless steels. This segregation is enhanced by the presence of molybdenum which stabilisers nitrogen in the grain boundary regions.

Therefore, even relatively small amounts of nitrogen have a pronounced effect on the sensitisation properties of the steel, by virtue of the segregation of the nitrogen at the grain boundaries. Problems of sensitisation in high carbon austenitic stainless steels in the critical temperature range can also be reduced by the addition of nitrogen[53].

Tests carried out on AISI 304 stainless steel with nitrogen ranging from 0.04-0.25 wt% and carbon content 0.045 wt% revealed that nitrogen additions up to 0.16 wt% also retard sensitisation but a nitrogen addition of 0.25 wt% does not retard sensitisation[54,55]. These tests also showed that the chromium concentration at the carbide/austenite interface increases from 11.2 to 12.4 wt% as nitrogen is increased from 0.04-0.16 wt% (see Figure 2.16)[54].

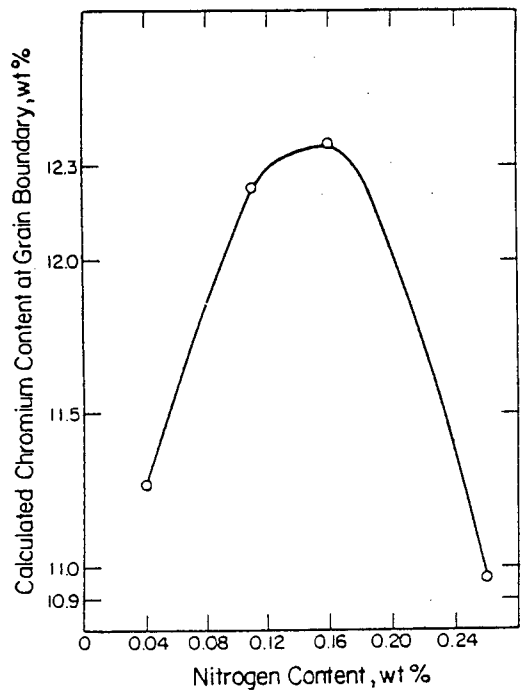

Figure 2.16 Calculated chromium concentration at carbide interface, as a function of nitrogen content, at 600°C[54].

This increase in chromium concentration is thought to lower the concentration gradient between the austenite matrix and the grain boundaries and hence retard carbide growth by reducing the sensitisation kinetics, since chromium diffusion in austenite is rate-controlling. Nitrogen additions of 0.25 wt% lowers the chromium concentration at the interface, increases the concentration gradient and sensitisation kinetics are not retarded[54].

2.7.2 EFFECT OF MARTENSITE ON SENSITISATION

In an investigation on the effects of deformation-induced martensite on the sensitisation of austenitic stainless steels[56], work was carried out to compare the effects of deformation which does not induce martensite with deformation which does on the sensitisation of austenitic stainless steels. In order to do this, the effect of deformation on the sensitisation of AISI Type 316 and 304 stainless steel was determined. In the undeformed state, the sensitisation kinetics of the two steels were remarkably similar, and the sensitised samples corroded intergranularly. However, deforming the samples to within 34.5 MPa of the maximum tensile stress produced martensite in the AISI 304 alloy but does not in the AISI 316 alloy. The presence or absence of martensite leads to quite different sensitisation behaviour. This can be explained by the following:

Deformation reduces the times required for sensitisation. However, the effect is much greater in the martensite containing AISI 304 stainless steel than in the AISI 316 type. The rapid sensitisation of AISI 304 results directly from the presence of martensite. Because chromium and carbon can diffuse more rapidly in the body-centred tetragonal (BCT) martensite than in the face-centred cubic (FCC) austenite, precipitation of chromium carbides can occur at lower temperatures. These intragranular carbides produce intragranular corrosion. No carbides or corrosion were observed in the deformed AISI 316 samples after ageing at these temperatures (below 600°C).

At temperatures of between 600 and 650°C, sensitisation occurs rapidly in the undeformed alloys. Deformation increased the kinetics of sensitisation in both alloys in this temperature range. However, samples of AISI 316 alloys sensitised for short times corroded intergranularly and only with continued sensitisation did intragranular corrosion accompany the intergranular attack. Deformed samples of AISI 304 stainless steel aged for short periods immediately showed both inter- and intragranular corrosion.

In both alloys, any intragranular corrosion which occurred after heat treatments in the temperature range 600-650°C could be associated with intragranular carbides. However, in the AISI 304 alloy, carbides can nucleate easily both at the grain boundaries and within the martensite leading to a high density of carbides. In the AISI 316 alloy, the grain boundaries remain the preferred location for carbide precipitation and only with time do intragranular carbides form.

The deformed AISI 316 alloy sensitised readily at 700°C and after heat treatments of 3 to 24 hours exhibited failure in the modified Strauss test. However, the AISI 304 alloy was either partially attacked or completely healed after the same treatment.

This "healing" phenomenon results from the ageing of martensite. Even at very short ageing times at 650-700°C, many carbides precipitate at the grain boundaries as well as within the martensite. This high density means that chromium depletion around any carbide will never be as great as the depletion around a low density of intragranular or grain boundary precipitates. Furthermore, the martensite is especially efficient at precipitating carbides because the solubility of carbon is lower in the martensite than in austenite. This means that most of the carbon in the martensite rapidly goes into the formation of carbides, giving a high density of fine carbides.

In summary, it was found that martensite formed during deformation produces very rapid sensitisation at temperatures below 600°C. This deformation-induced martensite is a site of extensive carbide precipitation during ageing and causes extensive intragranular corrosion. Between 650-700°C, a "healing" phenomenon may occur during the ageing of the deformation-induced martensite. This "healing" reduces the deleterious effects of sensitisation. Cold work alone, without the formation of martensite, noticeably increases the kinetics of sensitisation only in the temperature range where the undeformed samples are also rapidly sensitised. It does not lead to rapid "healing", and the grain boundaries remain the preferred site for carbide precipitation.

CHAPTER 3
EXPERIMENTAL TECHNIQUES

3.1 EXPERIMENTAL MATERIALS

Three novel austenitic stainless steel alloys were used in this experimental programme. These alloys were supplied by Columbus Stainless (Middelburg, South Africa) and are based on the AISI 301 series of stainless steels. These three alloys have reduced nickel levels (5.25 to 5.44 wt%) and increased nitrogen (0.23 to 0.26 wt%) and copper (0.07 to 3.34 wt%) levels. In addition to these three alloys, the experimental programme included the AISI 301 and 304L standards for comparison. All castings were hot rolled to a thickness of 10mm and were supplied in 4kg plates. The three novel alloys were designated 0Cu (0.07 wt%), 1Cu (1.23 wt%) and 3Cu (3.34 wt%) relating to their copper contents. The exact chemical compositions are given in Table 3.1.

Alloy	**C**	**Cr**	**Ni**	**N**	**Cu**	**Mn**	**S**	**Ti**	**Nb**	**Si**
0Cu	0.05	17.37	5.44	0.26	0.07	1.28	0.010	0.001	0.005	0.22
1Cu	0.03	17.73	5.30	0.23	1.23	1.49	0.008	0.001	0.004	0.22
3Cu	0.03	17.21	5.25	0.24	3.34	1.34	0.008	0.001	0.004	0.28
301	0.02	17.47	7.41	0.07	0.06	1.73	0.006	0.026	0.006	0.62
304L	0.02	18.34	8.12	0.08	0.05	1.93	0.005	0.002	0.007	0.52

Table 3.1 Composition of experimental alloys (wt%)

Austenite stabilities as ranked by $M_{s(\alpha')}$ temperatures (Section 2.1.1(b)) are given in Table 3.2.

Alloy	0Cu	1Cu	3Cu	301	304L
$M_{s(\alpha')}$ (°C)	-251.3	-263.7	-380.2	-58.4	-105.0

Table 3.2 $M_{s(\alpha')}$ temperatures (°C) of experimental alloys

3.2 MICROSCOPY

The microstructures of the various materials were characterised using both light and scanning electron microscopy.

3.2.1 OPTICAL MICROSCOPY

Optical light microscopy was employed before any corrosion tests were carried out in order to qualify the microstructures of the three novel alloys. Both bright field and Nomarski interference contrast modes were employed. Specimens were mechanically ground finishing with 1200 grit paper and then polished using a 3μm diamond paste cloth. They were then electropolished and electro-etched (to remove any residual martensite formed in the polishing process) using the following procedures:

a. Electropolishing

Solution:	25g CrO_3
	133ml acetic acid
	7ml distilled water
Current Density:	0.09-0.22 A/cm^2
Voltage (DC):	20V
Temperature:	17-19°C
Time:	6 minutes
Cathode:	Stainless Steel

b. Electro-etching

Solution:	10g oxalic acid
	100ml distilled water
Voltage (DC):	6V
Temperature:	15-20°C
Time:	45-60 seconds
Cathode:	Stainless Steel

3.2.2 SCANNING ELECTRON MICROSCOPY (SEM)

A Cambridge Model S.200 scanning electron microscope (SEM) was used in order to examine the surfaces of the various microstructures after corrosion and to identify the mode of corrosion which took place e.g. general corrosion, intergranular corrosion, intragranular corrosion, pitting corrosion, etc. Images were obtained from secondary electrons at an accelerating voltage of 30kV.

3.3 CORROSION TESTS

3.3.1 INSTRUMENTATION

Corrosion tests were carried out using an AMEL System 5000 Electrochemical Potentiostat which is linked to an AMEL EASYCORR Corrosion Software package. This software allows potentiodynamic polarisation scanning (including pitting cyclic scans), polarisation resistance measurements as well as Tafel plots to be conducted. The potentiostat is linked to the corrosion cell via cables to the reference electrode, working electrode and counter electrodes.

In order to eliminate any pick-up of electrical noise which may be present in the surroundings, a Faraday type cage was constructed which consisted of a wooden box lined on the inside with copper sheeting. This box contained only the corrosion cell, immersed in a temperature bath, thereby isolating the sensitive measurements from the surrounding environment.
A second bath (which contained the thermo-regulator and a small bilge pump) was placed outside the Faraday cage. This allowed for water to be pumped at temperature into the cage containing the corrosion cell, without both these motor driven devices contributing to any electrical noise. Figure 3.1 shows the instrumentation used during testing.

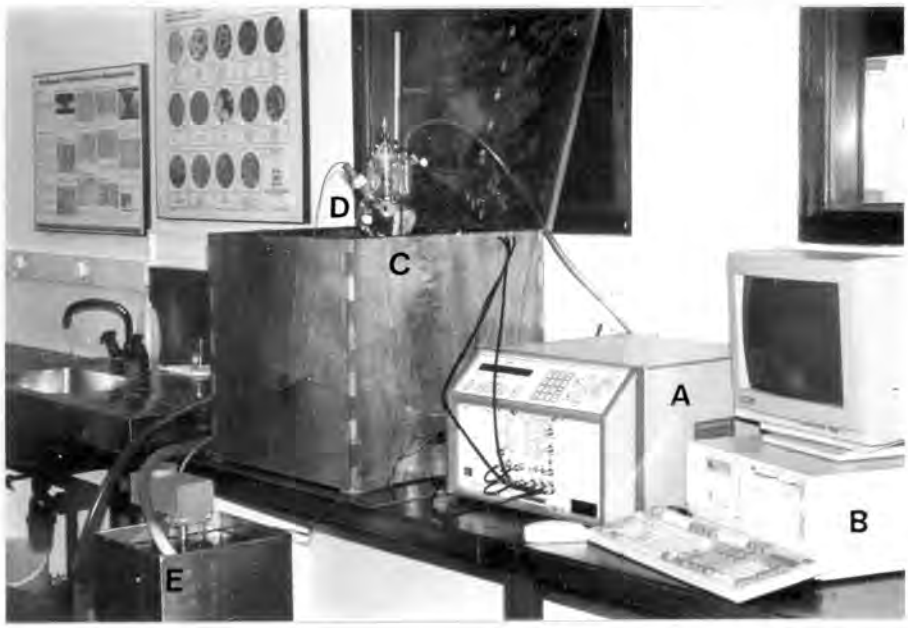

Figure 3.1 Corrosion Instrumentation

a. AMEL System 5000 Potentiostat
b. Computer containing AMEL EASYCORR software
c. Faraday cage containing test cell immersed in a water bath
d. Test cell
e. External water bath with thermo-regulator and bilge pump

The glass corrosion cell along with its accessories are shown in Figure 3.2. This corrosion cell, which has a capacity of 1 litre, has specially ground joints for accommodating the reference electrode, the graphite counter electrodes, the purge gas tube and the working electrode holder. Potential measurements were recorded against a saturated calomel electrode (SCE) which has a potential of 0.241V with reference to the standard hydrogen electrode. All results are thus quoted as voltage vs. SCE unless otherwise indicated.

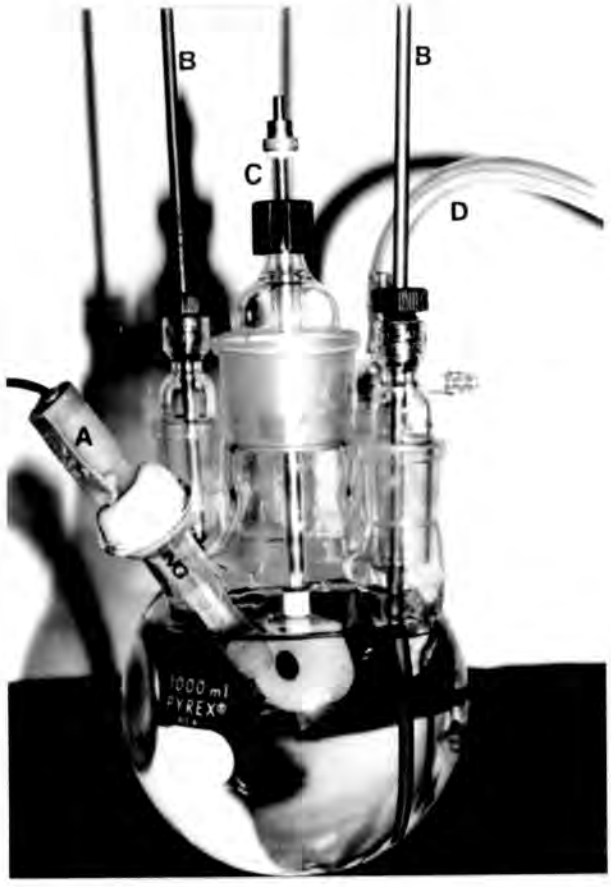

Figure 3.2 Glass Corrosion Test Cell

a. Saturated Calomel reference electrode
b. Graphite counter electrodes
c. Working electrode (specimen)
d. Purge gas tube

3.3.2 TESTING PROCEDURE

To ensure that the system was functioning correctly, a test was performed in accordance with the ASTM standard G5-78[57] on AISI 430 stainless steel in a 1*N* H_2SO_4 (sulphuric acid) solution. Figure 3.3 shows the result of the potentiodynamic test scan and indicates the good correspondence with the ASTM standard reference curve.

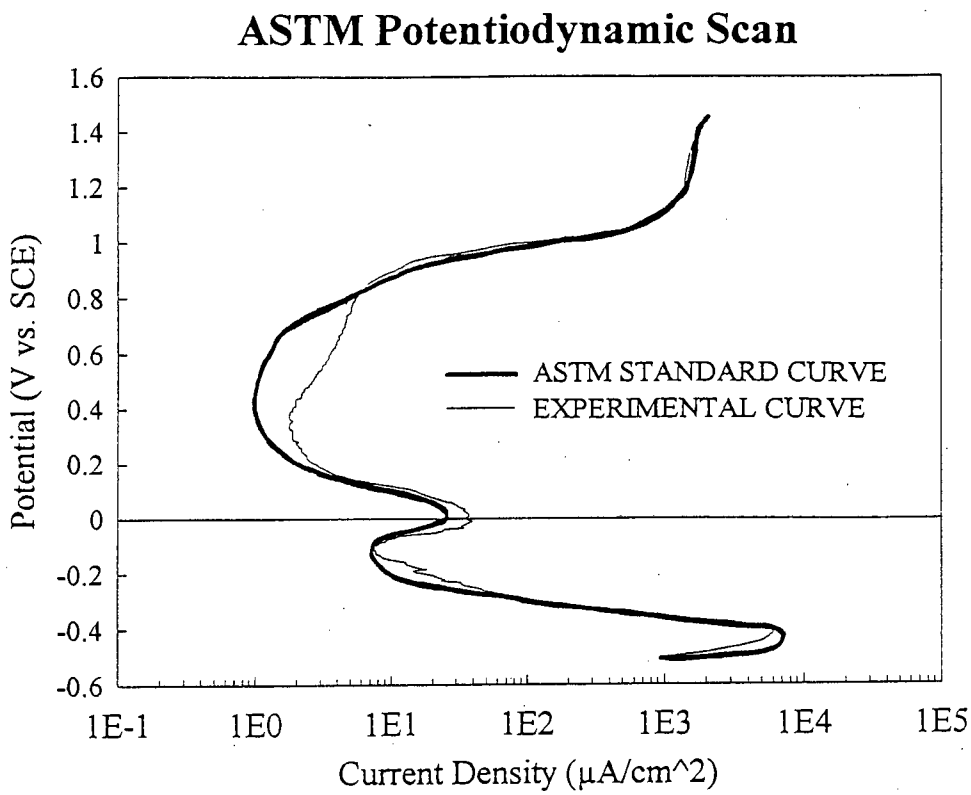

Figure 3.3 Potentiodynamic scan of AISI 430 in 1*N* H_2SO_4 compared to ASTM standard reference test.

Both potentiodynamic scans (including cyclic pitting scans) and Tafel plots were carried out on the specimens. The potentiodynamic scans enabled characterisation of the overall corrosion behaviour such as maximum dissolution rates, passivation behaviour, transpassivity and pitting tendencies, while the Tafel plots allowed for accurate corrosion rate measurements.

All tests (with the exception of pitting tests) were carried out in a 5 volume % sulphuric acid solution. The solutions were maintained at a constant temperature of 30°C using the thermo-regulator throughout the test. Argon gas was used to purge and thereby de-aerate the electrolyte for at least one hour before specimen immersion. This purging continued until completion of the scan.

Specimens were immersed at least one hour before commencement of the scan to allow the corrosion potential, E_{corr}, to stabilise. All potentiodynamic plots were scanned from a cathodic potential of -500mV_{SCE} to an anodic potential of 1200mV_{SCE} while Tafel plots were scanned over a potential amplitude of 300mV_{SCE}. All scans were performed at a rate of 167μV/second. Section 3.7 describes the procedures carried out for pitting tests.

3.3.3 CALCULATION OF CORROSION RATES

Corrosion rates were calculated using the Stern-Geary equation[12,58,59]:

$$I_{corr} = \left[\frac{\beta_a \beta_c}{2.3(\beta_a + \beta_c)}\right]\frac{1}{R_p}$$

where I_{corr} = corrosion current density in mA/cm^2

βa = anodic Tafel slope in mV/decade of current

βc = cathodic Tafel slope in mV/decade of current

R_p = polarisation resistance in ohms

2.3 = natural log of 10

The values for β_a and β_c were obtained from the Tafel plots. These Tafel plots involved potentiodynamically polarising the alloys starting at a potential (overvoltage) of 150mV below E_{corr} and ending at a potential of 150mV above E_{corr}. In this procedure, the specimen is made to initially act as a cathode in the electrochemical cell containing the electrolyte and by increasing the applied potential in the more noble direction, the specimen is made to act as an anode. This yields a curve known as an Evans diagram as shown in Figure 3.4.

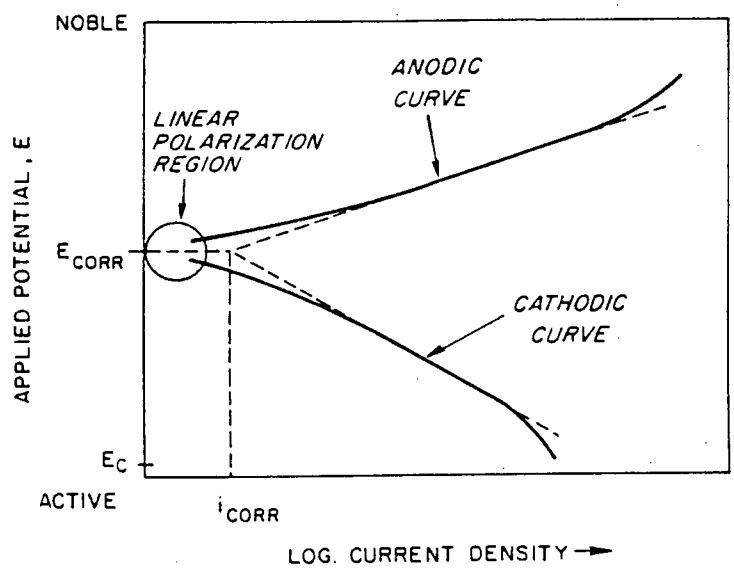

Figure 3.4 Evans diagram essentially used for determining corrosion rates[12]

Theoretically, both the anodic and cathodic potential-current density curves should be linear intersecting at a point corresponding to E_{corr} and I_{corr}. However, this is not the case as the measured curves deviate from linearity on approaching E_{corr}. The reason for this is thought to be the result of both anodic and cathodic sites developing on the specimen surface as the applied currents become increasingly small[12].

Despite this, both the measured cathodic and anodic potential-current density curves contain linear regions on a semilogarithmic plot within approximately 50mV of E_{corr}. These regions of linearity are referred to as Tafel regions and it is the slopes of these linear regions that yield values for β_a and β_c[33].

The value for polarisation resistance, R_p, is obtained from the slope of the potential-applied current curve (as opposed to the potential-current density curve) as shown in Figure 3.5. The slope of this curve at potentials within 10mV of E_{corr} (circled region in Figure 3.4) is approximately linear. This slope, $\Delta E/\Delta I$, has the units of resistance and represents the resistance, within the electrolyte, between the reference electrode and the polarised electrode (specimen).

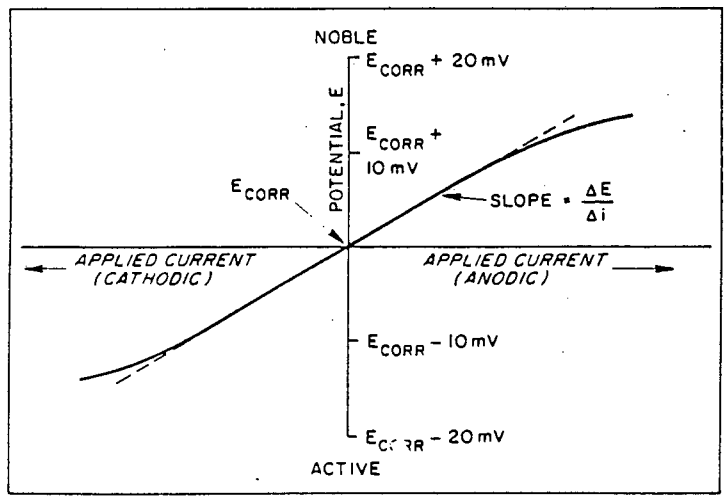

Figure 3.5 Measurement of linear polarisation resistance, R_p[12].

Once the values for β_a, β_c and R_p were obtained, I_{corr} could be calculated in mA/cm^2. To convert this corrosion current density to a corrosion rate in mmpy (millimetres per year), the following relationship was used:

$$mmpy = \frac{(3.3 \times mA/cm^2 \times E.W.)}{d}$$

where 3.3 = metric/time conversion factor

d = density of specimen in grams per cm^3

E.W. = equivalent weight in grams

This equation describes the corrosion rate of a pure metal which has a certain density and equivalent weight. Since stainless steels comprise a number of major alloying elements of differing equivalent weights, a computation must be made of the partial contributions of the various alloying elements. This computation is set out as follows:

$$E.W. = \Sigma \text{ ((volume element in alloy} \times \text{atomic mass)/valency)}$$

3.4 COMPRESSION TESTS

Compression tests were conducted for the section of tests that required all the alloys to have equal amounts of deformation-induced martensite. Since all alloys represent different austenite stabilities (determined by the copper content), each alloy needs to be deformed at a different temperature to achieve these equal martensite volume fractions. If the alloys were all deformed at room temperature, martensite volumes would increase from the lowest in 3Cu to the highest in 0Cu since the copper addition in 3Cu stabilises the austenite during deformation.

3.4.1 INSTRUMENTATION

Compression testing was carried out using an electro-servo hydraulic testing machine (ESH). This rig was used as it was able to facilitate a temperature bath. The rig as well as the temperature bath are shown in Figure 3.6 (a) and (b).

a.

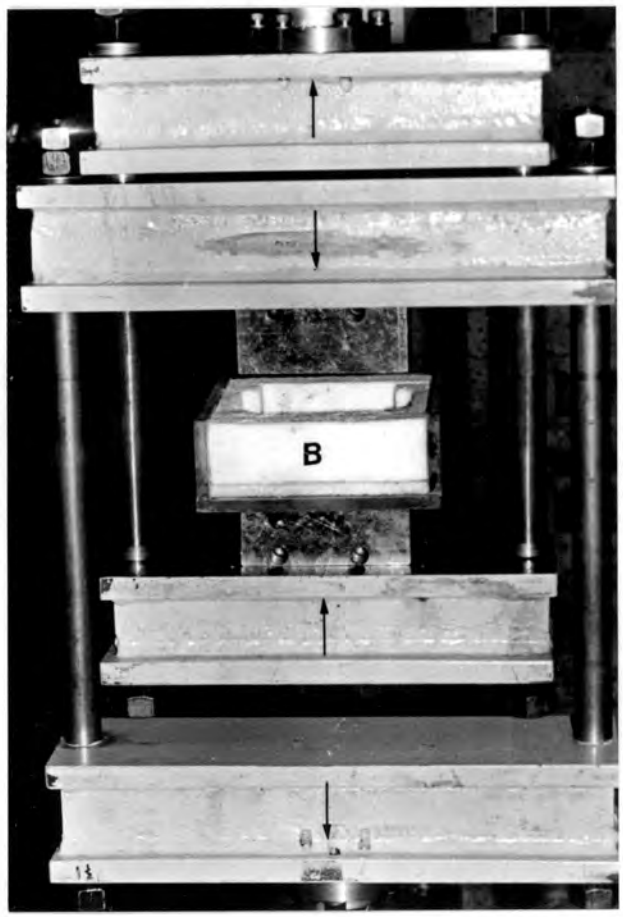

b.

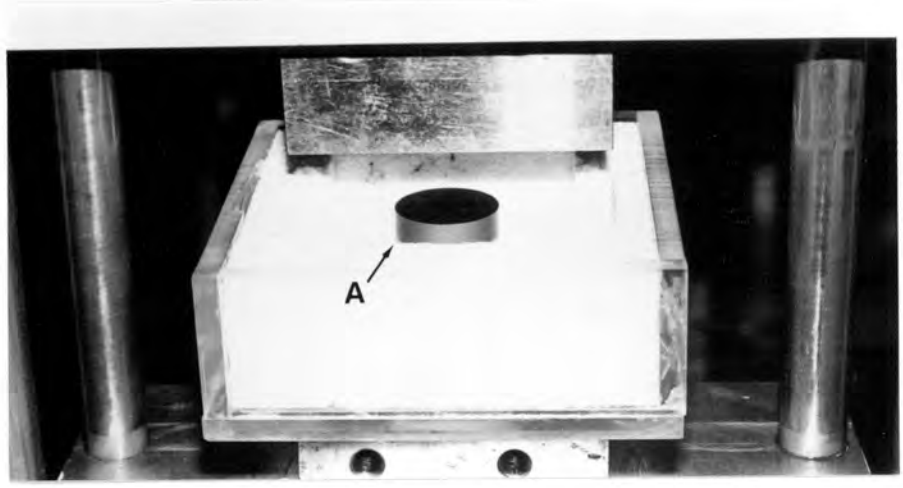

Figure 3.6 ESH Compression Rig

a. Overall view of compression rig with temperature bath (B). The arrows show the direction of movement of the components during testing.

b. Perspex temperature bath lined with polystyrene showing the hard metal anvil (A).

The bath is lined on the inside with an insulating polystyrene foam which helped maintain the required temperatures during the compression tests. Solutions of both hot water and alcohol containing dry ice were used to achieve the deformation temperatures. A hole was drilled at the base of the bath to accommodate one of the hard metal anvils. The specimen was held between this and another anvil. A spacer was made to fit around the circular specimen. This spacer had a thickness of exactly 5.6mm which did not allow the specimen to be strained to more than 30%.

3.4.2 COMPRESSION SPECIMENS

The dimensions of the compression specimens were carefully considered. The ESH test cell could safely withstand loads of up to 100kN. Thus a maximum diameter of 7mm was calculated taking into account the tensile strengths of these alloys. A larger diameter would mean a higher risk of rig failure, while a smaller diameter would result in insufficient surface area available for corrosion measurements. The thickness of the specimens were 8mm. Friction between the specimen and the anvils (resulting in barrelling) was largely reduced by the use of a molybdenum disulphide anti-scuff paste.

3.4.3 DETERMINATION OF DEFORMATION TEMPERATURES

A suitable martensite volume needed to be chosen which would yield representative corrosion results. 3Cu (containing the most copper and hence the most stable alloy) was compressed at temperatures between 0 and -70°C and the resultant martensite volume fractions were recorded. The results are graphed in Figure 3.7.

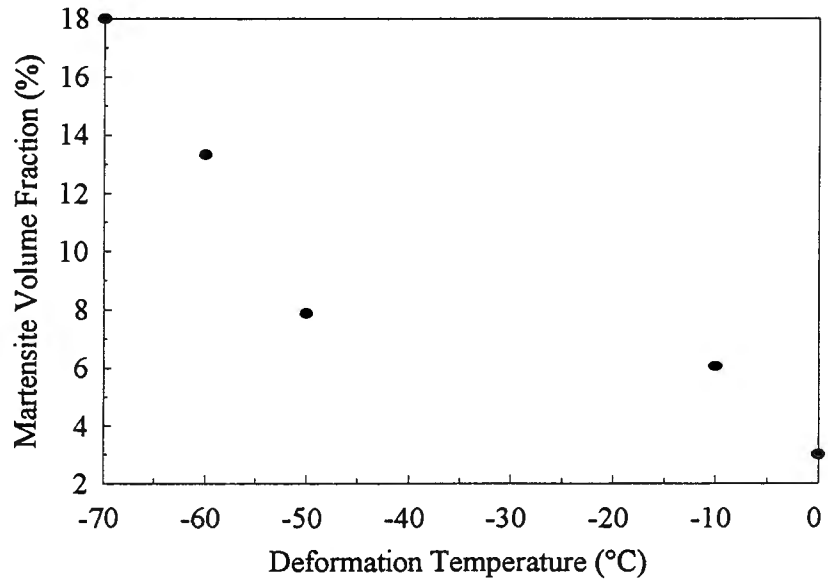

Figure 3.7 Martensite volume fraction vs. compression temperature for 3Cu

From this graph, a martensite content of ±20 volume % was chosen since this was the maximum martensite volume which formed in the most stable alloy at the lowest attainable temperature (approximately -70°C). An iterative process was used to determine the temperatures at which 0Cu and 1Cu would form a ±20% martensite volume. These temperatures were found to be 65-85°C for 0Cu and 15-25°C (room temperature) for 1Cu.

3.5 CORROSION SPECIMEN PREPARATION

3.5.1 SOLUTION TREATMENT

Solution treatment of all the alloys were carried out at 1050°C in a vacuum furnace under an argon atmosphere. The alloys were soaked at this temperature for 30 minutes and then quenched in water. All the alloys were subjected to this annealing process following the manufacture of the specimens. In the case of corrosion tests being carried out on specimens in the standard solution treated condition, specimens were machined into discs with a 15.7mm diameter. Following solution treatment, the discs were ground (starting first with 320 grit paper and finishing with 1200 grit) and finally polished using a 3μm diamond paste cloth.

3.5.2 ROLLING

Cold rolling was employed whenever the alloys needed to be deformed at room temperature i.e. whenever it was not necessary for equal martensite volume fractions. The rolling procedure involved first machining the alloys down to a thickness of 6mm. Following solution treatment, the plates were cold rolled to a 30% strain. After rolling, discs of 15.7mm were machined from the plate. Specimens were ground and polished (as described in Section 3.5.1) before corroding.

3.5.3 AGEING

All ageing procedures were carried out under an argon atmosphere at 700°C using the vacuum furnace. Following ageing, alloys were quenched in a water bath. Alloys tested in the solution treated and aged condition were aged for periods of 0.5, 3 and 10 hours while alloys in the solution treated and compressed condition were aged for 0.5 and 3 hour periods. Solution treated and rolled alloys were aged for 30 minute and 5 hour periods. Following ageing, all alloys were ground and polished.

3.5.4 COMPRESSED SPECIMENS

Following solution treatment, specimens (7mm diameter x 8mm thickness) were compressed to an equivalent 30% macro-strain. During compression, the friction between the specimen and the anvils results in the restriction of material deformation at either end of the specimen, despite the use of anti-friction paste. This means that the material strains differently at the ends of the specimen to the centre of the specimen. An experiment was conducted to determine how the martensite volume fraction (determined by XRD), indicative of the strain, varies along the length of the compressed specimen. Figure 3.8 shows the results of this experiment.

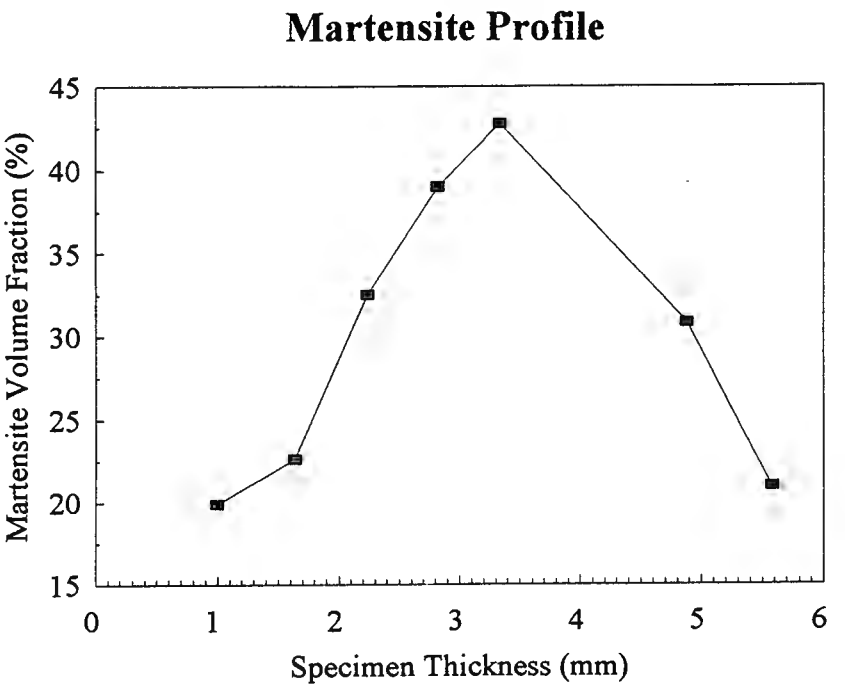

Figure 3.8 Variation of martensite volume fraction along the length of 0Cu compressed at room temperature

This graph shows that the martensite volume fraction is lowest at the ends of the compressed specimen and rises to a maximum in the centre of the specimen. This implies that the original applied macro-strain of 30% is not achieved uniformly along the specimen. Instead, there is a higher equivalent micro-strain (of unknown value but greater than 30%) in the centre of the specimen. It was assumed that the magnitude of the micro-strain found at the centre of the compressed specimens will be the same for all alloys. It is for this reason that, after compression, the test pieces were machined down to 2.8mm (half the length of the compressed specimen). All strains are still, however, quoted as 30% for simplicity.

The compressed discs (now ±8.4mm in diameter) were too small to fit in the conventional Teflon (PTFE) specimen holder which exposes a surface area of $1cm^2$ i.e. a diameter of 11.28mm. Specimens were therefore mounted in Pratley epoxy clear glue which offered the best adhesion to the specimen thereby preventing crevices from forming during corrosion. A hole was drilled through the side of the epoxy to facilitate the working electrode rod. These two specimen holders are shown in Figure 3.9.

Figure 3.9 Two specimen holders used for corrosion tests

a. Teflon holder (exposing a surface area of 1cm^2) used for all but the compressed specimens

b. Compressed specimen mounted in Pratley epoxy glue

Figure 3.10 shows a detailed schematic of the Teflon holder photographed in Figure 3.9 (a).

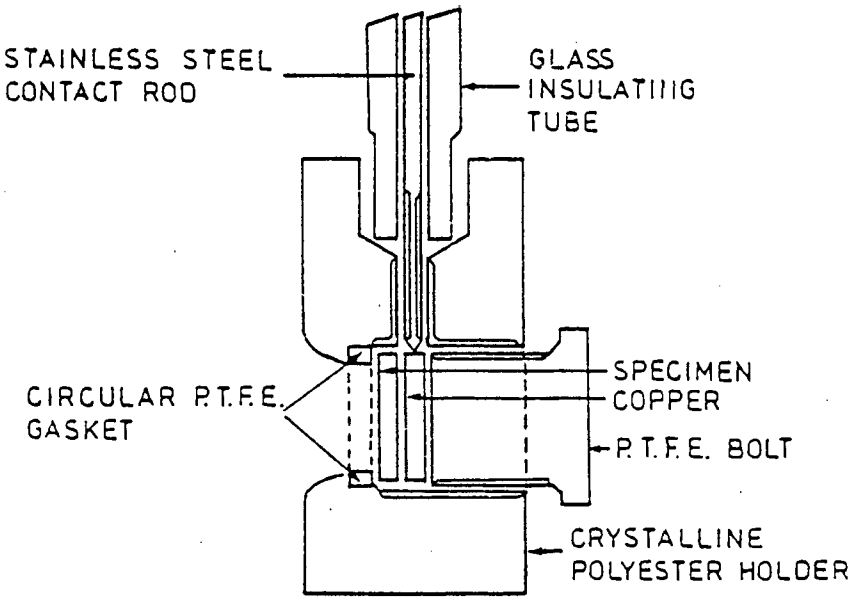

Figure 3.10 Schematic of Teflon holder showing detail of Teflon gasket[60]

All mounted compressed specimens were ground for 2 minutes first using 500 grit paper, then for 1 minute using 1200 and then 4000 grit paper. Polishing then took place for 2 minutes using a Struers OP-U suspension solution. Specimens were corroded after XRD analysis (to determine the deformation-induced martensite volume fraction). For the compressed and aged condition, corroded compressed specimens were broken out of the mould, ultrasonically cleaned, and then aged (either 0.5 or 3 hour periods). After ageing, the specimens were again mounted in Pratley epoxy glue and ground with 1200 grit paper for 30-60 seconds and then 4000 grit paper for 1 minute. Great care was taken to remove a minimal amount of surface material after ageing thereby maintaining the position of maximum strain (in the centre of the specimen). Polishing then took place for 2 minutes using the Struers suspension solution.

3.6 X-RAY DIFFRACTION

X-Ray diffraction techniques were used to determine martensite volume fraction. The complex morphology of martensite does not allow for easy measurement of its volume fraction by light microscopy. Martensite laths occur in sheaves or elongated clusters and are too small to be resolved individually. As a result, optical microscopy indicates greater amounts of strain-induced martensite than actually exists[61]. X-Ray diffraction is potentially the most accurate method for quantitative detection of martensite.

3.6.1 CALCULATION OF MARTENSITE VOLUME FRACTION

The X-ray intensity diffracted from each crystal phase is proportional to the volume fraction of that phase present. X-Ray diffraction results in a trace of reflected intensity against 2θ (where θ is the Bragg angle). The Bragg angle is related to the interplanar spacing of the crystal by Bragg's Law[62]:

$$n\lambda = 2d\sin\theta \qquad \text{eqn. 3.1}$$

where $n = 1, 2, 3...$

λ = X-ray wavelength

d = interplanar spacing

θ = angle between the atomic plane and the X-ray beam

The X-ray intensity (measured from the heights on the X-ray plot) of each phase is not proportional to the integrated peak area (which is proportional to the phase volume fraction). The volume fraction of each phase is therefore calculated using the area under the peak, rather than the peak height.

For microstructures consisting essentially of austenite and martensite, the ratio of the volume fraction of austenite (V_γ) and martensite ($V_{\alpha'}$) can be written as:

$$V_\gamma / V_{\alpha'} = I_\gamma^{hkl} R_{\alpha'}^{hkl} / I_{\alpha'}^{hkl} R_\gamma^{hkl} = S \qquad \text{eqn. 3.2}$$

I_{hkl} is the integrated intensity of a particular hkl reflection in a phase while R_{hkl} is a factor depending on the specimen crystal structure, the reflecting set of planes and θ.

If $V_\gamma + V_{\alpha'} \approx 1$ (provided that the volume contributed by carbides and/or nitrides is very small) then:

$$V_{\alpha'} = 1 / [1 + S] \text{ and } V_\gamma = S / [1 + S] \qquad \text{eqns. 3.3}$$

Diffraction line broadening usually occurs and the intensity of an X-ray at a particular Bragg angle follows a Gaussian distribution. The area under the peak was thus calculated using a programme called XPROC which uses two different techniques: first, it fits a straight line through the left and right backgrounds and secondly it fits a polynomial. Two integrated areas under the peak are thus obtained which are then averaged to give the integrated intensity (I_{hkl}) corrected for the background

R_{hkl} can be calculated from basic principles and a list of these values are given in Table 3.3.

Peak	**Bragg Angle**		$\mathbf{R_{hkl}}$
	θ	2θ	
$200_{\alpha'}$	32.5	65	32
$211_{\alpha'}$	41.2	82.4	61
$310_{\alpha'}$	58.0	116.0	19
200_{γ}	25.4	50.8	82
220_{γ}	37.3	74.6	44
311_{γ}	45.5	91.0	51

Table 3.3 Bragg angles and R-factors of three austenite (γ) and martensite (α′) peaks used for CuKα radiation[63]

These R-factors, together with the I_{hkl} values for each reflection were then substituted into eqn. 3.2 to obtain **S**, which was then used in eqns. 3.3 to obtain the martensite volume fraction.

3.6.2 XRD INSTRUMENT SETTINGS

Data was collected using a computer-interfaced Phillips X-Ray Diffractometry (XRD) machine. A copper (CuKα) tube was used for radiation. Although this source of radiation only reaches a penetration depth of 2μm in stainless steel[63], it was found to be adequate for this work. A voltage of 40kV and current of 25mV were the optimum settings for this tube. An investigation into the count time and degree interval found a 10 second time and a 0.05° interval to be adequate. Samples were scanned over a range of 2θ from 62° to 93°.

Due to practical limitations such as peak overlap making some peaks difficult to resolve and also time constraints, it was decided to use only two peaks for each of the martensite and the austenite phases. Although the final analysis is more accurate when as many peaks as possible are included for each phase, work has shown that if only the 220_γ and 311_γ peaks are used for the austenite phase, the analysis yields virtually the same results as for the analysis using three peaks for this phase[37]. Due to difficulty in resolving peak overlap between $310_{\alpha'}$ (θ_{Cu} = 58.0°) and 400_γ (θ_{Cu} = 59.3°) it was decided to use only the $200_{\alpha'}$ and $211_{\alpha'}$ peaks for the martensite phase. Figure 3.11 shows a typical XRD trace obtained for 1Cu compressed at room temperature. The austenite and martensite peaks used in the calculation of martensite volume fraction are clearly shown.

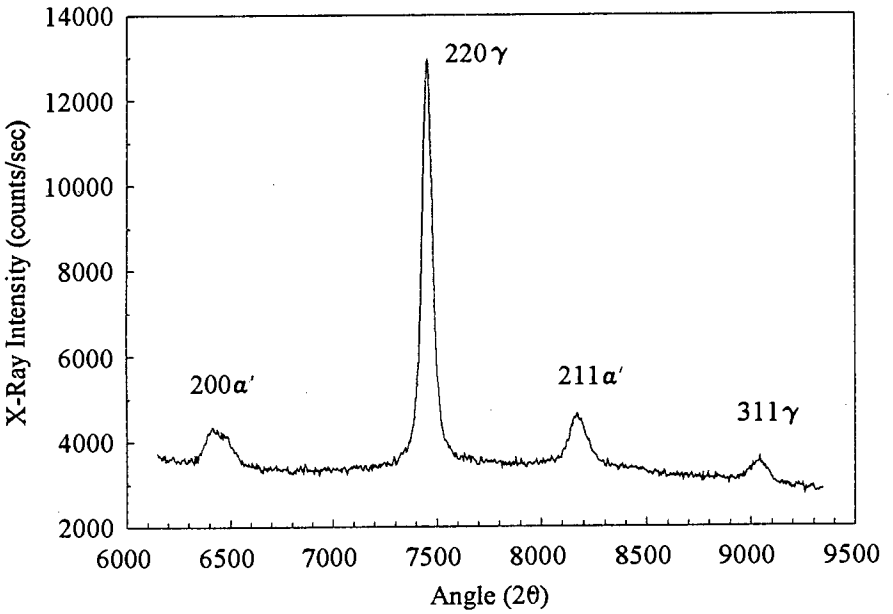

Figure 3.11 XRD trace for 1Cu compressed at room temperature.

3.7 PITTING TESTS

Pitting tests were conducted by cyclic polarisation first in a salt water solution (3.5 wt% NaCl) as well as solutions containing 100, 200, 500 and 1000ppm of chloride. Examination of all the specimens following these tests showed severe evidence of crevice corrosion while there was no evidence of pit formation.

Pitting tests thus posed a problem in this project as it was very difficult to eliminate the problem of crevice corrosion. This crevice corrosion occurs at the interface between the metal surface under study and the insulating material used to isolate part of the test specimen from the surrounding halide solution. Any small flaw at this interface results in a depletion of oxygen and localised corrosion starts in this region. The occurrence of crevice corrosion leads to an artificially low and inconsistent value of "pitting" potential in a series of measurements on a given alloy as well as incorrect ranking of different alloys[64,65].

The problem in the initial tests lay in the integrity of the seal of the mounting technique. The Teflon (PTFE) specimen holder (shown in Figure 3.9 (a)) was used in these initial tests. This technique involves having a circular Teflon gasket being pushed up against the specimen surface as shown in Figure 3.10. If this gasket is not perfectly smooth or if it is over tightened so that it bulges, crevices are formed leading to localised corrosion.

Specimens were then mounted using the technique shown in Figure 3.9 (b) using Pratley epoxy glue. This technique was also not successful due to the integrity of the adhesion of the glue to the specimen as well as the porosity of the glue.

Pawel *et al*[64,65] acknowledged the problem of crevice corrosion during pitting tests. They tried a technique whereby the samples, following mounting and metallographic surface preparation, were prepassivated in 50 volume % nitric acid (mixed with water) for 30 minutes at 50°C. The metal/epoxy interface was then covered with an enamel which was painted on with a fine brush. Immediately before testing, provided the enamel had dried, the exposed surface area of the sample was lightly repolished with a cotton swab using 1μm diamond paste to remove the passive film from the surface, but allowing the passive film to remain under the enamel. This technique proved to be successful for Pawel *et al* for pitting tests in 1*N* sulphuric acid with 0.5M NaCl at 27°C.

This technique was tried in this study, except the samples were mounted using a cold resin and instead of the enamel, Pratley epoxy glue was used to paint over the metal/resin interface. A 500ppm de-aerated chloride solution was used at 30°C. The cyclic pitting scans were started at 50mV below E_{corr} and were reversed when the current reached 1mA/cm^2.

CHAPTER 4
RESULTS AND DISCUSSION

4.1 PRELIMINARY WORK

Previous corrosion tests had been carried out on alloys similar in composition to those used in this experimental programme[2]. These tests were initiated after it was found that alloys containing reduced nickel levels (5.4 wt%) and nitrogen additions between 0.2-0.25 wt%, cracked a few hours following deep drawing[1]. This was found to be due to the nitrogen having an embrittling effect on the martensite formed during the deep drawing process. To overcome this, it was suggested that the martensite be softened by a post-forming stress relieving heat treatment. On the other hand, delayed cracking is prevented when copper is added to these alloys. It is to this end that tests were carried out to determine the effect of both tempering and copper additions on the corrosion resistance of these alloys. These tests included determining the corrosion rates of the alloys in

a. the solution treated condition and
b. the solution treated, deformed (30% cold rolled) and aged condition.

The initial stages of this experimental programme involved reproducing the results obtained in the preliminary work using the present alloys. The tests reproduced involved determining the corrosion rates of the alloys in the two microstructural conditions mentioned in (a) and (b) above. The results of the corrosion tests performed in de-aerated 5 volume % sulphuric acid for the alloys in the solution treated only condition (a) are shown in Figure 4.1

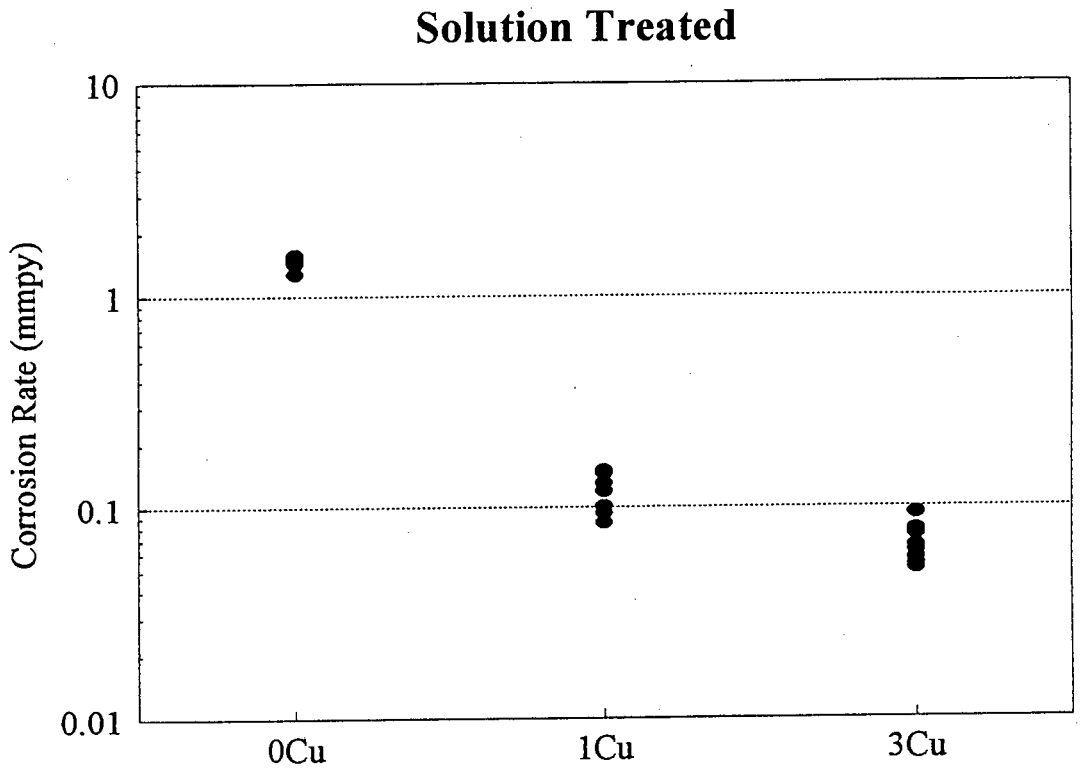

Figure 4.1 Corrosion rates of the experimental alloys in 5 volume % de-aerated sulphuric acid at 30°C for the solution treated condition.

These results show that there is a clear decrease in corrosion rate from 0Cu to 3Cu indicating that the corrosion rate decreases with an increase in copper content. This could suggest that either copper decreases the dissolution rates of these alloys or that 0Cu, being the least stable alloy, forms that much more residual martensite during metallographic preparation to raise the corrosion rates above those of 1Cu and 3Cu. An XRD analysis of the alloy surfaces following metallographic preparation in the solution treated condition revealed martensite contents of approximately 8, 3 and 1% for 0Cu, 1Cu and 3Cu respectively. Martensite, being a high energy phase, is expected to corrode preferentially to austenite.

The corrosion rates for the solution treated, deformed and aged condition (b) are graphed in Figure 4.2 and the values are given in Table 4.1. Deformation was achieved by cold rolling all the alloys at room temperature to a 30% strain. Subsequent ageing was carried out under an argon atmosphere at 700°C for 0.5 and 5 hour periods. This was an attempt to determine what effect the post-forming stress relieving heat treatment would have on the corrosion properties of the alloys, especially 0Cu.

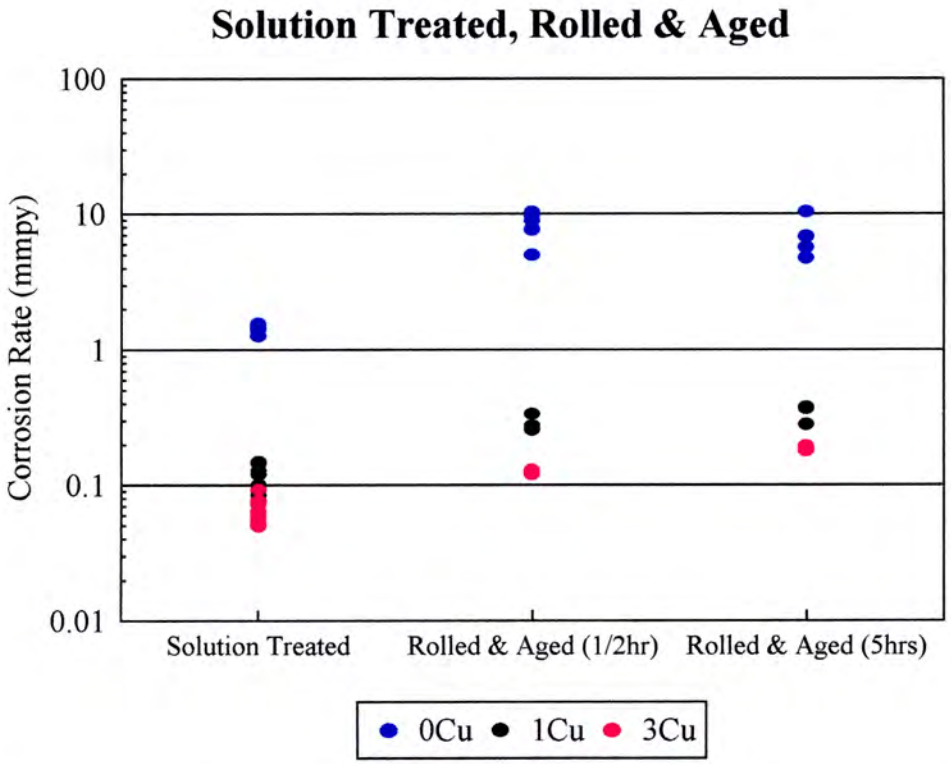

Figure 4.2 Corrosion rates of the experimental alloys in de-aerated 5 volume % sulphuric acid for the solution treated, rolled and aged condition

ALLOY	CORROSION RATE (mmpy)		
	Solution Treated	**Solution Treated, Rolled & Aged (1/2 hr)**	**Solution Treated, Rolled & Aged (5hrs)**
0Cu	1.42	7.70	7.66
1Cu	0.12	0.29	0.33
3Cu	0.06	0.12	0.19

Table 4.1 Corrosion rate values (mm per year) in 5 volume % sulphuric acid for both the solution treated condition and the solution treated, rolled and aged condition.

The corrosion rates given in the table were obtained by taking the median of the values shown on the scatter graph i.e. the average of the highest and lowest point. It is clear that following deformation and ageing, the relatively poor corrosion performance of 0Cu is exacerbated. The corrosion rates for 1Cu and 3Cu following deformation and ageing have also increased relative to the solution treated only condition, although these corrosion rates are still very low compared to 0Cu. From the values shown in Table 4.1, the amount of increase in corrosion rate from the solution treated only condition to the solution treated, rolled and aged (1/2 hr) condition is approximately a factor of 5.42, 2.42 and 2.00 for 0Cu, 1Cu and 3Cu respectively. The addition of copper could therefore be important for two reasons:

a. Copper reduces the anodic dissolution rate and
b. Copper increases the stability of the austenite during deformation.

The appropriate addition of copper to metastable austenitic stainless steels thus appears beneficial in that it improves both the corrosion properties in de-aerated sulphuric acid and prevents delayed cracking after deep drawing.

The results of the preliminary work cannot be fully explained in that a number of overlapping variables occur. In the first instance, the influence of copper on the anodic dissolution in the solution treated condition is plausible (despite small variations in residual martensite volumes formed during metallographic preparation) and these results seem to agree with the reported literature for austenitic stainless steel. Secondly, the role of copper on the dissolution properties after deformation and ageing is not clear since an additional variant in the form of martensite volume fraction is introduced. Martensite volumes of approximately 33, 20 and 3% were present in 0Cu, 1Cu and 3Cu respectively following 30% cold rolling. The martensite formed during deformation is expected to affect both the energy state of the alloy as well as precipitation during ageing. So the following questions are posed regarding the relatively poor corrosion performance of 0Cu following deformation and ageing:

i. Is this due to more rapid precipitation (leading to sensitisation) associated with the increase in martensite formed during deformation, OR
ii. The higher martensite volume fraction leads to preferential attack due to its high energy state, OR
iii. The copper additions in 1Cu and 3Cu could markedly retard the precipitation kinetics due to its stabilising effect on the austenite and thereby hinder the sensitisation phenomenon.

Of course it is most likely a combination of all three possibilities, but the relative contributions need to be ascertained.

It is expected that if the martensite content of an austenitic steel is increased, the tendency to enhanced anodic dissolution increases. Martensite is a highly dislocated, high energy phase and is expected to corrode preferentially to the more corrosion resistant austenite phase. What is not known is:

Does copper influence the dissolution rate of martensite?

Does copper influence precipitation kinetics during ageing or does it influence the sensitisation of martensite in any way?

In order to answer these questions and to try and explain the results obtained in the preliminary work, further corrosion tests were carried out on all the alloys in the following conditions:

1. Solution treated and aged only
2. Solution treated and rolled only
3. Solution treated and deformed (at controlled temperatures so that an equal martensite volume fraction is achieved amongst all three alloys)
4. Solution treated, deformed (with equal martensite volume fractions) and subsequently aged

4.2 SOLUTION TREATED AND AGED ONLY

This first set of tests were performed in order to determine, for the given alloy compositions, the influence of ageing following solution treatment on the corrosion properties. More particularly, this is an attempt to establish the influence of copper on the precipitation kinetics, and hence sensitisation of the alloys during ageing.

4.2.1 OPTICAL MICROSCOPY

Before the corrosion tests were performed, the microstructures were examined following solution treatment at 1050°C for 30 minutes and ageing at 700°C for 0.5 hour, 3 and 10 hours. These micrographs are shown in Figures 4.3 to 4.5.

a. b.

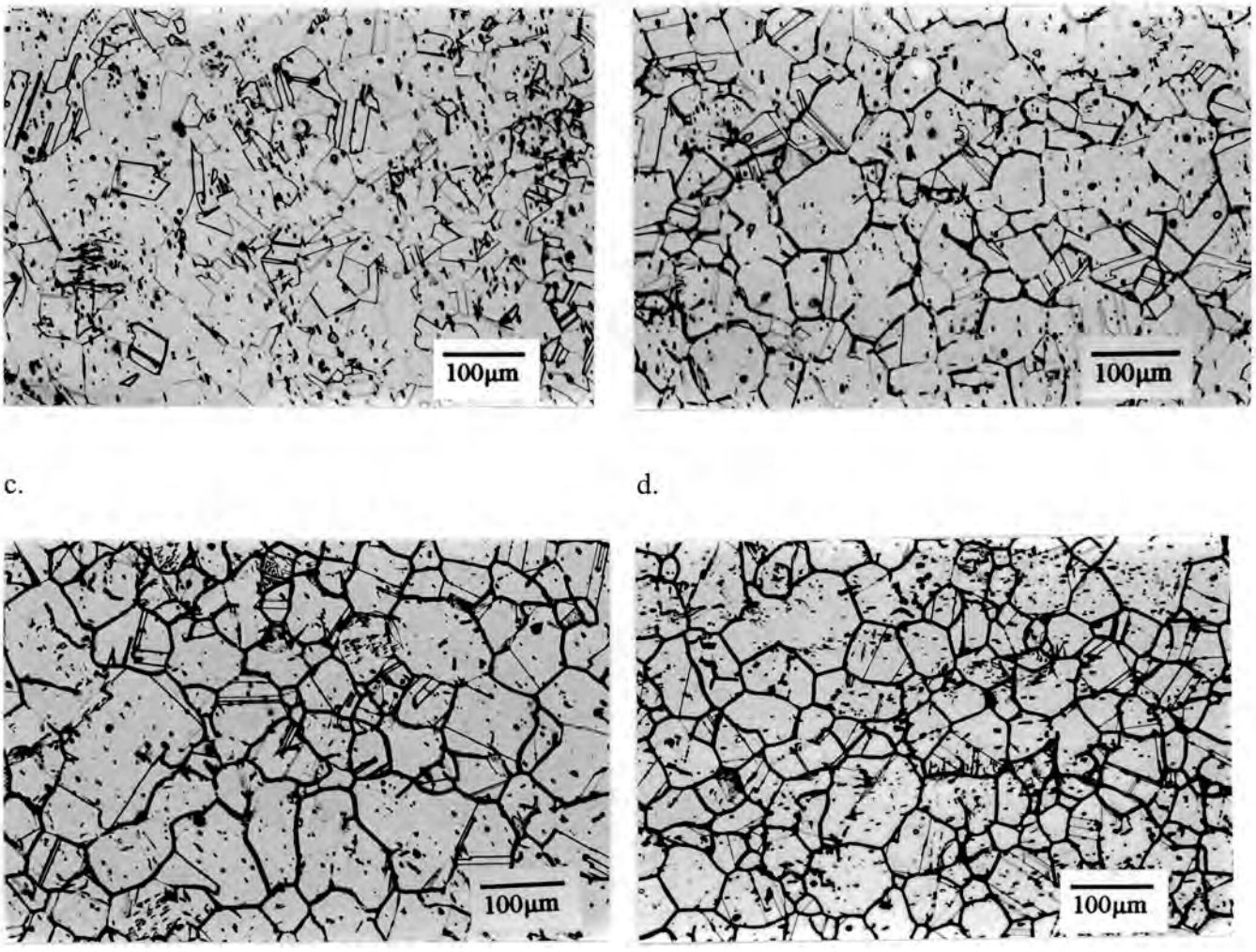

c. d.

Figure 4.3 Optical micrograph showing microstructure of 0Cu

a. Solution Treated

b. Solution Treated and Aged (1/2 hour)

c. Solution Treated and Aged (3 hours)

d. Solution Treated and Aged (10 hours)

a.

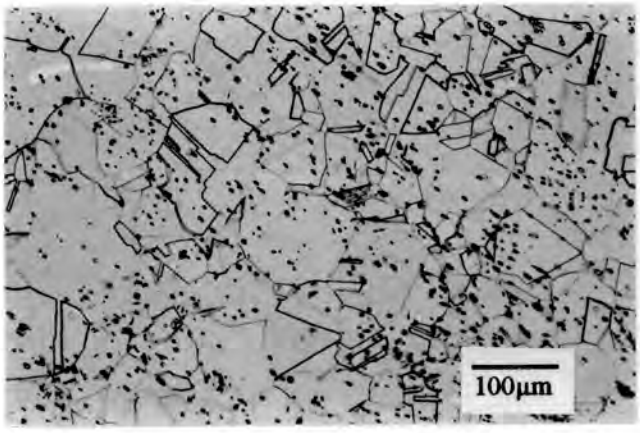

b.

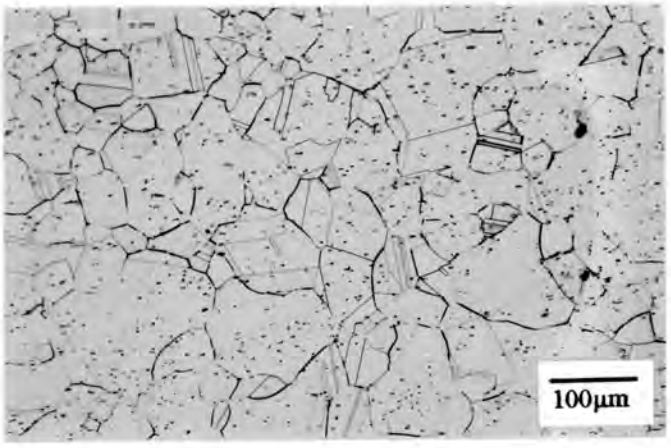

c.

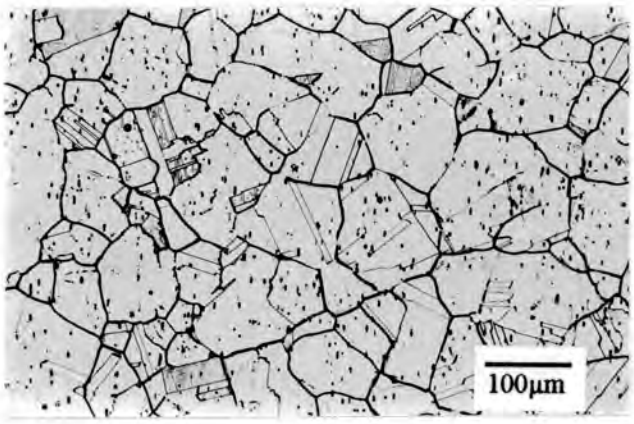

d.

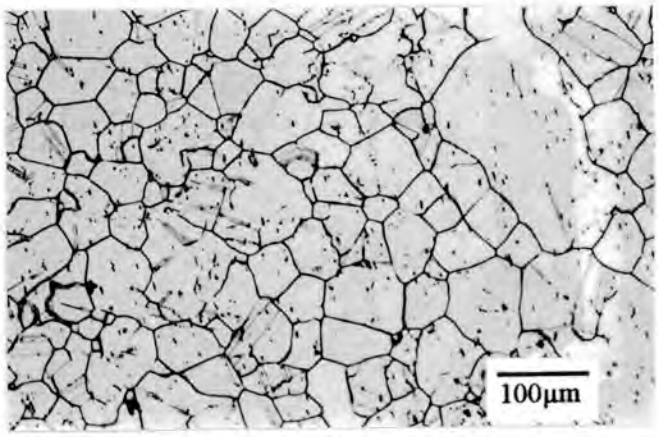

Figure 4.4 Optical micrograph showing microstructure of 1Cu

a. Solution Treated

b. Solution Treated and Aged (1/2 hour)

c. Solution Treated and Aged (3 hours)

d. Solution Treated and Aged (10 hours)

a.

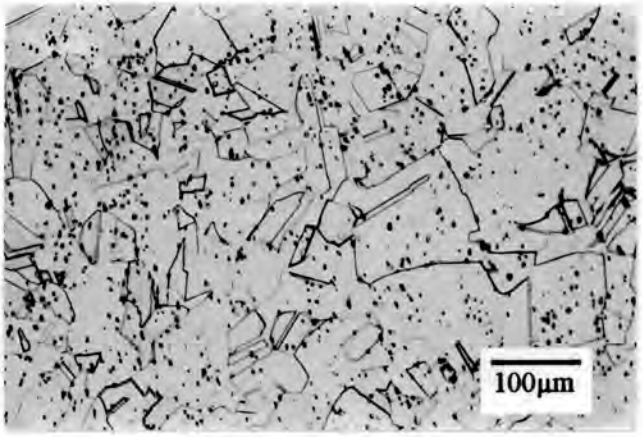

b.

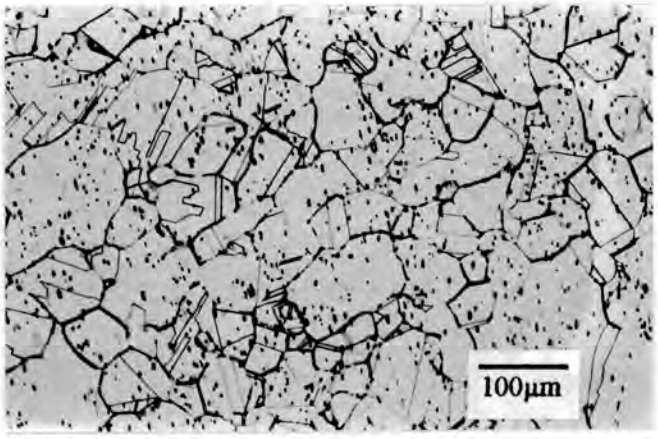

c.

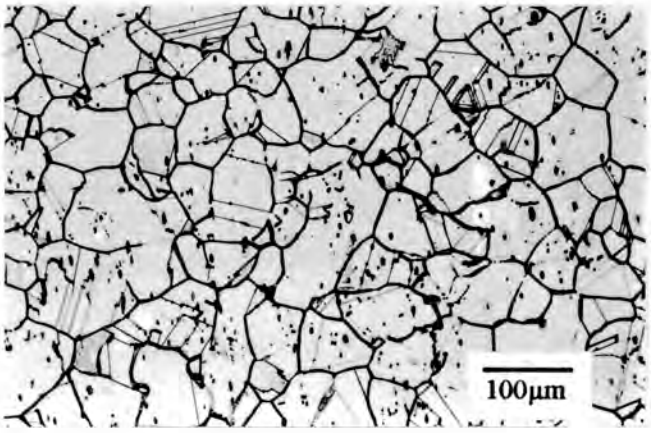

d.

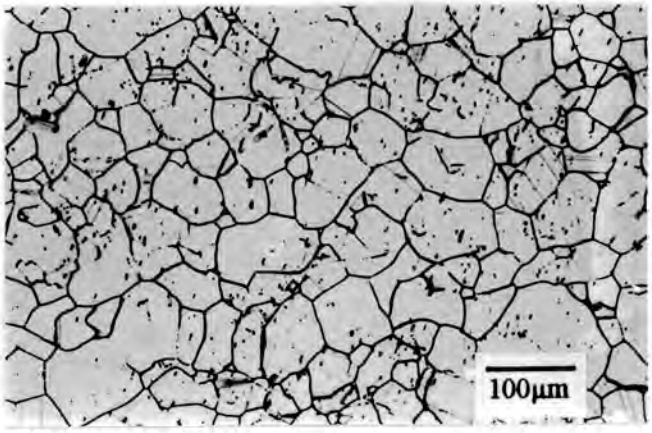

Figure 4.5 Optical micrograph showing microstructure of 3Cu

a. Solution Treated

b. Solution Treated and Aged (1/2 hour)

c. Solution Treated and Aged (3 hours)

d. Solution Treated and Aged (10 hours)

The micrographs of the three alloys in the solution treated condition all show very similar microstructures. This microstructure consists essentially of austenite. The microstructures also seem to be polluted with oxides. These are assumed to be oxides and not ferrite as the latter is not expected to form at 1050°C in these alloys. There is also evidence of the usual annealing twins amongst all three alloys.

Following ageing, there appears to be some sort of precipitation occurring along the grain boundaries of the alloys. The actual precipitates are not visible using the bright field mode but show up as areas where the etchant has attacked preferentially (i.e. at the carbide/austenite interface). So the grain boundaries appear as black lines after ageing and since the alloys were all etched for the same times, it can be assumed that the thicker these grain boundaries appear, the more precipitation has occurred. It can therefore be said that after long ageing periods (10 hours), there is more precipitation occurring than there is after 0.5 hours. This trend is picked up for all three alloys but is particularly evident in 0Cu.

Examination of the micrographs for the aged (10 hours) condition shows that 0Cu has considerably more precipitation occurring along the grain boundaries relative to 1Cu and 3Cu, which both show similar degrees of precipitation. This could suggest that copper retards precipitation kinetics in 1Cu and 3Cu. The lack of copper in 0Cu could thus be the reason for the relatively large degree of grain boundary precipitation after ageing for 10 hours. This could also be due to the fact that 0Cu contains 0.02 wt% more carbon than the other two alloys. Since carbon has an affinity for chromium, this could lead to enhanced precipitation of chromium carbides.

4.2.2 CORROSION RESULTS

The results of the corrosion tests for the alloys in the solution treated and aged (0.5, 3 and 10 hours) are graphed in Figure 4.6. The solution treated only condition is represented by an ageing time of 0 hours.

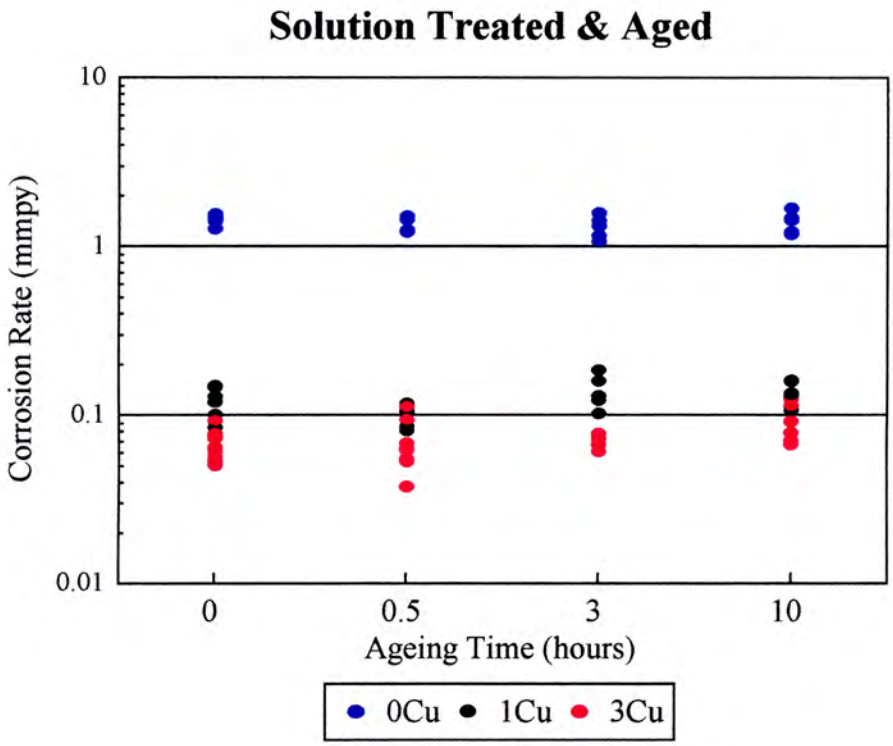

Figure 4.6 Corrosion rates of the experimental alloys in de-aerated 5 volume % sulphuric acid at 30°C for the solution treated and aged condition

These results surprisingly show that there is very little difference in the corrosion rates between the solution treated condition and the aged condition. It is expected that ageing results in sensitisation due to precipitation of chromium carbides or chromium carbo-nitrides along the grain boundaries and that this would lead to higher corrosion rates in the aged condition relative to the solution treated only condition. However, this does not seem to be evident looking at the values graphed in Figure 4.6.

It was also noted that for all three alloys, the corrosion rates do not increase with longer ageing times. This suggests that copper may not have an influence on precipitation kinetics leading to sensitisation of these alloys. Figure 4.6 implies that the relatively severe grain boundary dissolution (presumably caused by sensitisation associated with precipitation) shown in the optical micrographs for 0Cu in the aged (10 hours) condition, does not seem to have an effect on the corrosion rate. One would expect that if copper did in fact retard precipitation kinetics leading to sensitisation, there would at least be an increase in corrosion rate from the 1/2 hour aged condition to the 10 hour aged condition in 0Cu. This, however, is also not evident in the corrosion results.

It is still evident though that 0Cu displays consistently higher corrosion rates than the other two copper containing alloys and that 3Cu offers the most corrosion resistance.

4.2.3 SCANNING ELECTRON MICROSCOPY

The SEM micrographs shown in Figures 4.7 to 4.9 were obtained after stopping the potentiodynamic scans at $1200mV_{SCE}$.

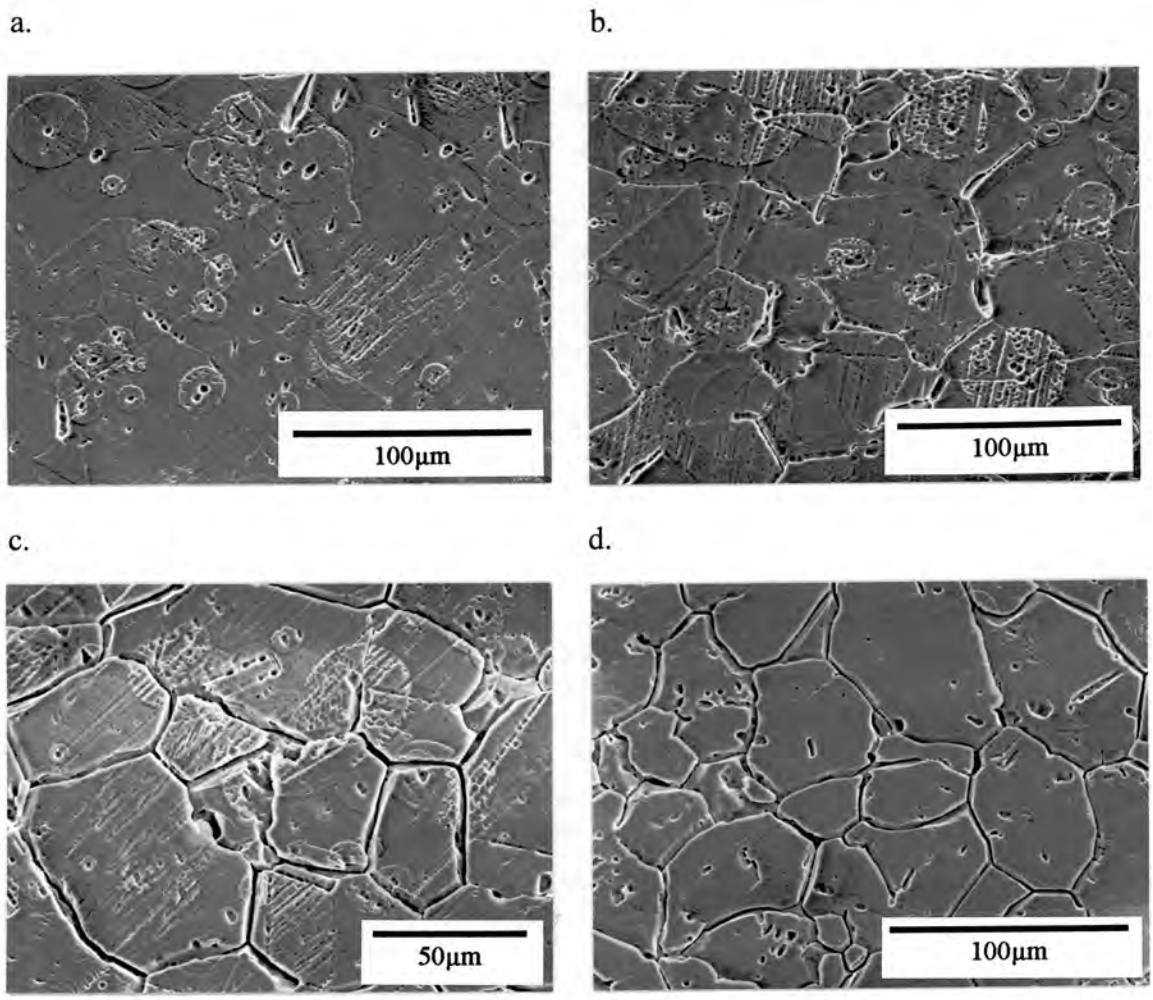

Figure 4.7 SEM micrograph of 0Cu showing corrosion damage

a. Solution Treated

b. Solution Treated and Aged (1/2 hour)

c. Solution Treated and Aged (3 hours)

d. Solution Treated and Aged (10 hours)

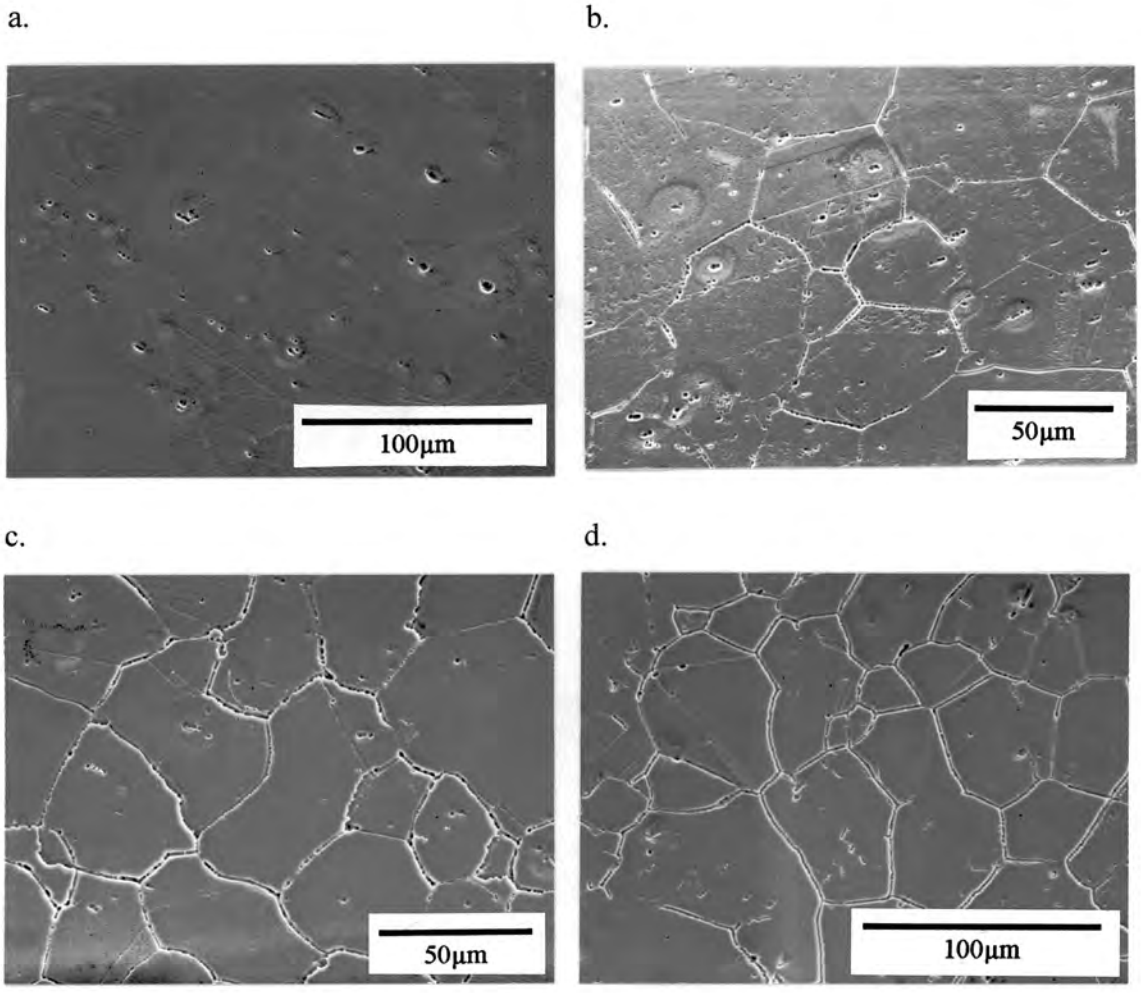

Figure 4.8 SEM micrograph of 1Cu showing corrosion damage

a. Solution Treated

b. Solution Treated and Aged (1/2 hour)

c. Solution Treated and Aged (3 hours)

d. Solution Treated and Aged (10 hours)

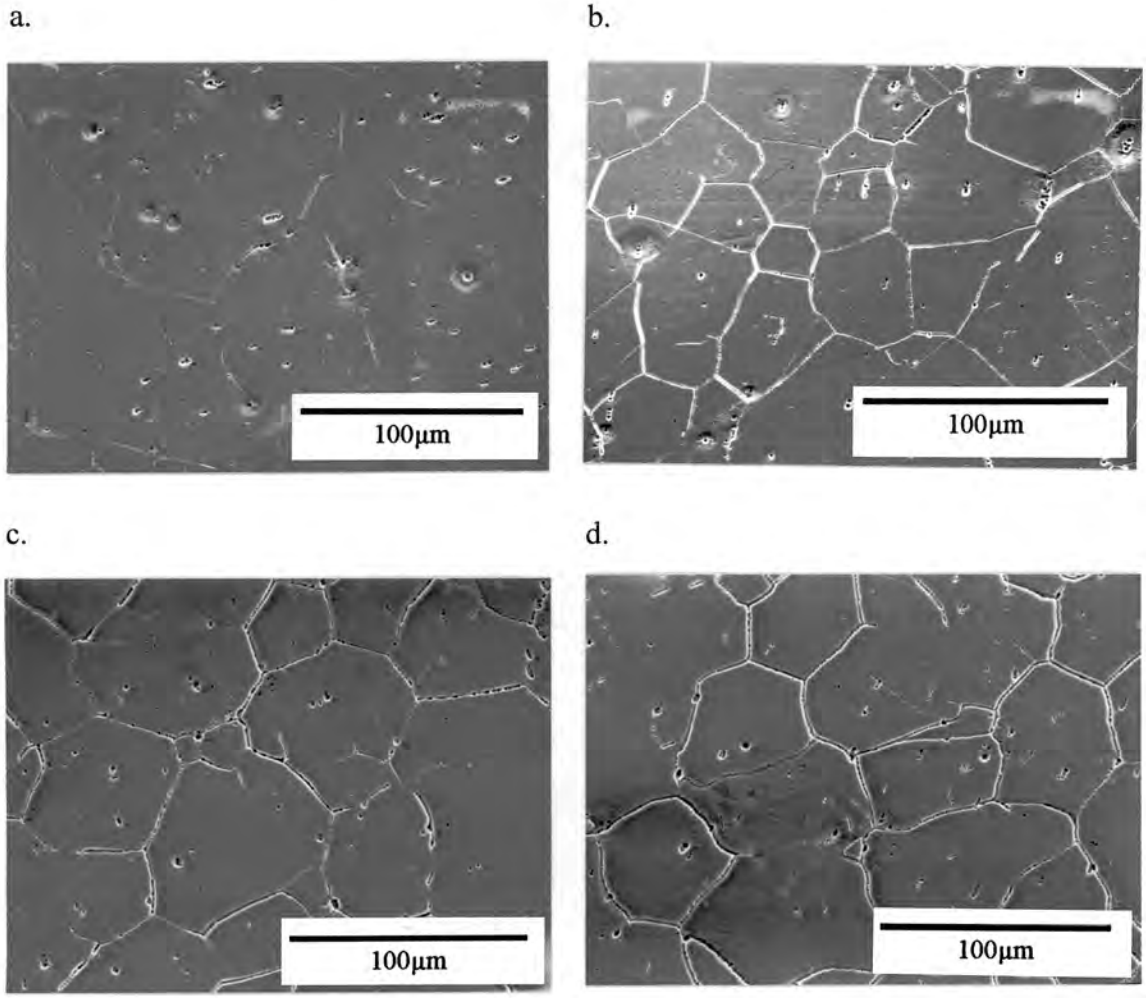

Figure 4.9 SEM micrograph of 3Cu showing corrosion damage

a. Solution Treated

b. Solution Treated and Aged (1/2 hour)

c. Solution Treated and Aged (3 hours)

d. Solution Treated and Aged (10 hours)

Once again, as for the optical micrographs, there is a noticeable increase in the amount of grain boundary attack as the alloys are aged from 0.5 to 10 hours. No grain boundary attack is evident in the solution treated condition for any of the three alloys. 0Cu shows the most general (uniform) corrosive attack in the solution treated condition while 3Cu shows the least.

The grain boundary attack which is evident after ageing suggests that these alloys have indeed been sensitised. This sensitisation phenomenon seems consistently most severe in 0Cu. Sensitisation occurs when precipitates (chromium carbides or -carbo-nitrides) form along the grain boundaries during ageing. These precipitates are rich in chromium which has diffused from the areas immediately adjacent to the grain boundaries. The percentage of chromium in these adjacent areas drops significantly so that there is a chromium differential between the grain boundary region and the internal grain area. This differential in chromium means that during corrosion, the grain boundary region (representing the low chromium region) forms a less protective passive layer and becomes the anode which corrodes preferentially and locally. The internal grain area forms a more stable passive layer (due to the higher chromium levels) and is thus protected from corrosive attack. As ageing time increases, more chromium is taken up around the precipitates and these precipitates grow. This results in a higher chromium differential leading to broader and deeper bands being sensitised along the grain boundaries. Eventually, after long ageing times, precipitate growth would cease as the chromium has combined with all the available carbon (and perhaps nitrogen) at the grain boundaries. This means that the chromium would now have sufficient time and energy, at the ageing temperature, to diffuse from the areas of high concentration (deep within the grain area) to those of low concentration and thereby reduce the chromium differential. This results in a reduced sensitisation effect and is known as self-healing. This self-healing phenomenon was not, however, noticed for these experimental alloys aged for up to 10 hours.

The question still, however, remains why there is no increase in actual corrosion rates with ageing time, despite the increase in intergranular corrosion with ageing time for all the alloys (which is evident in Figure 4.7 to 4.9).

It was noticed that for all the alloys in the solution treated condition, general corrosion seems the obvious mode of attack i.e. the surface is attacked uniformly. However, following ageing, the uniform corrosion ceases to be the dominant mode of attack and the more severe localised intergranular corrosion prevails. This makes sense because as soon as grain boundary attack is initiated, an autocatalytic reaction occurs whereby the high energy grain boundaries take the role of the anode in the corrosion reaction while the matrix material becomes the cathode.

As corrosion proceeds, intergranular attack accelerates while the regions within the grains are effectively cathodically protected. This is a typical phenomenon associated with localised corrosion. Hence, as is evident in the SEM micrographs, there is a decrease in uniform attack while there is an increase in localised grain boundary attack as the ageing time increases.

The above finding could explain the reason why there is no noticeable increase in corrosion rate with increasing ageing times. In the solution treated only condition, there is a uniform removal of material from the entire surface area whereas, after ageing for 10 hours, the material is lost only from the grain boundaries; not uniformly from the matrix. Although the latter loss seems quite severe, the amount of localised material lost is probably the same as that lost uniformly in the solution treated condition. Since the unit of corrosion rate in Figure 4.6 is mm per year, which represents the thickness of the layer of material lost uniformly from a surface, this may explain the similar corrosion rates between the solution treated and aged (0.5, 3 and 10 hour) conditions. The above explanation, therefore, seems to indicate that the polarisation tests conducted are not a suitable method for determining the influence of sensitisation on corrosion rates. It was later discovered that Betrabet *et al*[55] used a technique known as the electrochemical potentiokinetic reactivation (EPR) technique which provides a quantitative electrochemical measurement of sensitisation. This technique is described as follows:

The specimen is immersed in a solution of de-aerated 0.5M $NaSO_4$ + 0.01M KSCN at 30°C. The specimen is then anodically polarised from the rest potential (E_{corr}) into the passive region ($200mV_{SCE}$) at a voltage scan rate of 100mV/min. The potential is then scanned (at the same rate) in the reverse direction (reactivation scan) down to E_{corr}. The resultant curve is illustrated in Figure 4.10. The reactivation polarisation causes breakdown of the passive film at sensitised regions in which chromium depletion has occurred. The maximum anodic current (I_a) and the maximum reactivation current (I_r) is measured from the anodic and reactivation curves respectively. The reactivation ratio, R_a, which is the parameter used to quantify the degree of sensitisation (DOS), is the ratio of the maximum reactivation current to the maximum anodic current (see Figure 4.10).

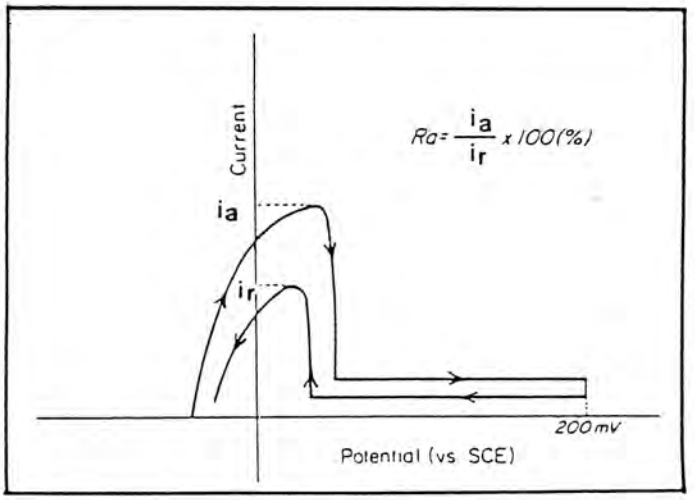

Figure 4.10 Definition of the reactivation ratio (R_a) in the EPR technique[55]

Due to time constraints, this technique was not conducted.

The SEM micrograph of 0Cu in Figure 4.7 (a) showed several raised circular features which seem to form predominantly around holes. It is not completely clear what these features represent. The SEM micrograph in Figure 4.11 shows a close-up of one of these circles with an inclusion situated in the centre.

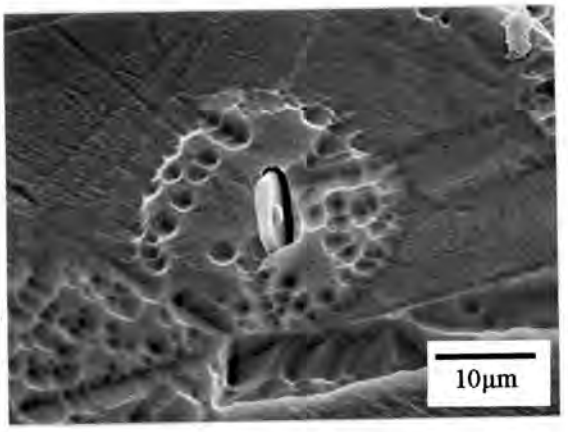

Figure 4.11 SEM micrograph of Cr rich inclusion found in the centre of the circular features noticed predominantly on 0Cu's surface following corrosion in the solution treated condition.

An Energy Dispersive Spectrometry (EDS) analysis on this inclusion showed that it is chromium rich. It is assumed that this inclusion is an oxide as it is highly unlikely that any carbides or nitrides would precipitate at 1050°C. It could be that during corrosion, these inclusions form a small crevice with the site in which it sits. This crevice is depleted of oxygen and therefore starts to corrode preferentially. This in turn initiates the autocatalytic reaction mentioned earlier and the site in which the inclusion is situated becomes an anodic site which corrodes rapidly. Since there are no other localised sites in the solution treated condition that might corrode preferentially, the rest of the surface corrodes uniformly except for the region immediately surrounding the inclusion. This region, sometimes termed the "throw", is the region which is effectively cathodically protected due to electrons being supplied by the highly corrosive anodic site. This would explain the circular shape of these features which sometimes impinge on one another if the inclusions are close enough. This process would eventually stop when the inclusion becomes dislodged.

The reason for this phenomenon occurring predominantly in 0Cu could be that 0Cu is the least corrosion resistant and therefore the surrounding matrix, which continues to corrode uniformly, experiences more material loss than the other alloys. This results in these cathodically protected "rings" to appear more prominent and to stand proud of the rest of the uniformly corroded area.

4.2.4 PERFORMANCE OF AISI 301 AND 304L ALLOYS

Included in the corrosion tests for the solution treated and aged condition were the AISI type 301 and 304L standard alloys. These commercial alloys were included to see how they compare with the novel alloys in the experimental programme. The 301 type alloy has the leanest composition and is employed in applications requiring formability especially where stretching is concerned. Type 304L stainless steel is more widely produced ("L" standing for low-carbon). It has a greater stability and improved corrosion resistance and is used considerably at elevated temperatures. Figure 4.12 shows the same corrosion results as in Figure 4.6 but with those of the 301 and 304L alloys superimposed.

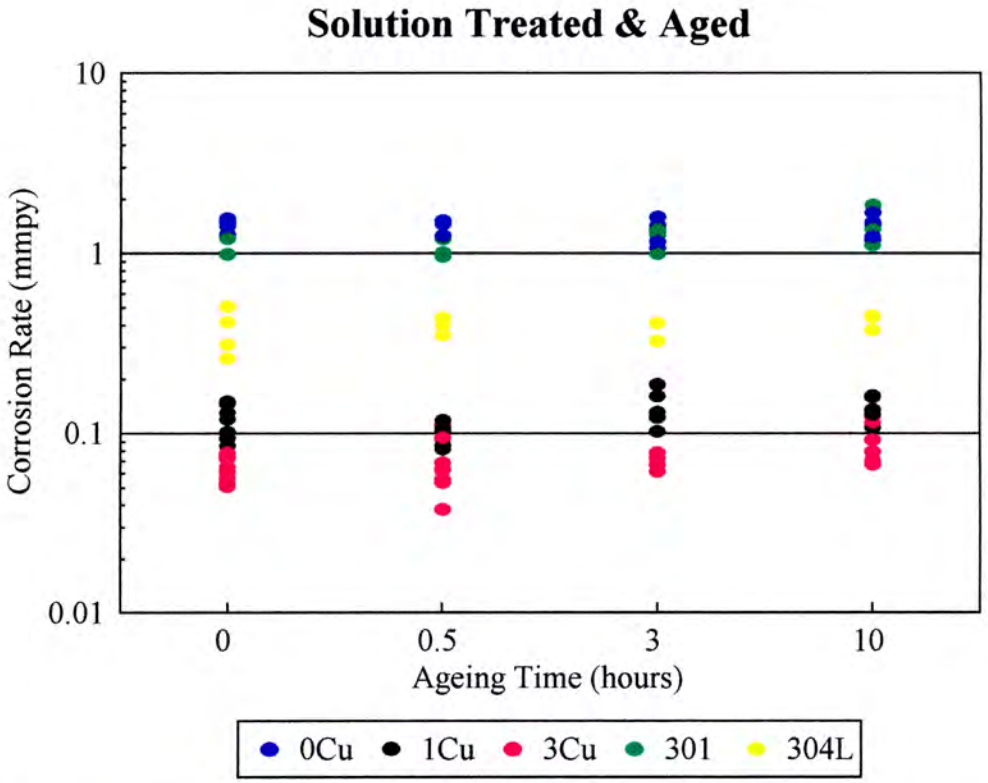

Figure 4.12 Comparison of AISI 301 and 304L type alloys with the novel experimental alloys for the solution treated and aged condition.

These results show that the 301 alloy performed in much the same way as 0Cu. The 304L alloy showed improved corrosion resistance compared to 0Cu and 301 but did not, however, perform as well as the copper rich 1Cu and 3Cu. Referring back to Table 3.1, one can see that the main compositional differences between the standard AISI alloys and the experimental alloys is that there is more nickel, less nitrogen and less copper in the conventional AISI alloys (the only exception being that of 0Cu which has a copper content similar to those for the AISI standard alloys). However, the 304L alloy has slightly more chromium, nickel and manganese than the 301 alloy and hence a possible reason for its superior corrosion performance.

It is somewhat surprising that both 1Cu and 3Cu show a consistently higher corrosion resistance than the AISI 304L standard, which is known for its good corrosion properties.

The only noticeable compositional difference between the 304L alloy and both 1Cu and 3Cu is the higher copper content in the latter. This once again strengthens the theory of the beneficial effects of copper on the anodic dissolution of these materials. As with the experimental alloys, the corrosion rates of the AISI standard alloys did not show an increase after ageing relative to the solution treated condition nor did these corrosion rates increase with ageing time. The SEM micrographs of these two alloys in the solution treated and aged condition, following corrosion, are shown in Figures 4.13 and 4.14

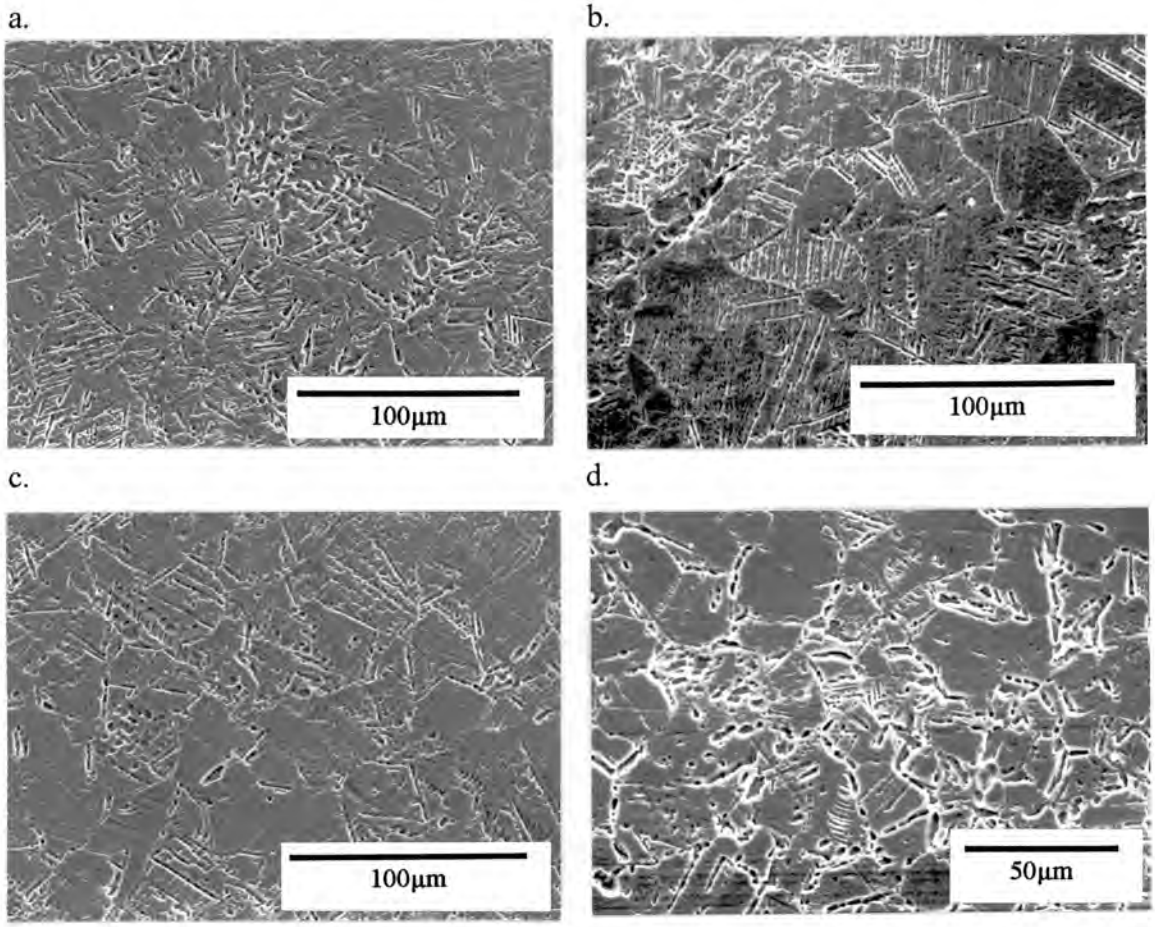

Figure 4.13 SEM micrograph of AISI 301 showing corrosion damage

a. Solution Treated

b. Solution Treated and Aged (1/2 hour)

c. Solution Treated and Aged (3 hours)

d. Solution Treated and Aged (10 hours)

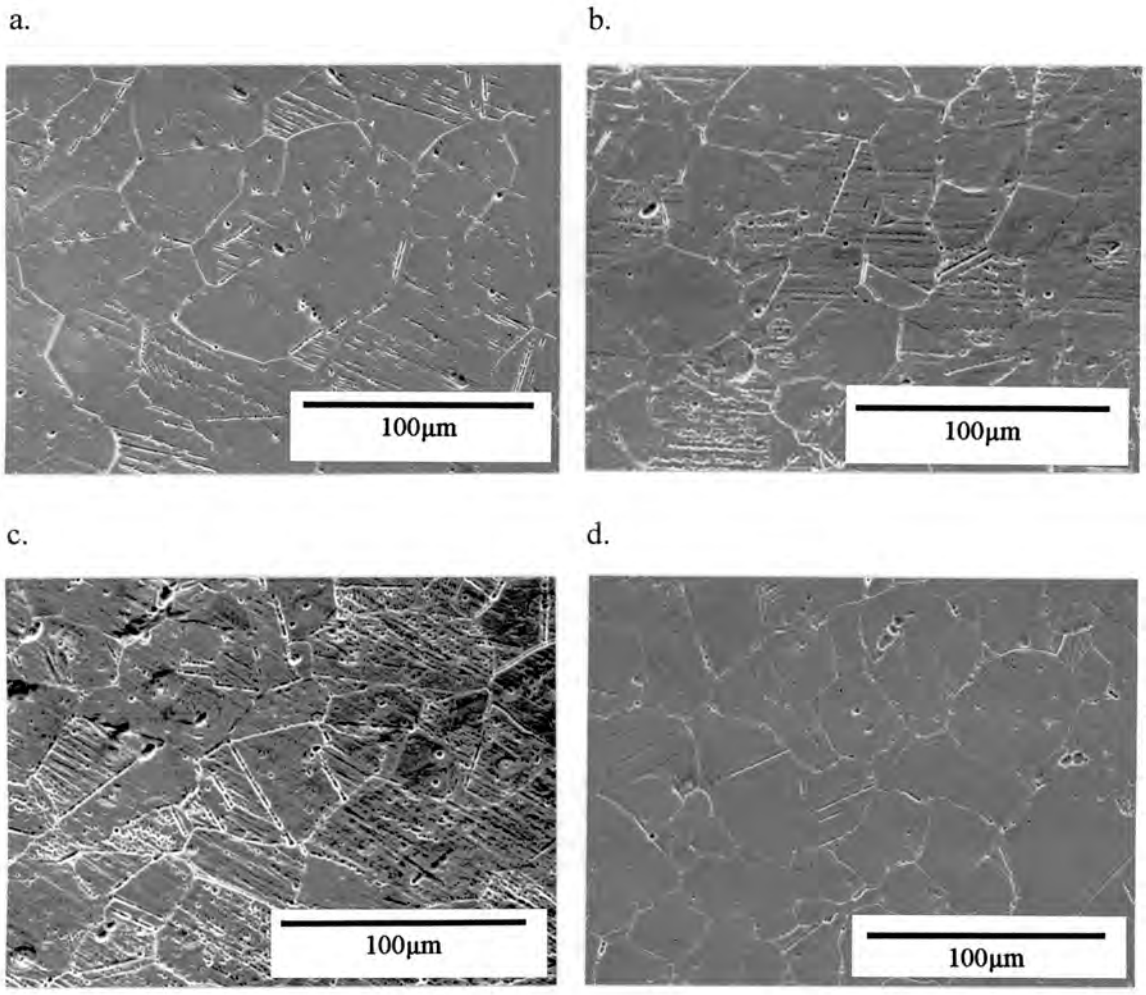

Figure 4.14 SEM micrograph of AISI 304L showing corrosion damage

a. Solution Treated

b. Solution Treated and Aged (1/2 hour)

c. Solution Treated and Aged (3 hours)

d. Solution Treated and Aged (10 hours)

It can be seen from these micrographs that AISI 301 is consistently more heavily corroded than AISI 304L, which complies with the results in Figure 4.12. There is also considerably less intergranular corrosion occurring in the aged conditions compared to the experimental alloys.

This may be because there is less carbon (0.022 wt%) and nitrogen (0.07-0.08 wt%) in these standard alloys which could result in less severe sensitisation than the novel alloys which contain 0.03-0.05 wt% carbon and 0.23-0.26 wt% nitrogen (carbon and nitrogen have an affinity for chromium and they combine together to form precipitates along preferential sites such as grain boundaries). The standard alloys also contain slightly more titanium and niobium which are elements known to reduce the sensitisation affects. It was also noticed that there is far more general corrosion occurring intragranularly than there is in the novel alloys.

To summarise the corrosion results in the solution treated and aged condition, copper does not appear to have an overriding influence on the sensitisation of the alloys during ageing. This is apparent since the corrosion rates for all the alloys in the aged condition do not vary much with ageing time. In other words, the same trends in corrosion rates are observed after ageing for all the alloys despite their large differences in copper contents. However, corrosion damage examined by electron microscopy revealed that (i) more severe intergranular corrosion occurred in 0Cu compared to the other two copper containing alloys for any given ageing period and (ii) the degree of intergranular corrosion increased with ageing time for each alloy. Thus, qualitatively one could say that copper does influence precipitation kinetics, but the polarisation tests do not seem to produce quantitative data consistent with this observation, possibly due to the localised nature of corrosion as mentioned earlier. Meanwhile, 0Cu still exhibits the poorest corrosion performance while 3Cu maintains its superior corrosion resistance after ageing.

The next set of tests involved deforming the alloys (at room temperature) following solution treatment. No subsequent ageing was performed so that the sensitisation phenomenon was eliminated (which has a detrimental effect on the corrosion performance and which also may be affected by copper additions).

4.3 SOLUTION TREATED AND ROLLED

Corrosion tests were performed on all the alloys following solution treatment and deforming. Deformation was achieved by rolling the alloys at room temperature to a strain of 30%.
This was done in order to establish the influence of martensite on the dissolution properties of the alloys and more particularly, the influence of copper on the dissolution of martensite.

4.3.1 OPTICAL MICROSCOPY

Following rolling, the microstructure of the three alloys was examined using the Nomarski polarisation contrast mode. Figure 4.15 shows these micrographs.

a.

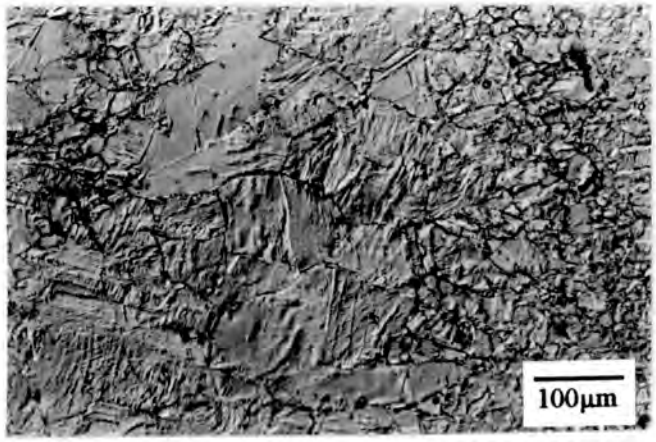

b.

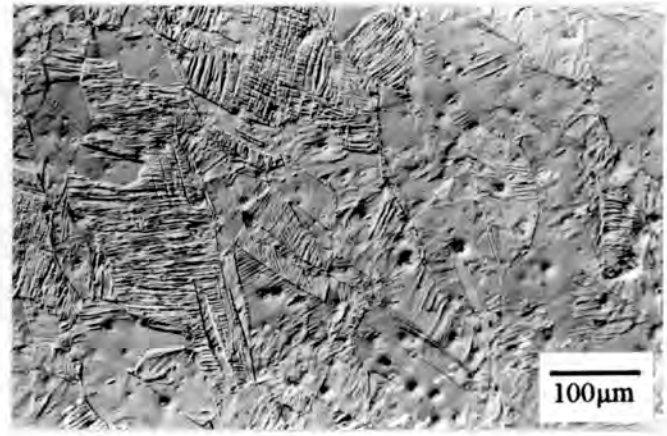

c.

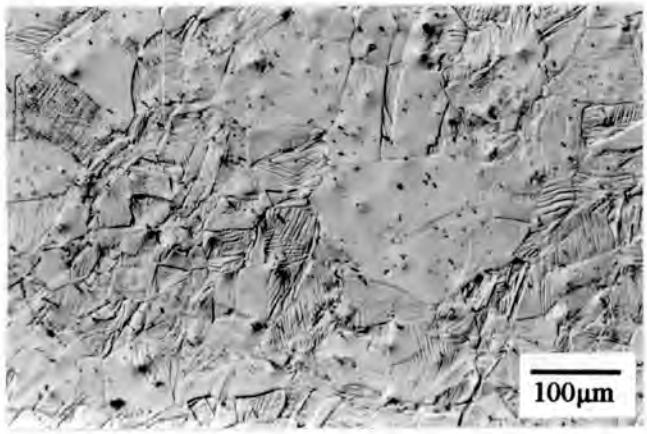

Figure 4.15 Optical micrographs of the alloys in the solution treated and rolled (room temperature) condition.

a. 0Cu (±33% martensite volume)

b. 1Cu (±20% martensite volume)

c. 3Cu (±3% martensite volume)

Figure 4.15 shows that the microstructures of all the alloys consist essentially of austenite and martensite. The given volume fractions of the deformation-induced martensite were obtained by XRD analysis.

4.3.2 CORROSION RESULTS

The corrosion rates of the three alloys in the solution treated and rolled condition are compared with those in the solution treated only condition and are shown in Figure 4.16.

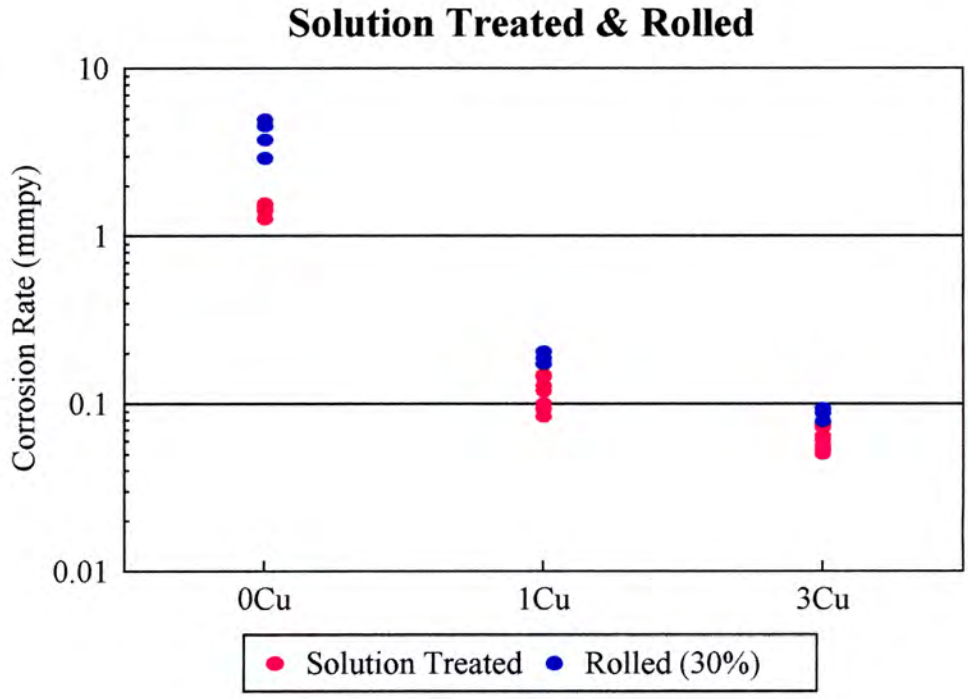

Figure 4.16 Corrosion rates of the experimental alloys in de-aerated 5 volume % sulphuric acid for the solution treated and rolled (room temperature) condition.

Following rolling, the corrosion rates of all the alloys increased with respect to those in the solution treated condition. This is to be expected as martensite is formed during deformation of these metastable alloys. Martensite has a high dislocation density and is a high energy phase, and thus provides for preferential corrosive attack over the more corrosion resistant austenite phase.

Once again, the corrosion rates after rolling are highest in 0Cu and lowest in 3Cu. The high martensite volume fraction in 0Cu (as shown in Figure 4.15) is attributed to the lack of copper in this alloy since copper is known to increase the stability of austenite during deformation. As mentioned in Section 2.1.2, copper has the ability to suppress the M_s and M_d temperatures of austenite and is an effective stabiliser of austenite once it has been formed. Since all the alloys were deformed at room temperature, this would mean that 3Cu, containing the most copper, would form the least amount of martensite upon deformation and therefore have a similar (or only slightly higher) corrosion rate to that in the solution treated condition.

The increase in corrosion rates for the solution treated and rolled condition with respect to those in the solution treated only condition was most marked in 0Cu and only slight in 3Cu. The amount of increase in corrosion rates from the solution treated only condition to the solution treated and rolled condition was approximately a factor of 2.78, 1.62 and 1.21 for 0Cu, 1Cu and 3Cu respectively. This could either be due to the fact that (i) there is more martensite in 0Cu which corrodes preferentially or (ii) it could be that the copper additions in 1Cu and 3Cu reduce the dissolution rate of martensite. One needs an equal amount of martensite in all the alloys in order to establish the latter. Thus, in order to eliminate the variation in martensite volume fraction amongst the alloys, deformation must take place at different controlled temperatures for each of the three alloys. This means that composition (i.e. copper) will be the only variable in the deformed alloys. The next set of tests were therefore carried out to establish the influence of copper on the dissolution rate of martensite.

4.4 SOLUTION TREATED AND DEFORMED (CONTROLLED TEMPERATURE)

In order to obtain equal martensite volume fractions at equivalent strains, the alloys need to be deformed at different temperatures due to their different austenite stabilities. The alloys were deformed by compression while submerged in a temperature bath. 0Cu, being the most unstable was deformed at a temperature of between 65 and 85°C while the more stable 3Cu was deformed at approximately -70°C. 1Cu, representing an intermediate stability, was deformed at room temperature (15-25°C). The procedure carried out for these compression tests is explained in detail in Section 3.4. All the alloys were compressed to an equal macro-strain of 30%. During compression, the specimens experience different micro-strains along their length due to friction between the specimen and the anvils. A maximum equivalent micro-strain (which exceeds 30%) occurs in the centre of the compressed specimen (as shown by the varying martensite volumes in Figure 3.8) and so all specimens were sectioned to obtain maximum martensite values and equal strains throughout the alloy range.

4.4.1 OPTICAL MICROSCOPY

Optical microscopy using the Namarski interference contrast mode was carried out after compression but before corrosion of the alloys. These micrographs are shown in Figure 4.17.

a.

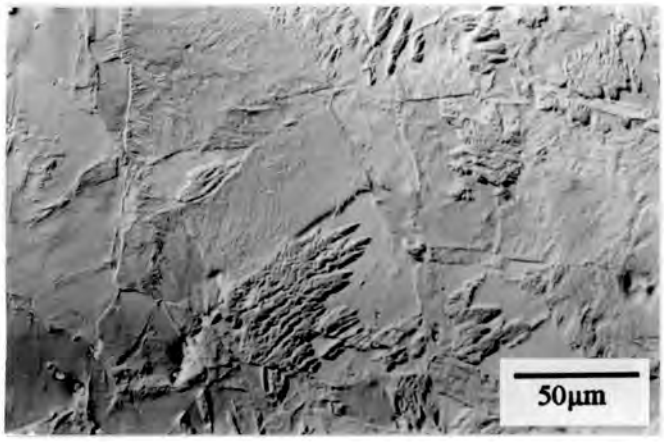

b.

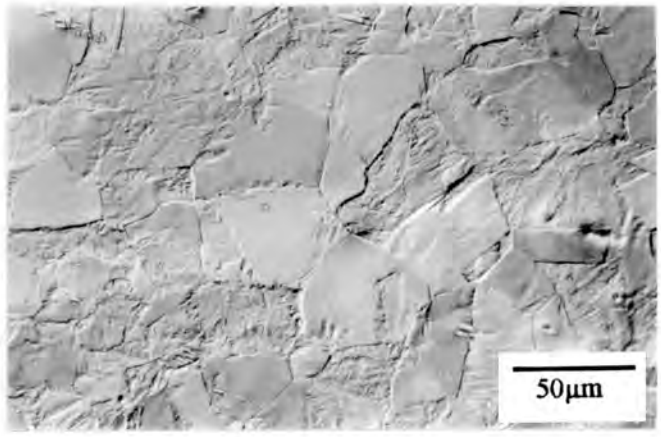

c.

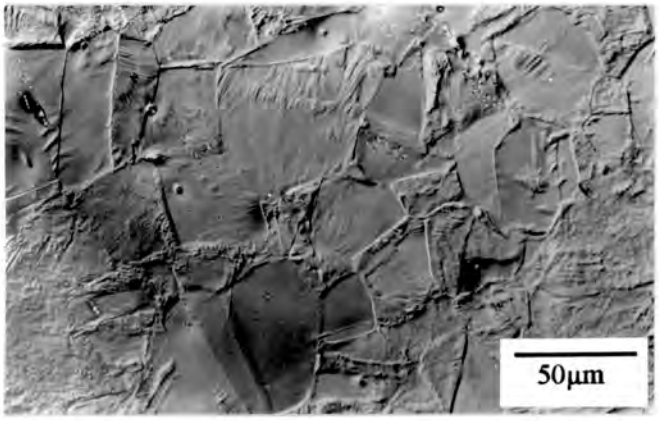

Figure 4.17 Optical micrographs of the alloys in the solution treated and deformed (controlled temperature) condition.

a. 0Cu (±19% martensite volume)

b. 1Cu (±17% martensite volume)

c. 3Cu (±18% martensite volume)

As desired, the microstructures consist of austenite and equal martensite volume fractions (within 2%) for the three alloys. The martensite volume fraction was determined by XRD analysis.

4.4.2 CORROSION RESULTS

Determination of the deformation temperatures which would result in equal amounts of martensite in all the alloys was achieved by trial and error (described in Section 3.4.3). The alloys were compressed at many different temperatures (to an equivalent 30% macro-strain) before those which would result in a martensite volume of 20±3% were found. Figure 4.18 displays the corrosion rates of all the alloys, compressed at these different temperatures (reflecting different martensite volume fractions), used in the trial and error process.

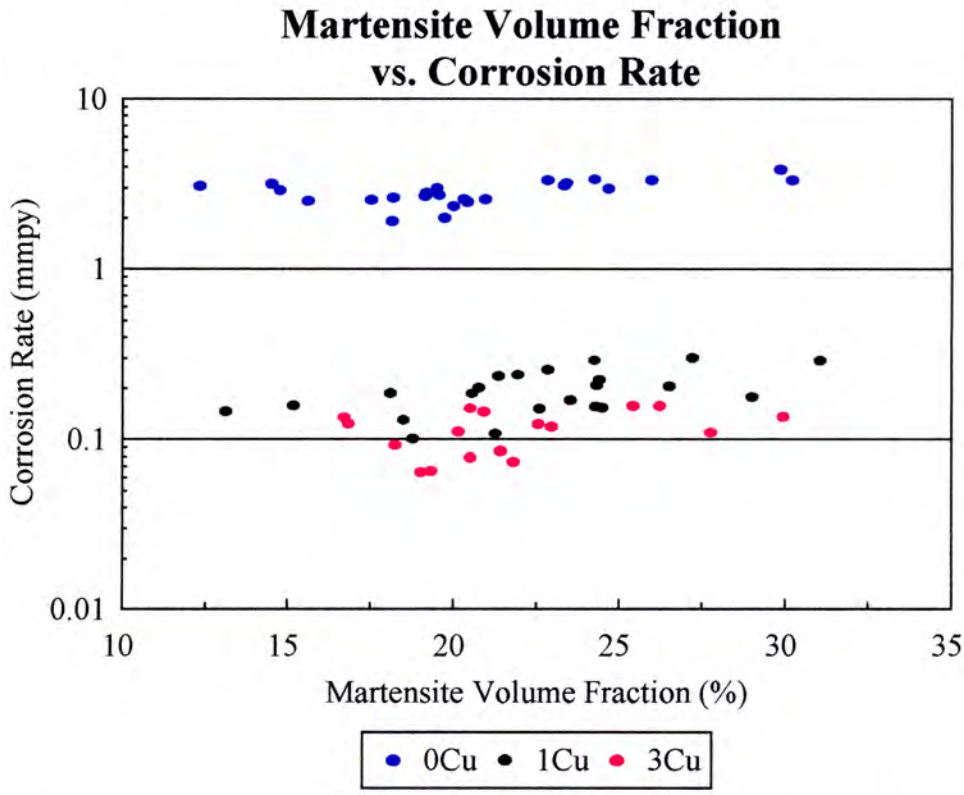

Figure 4.18 Corrosion rate vs. martensite volume fraction for the alloys which were compressed at different temperatures but equivalent macro-strains.

These results show that for each volume fraction of martensite, 0Cu consistently exhibits the poorest dissolution properties after deformation. The dissolution properties of 1Cu and 3Cu are remarkably similar although 3Cu still seems to have a higher corrosion resistance than that of 1Cu, albeit very slight.

The corrosion rates in Figure 4.18 also show very little variation with martensite volume fraction. This is surprising since it is expected that the corrosion rates should increase with increasing martensite volume fraction. As mentioned before, martensite is a highly dislocated, high energy phase which is expected to corrode preferentially. One would assume, therefore, that a larger amount of martensite would result in more severe corrosive attack which would reflect a higher value for the corrosion rate. This was, however, hardly evident within the martensite volume range of 12-33%.

It also seems that there is far more scatter in the corrosion rate measurements for 1Cu and 3Cu than in those for 0Cu. This could be explained by the fact that 1Cu and 3Cu have lower corrosion rates than 0Cu and therefore fewer ions are anodically removed from the surfaces of these alloys during corrosion. This results in very small currents being generated between the specimen surface and the counter electrodes. The potentiostat is especially sensitive in the measurement of these low currents as they are easily corrupted by the slightest pick-up of electrical noise or static.

The scatter in Figure 4.18 could also be attributed to the fact that, in this test, smaller alloy surfaces were exposed to the corrosive environment than in the other tests performed thus far (the reasons are explained in Section 3.4). A smaller surface area effectively means a smaller sample size. Data from a large sample size obviously yields a more representative and accurate result.

Figure 4.19 shows how the corrosion rates for the solution treated and compressed condition (with equal martensite volumes of 20±3%) compare with those for the solution treated only condition.

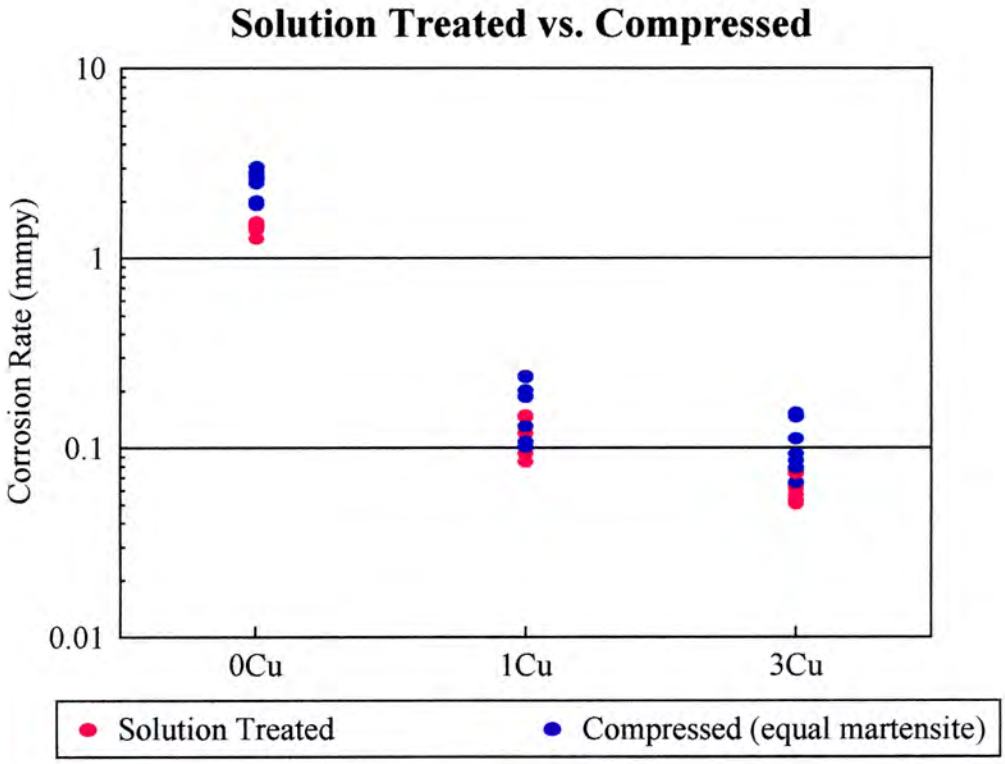

Figure 4.19 Comparison of corrosion rates for the solution treated condition with those of the compressed (controlled temperature) condition

As expected, there is an increase in corrosion rates for the compressed condition with respect to the solution treated only condition. There seems to be some overlap in values of corrosion rates for both the solution treated and the solution treated and compressed conditions in 1Cu and 3Cu i.e. the corrosion rates for the solution treated and compressed condition are not consistently higher than those for the solution treated only condition for these two alloys. These corrosion rates are, however, consistently higher in 0Cu. Since all the alloys contained an equal amount of martensite in the solution treated and deformed condition, the fact that the corrosion rates for the deformed state increase the most in 0Cu (from the solution treated only condition) and the least in 1Cu and 3Cu suggests that the copper in 1Cu and 3Cu could well have a beneficial effect on reducing the dissolution rate of martensite.

4.4.3 SCANNING ELECTRON MICROSCOPY

Examination of the corroded surfaces, following potentiodynamic polarisation of the alloys in the compressed (controlled temperature) condition, was undertaken using the scanning electron microscope. Prior to corrosion, these alloys had martensite volumes of approximately 19, 22 and 20% for 0Cu, 1Cu and 3Cu respectively. The micrographs are shown in Figure 4.20.

a.

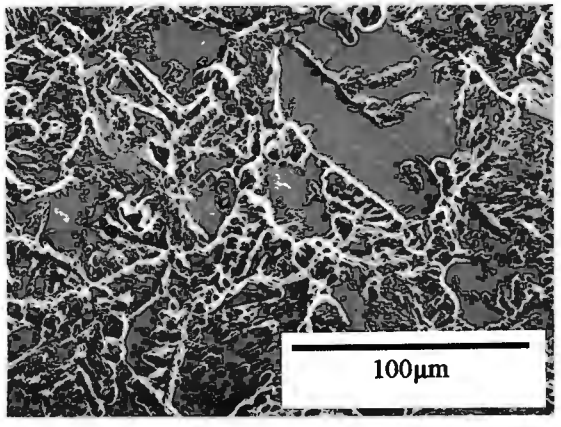

b.

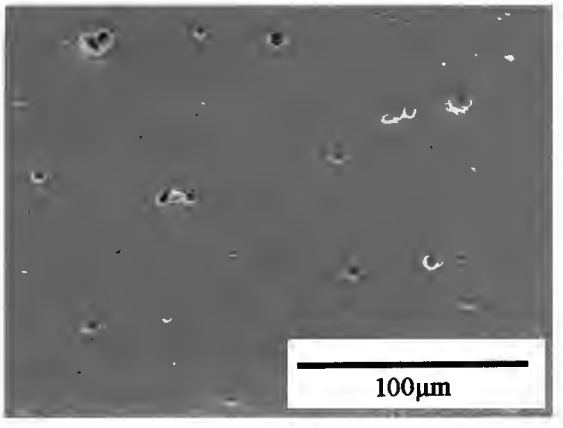

c.

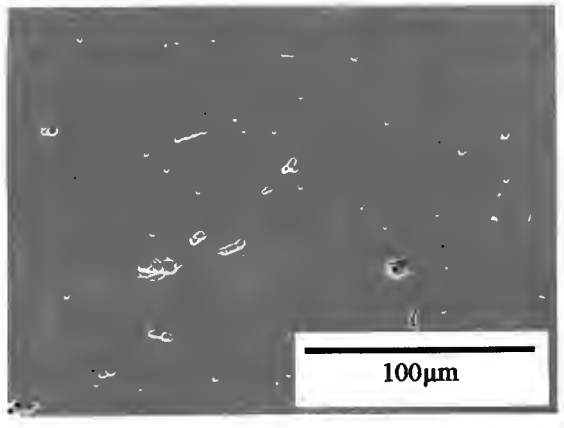

Figure 4.20 SEM micrographs of the alloys in the solution treated and compressed (controlled temperatures) condition showing corrosion damage

a. 0Cu

b. 1Cu

c. 3Cu

0Cu, as expected, has experienced the most severe intragranular corrosive attack as shown in Figure 4.20 (a). 1Cu and 3Cu however, despite their equal martensite volume fractions with 0Cu, showed very little evidence of dissolution. The only features noticed in Figure 4.20 (b) and (c) were those of oxide sites.

There should be no reason for 1Cu and 3Cu not to have the same heavily corroded surface as 0Cu, since equal martensite volume fractions were present throughout the alloys. The composition of the alloys is the only variable which remains. Since copper is the element that varies most markedly amongst the alloys, it can be deduced from these micrographs that the copper additions in 1Cu and 3Cu reduce the dissolution rates of the deformed microstructures of these alloys.

So to summarise this series of corrosion tests, the superior corrosion performance of 1Cu and 3Cu following deformation can be attributed to their copper additions. The corrosion rates shown in Figure 4.19 also suggest that copper has a beneficial effect on reducing the dissolution rate of martensite.

4.5 SOLUTION TREATED, DEFORMED (AT CONTROLLED TEMPERATURES) AND AGED

The next series of tests were conducted to determine whether copper has any effect on the sensitisation of martensite during ageing.

The exact same alloys that were solution treated and deformed (to equal martensite levels) in the previous series of tests were used for this test series, but now included ageing at 700°C for either 0.5 or 3 hour periods. The resulting microstructures of these alloys were first investigated before corrosion took place.

4.5.1 OPTICAL MICROSCOPY

The micrographs obtained by using the Nomarski interference contrast mode are displayed in Figure 4.21.

a.

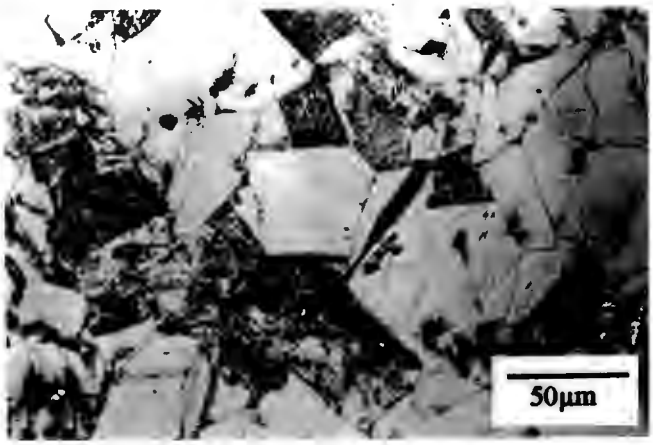

b.

c.

Figure 4.21 Optical micrographs of the alloys in the solution treated, deformed (controlled temperatures) and aged (3 hours) condition. Martensite levels before ageing were approximately 19, 17 and 18% for 0Cu, 1Cu and 3Cu respectively.

a. 0Cu

b. 1Cu

c. 3Cu

The alloys shown in these micrographs are the exact alloys shown in Figure 4.17. However, these micrographs show remarkably different features to those in Figure 4.17 due to ageing. The blackened areas are presumed to be the martensitic regions which now appear black because the precipitates formed within these martensitic regions have been attacked by the etchant. Once again, the actual precipitates are not visible in these micrographs as the etchant attacks the interface formed between the precipitate and the matrix. There also seems to be precipitation of some form along the grain boundaries as well as along twin boundaries. The light areas represent the austenitic regions.

4.5.2 CORROSION RESULTS

The corrosion rates for the alloys in the solution treated, compressed (controlled temperature) and aged condition are first compared with those for the solution treated and compressed only (controlled temperature) condition and then with those for the solution treated and aged only condition.

a. Comparison with the solution treated and compressed only (unaged) condition

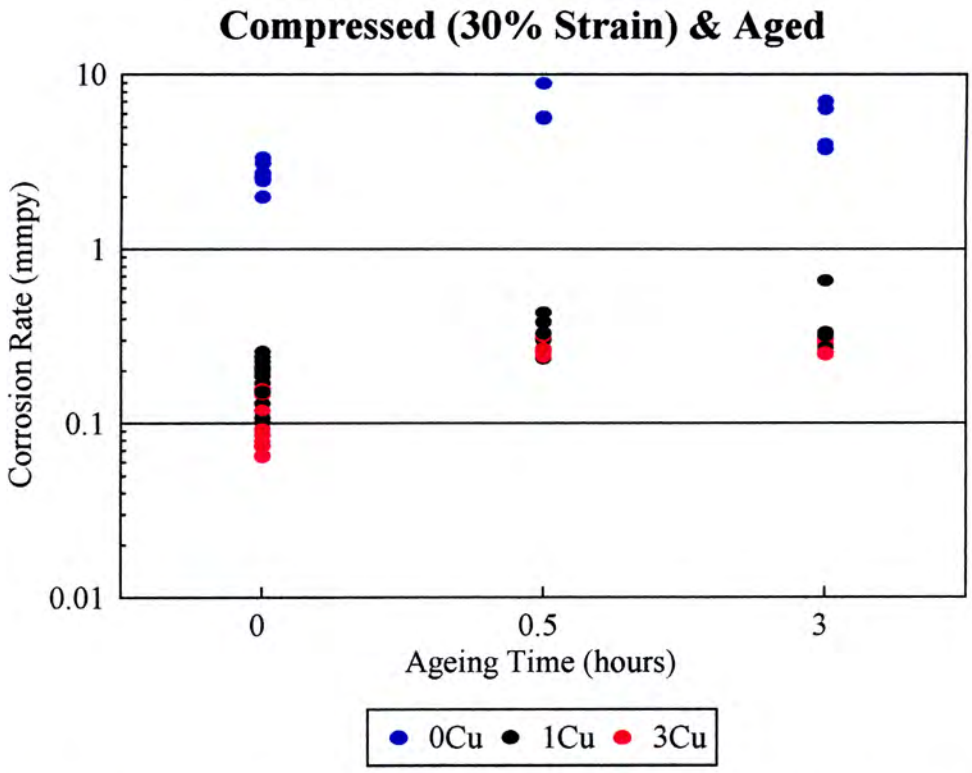

Figure 4.22 Corrosion rates of the alloys after solution treatment, deformation (to form equal martensite volume fractions) and ageing (0.5 and 3 hours) compared with those for the solution treated and deformed only condition (i.e. 0 ageing time).

The resultant effect of ageing after deformation of these alloys is to increase their corrosion rates. This increase was evident in all three alloys for the deformed and aged (1/2 hour) condition from the deformed only condition and it seems that the degree of increase is similar for all three alloys. Once again, 0Cu exhibits a consistently poorer corrosion performance than 1Cu and 3Cu for the compressed and aged condition. No further increase in corrosion rate was evident after longer ageing times.

The increase in corrosion rates after deformation and ageing (relative to the deformed only condition) can be attributed to sensitisation. The corrosion due to the presence of high energy martensite in the deformed only condition is less severe than that due to the sensitisation of this martensite after ageing. A discussion of this will follow.

b. Comparison with the solution treated and aged (undeformed) condition

The corrosion rates for the deformed and aged condition are compared with those for the undeformed and aged condition in Figure 4.23.

a.

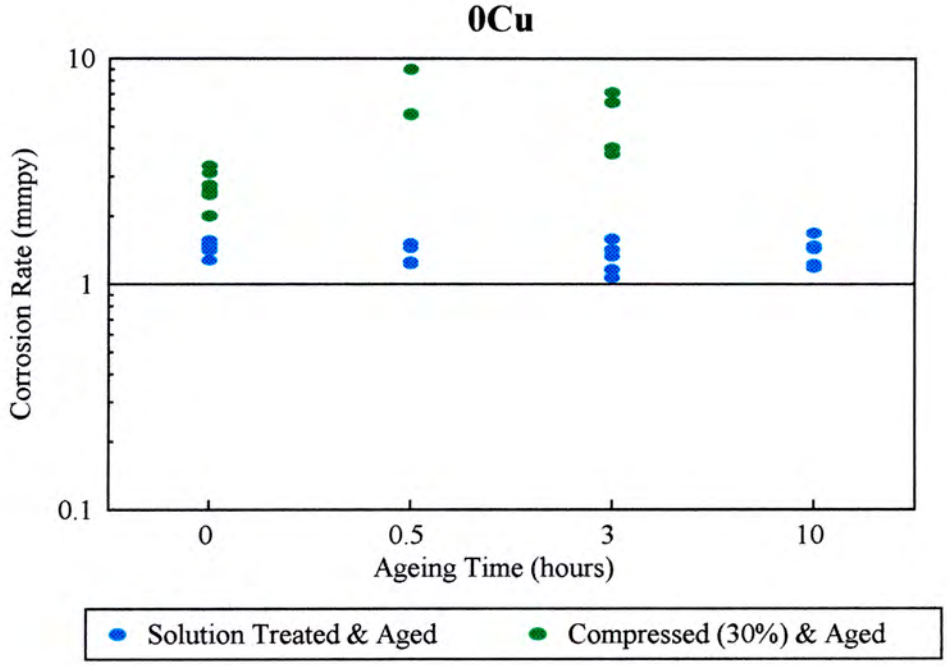
0Cu
10
1
0.1
Corrosion Rate (mmpy)
0
0.5
3
10
Ageing Time (hours)
Solution Treated & Aged
Compressed (30%) & Aged

b.

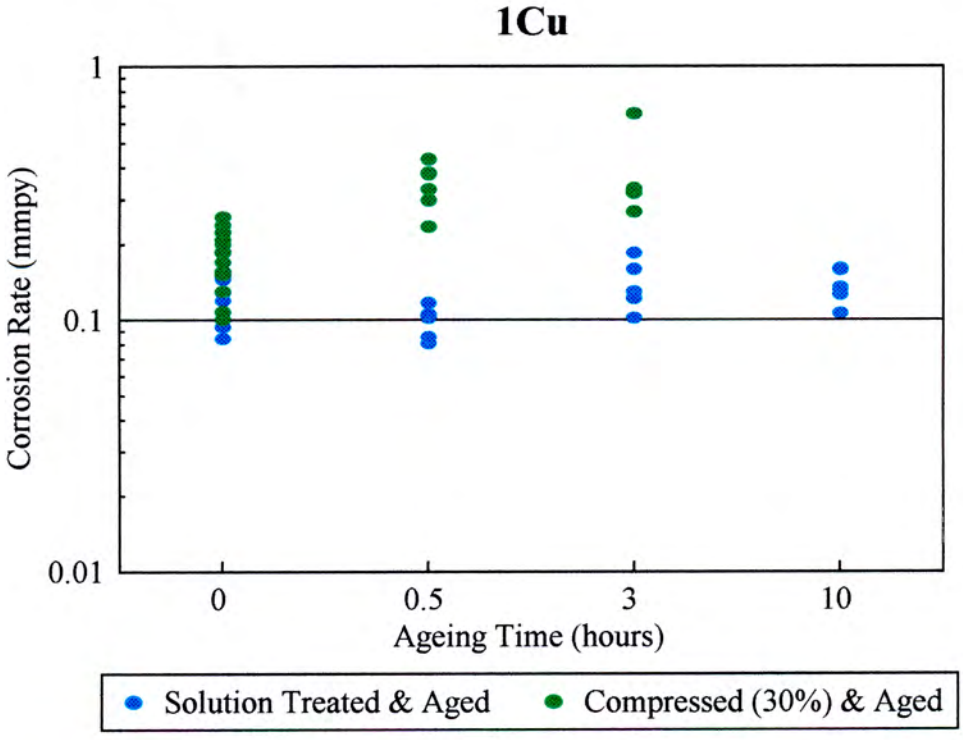
1Cu
1
0.1
0.01
Corrosion Rate (mmpy)
0
0.5
3
10
Ageing Time (hours)
Solution Treated & Aged
Compressed (30%) & Aged

c.

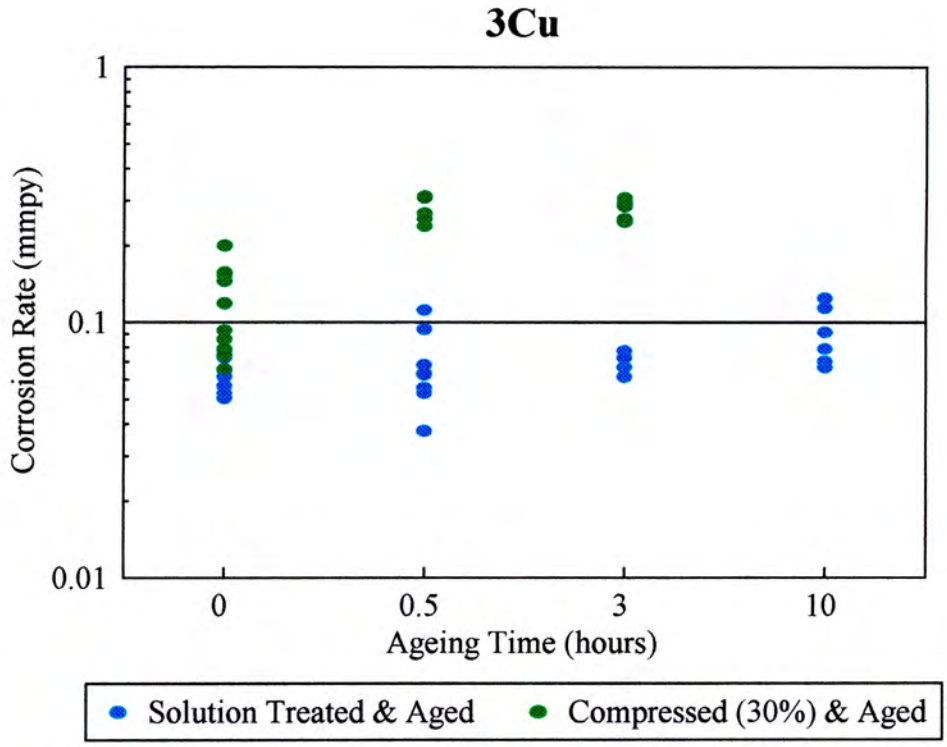

Figure 4.23 Comparison of corrosion rates for the solution treated (undeformed) and aged condition with those of the solution treated, deformed and aged condition.

a. 0Cu

b. 1Cu

c. 3Cu

The ageing time labelled zero (0 hours) represents the solution treated only and deformed only conditions (i.e. without subsequent ageing). It can be seen in these graphs that for each alloy, the corrosion rates for the solution treated, deformed and aged condition are consistently higher than those for the solution treated and aged only condition. Looking at the corrosion rates of the alloys after 0.5 hours of ageing, it seems that the amount of increase in corrosion rates from the solution treated and aged only condition to the solution treated, deformed and aged condition is greatest in 0Cu. This, however cannot be said with 100% certainty due to the scatter of the corrosion rate values in these conditions. These results will be discussed after the microscopic examination of these alloys in the solution treated, deformed and aged condition using the SEM.

4.5.3 SCANNING ELECTRON MICROSCOPY

The scanning electron micrographs of the three alloys (following potentiodynamic scans in 5 volume % de-aerated sulphuric acid) in the solution treated, deformed and aged (3 hour) condition are shown in Figure 4.24.

a.

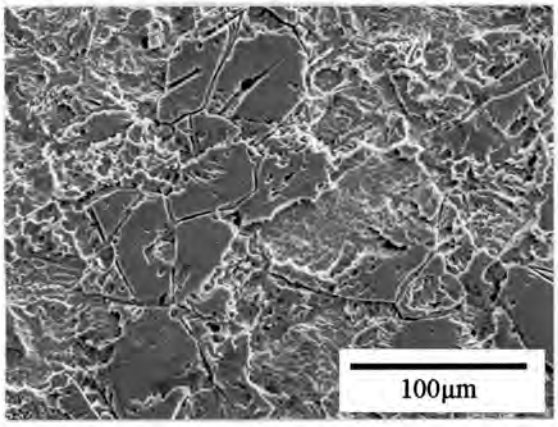

b.

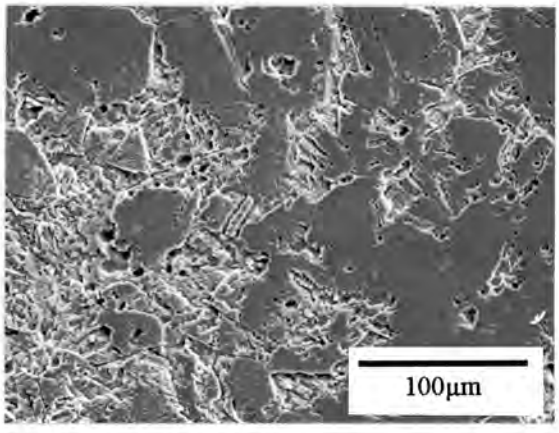

c.

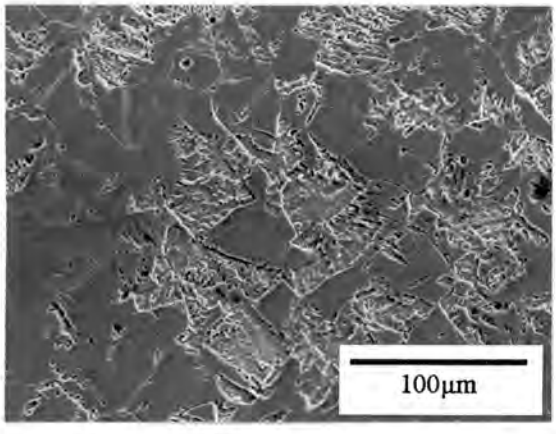

Figure 4.24 SEM micrographs of the alloys in the solution treated, deformed (controlled temperatures) and aged (3 hours) condition. Martensite levels before ageing were approximately 19, 21 and 22% for 0Cu, 1Cu and 3Cu respectively.

a. 0Cu

b. 1Cu

c. 3Cu

When comparing these micrographs to those shown in Figure 4.20 (for the compressed only condition), the most obvious difference is that following ageing, 1Cu and 3Cu have experienced a considerable amount of intragranular corrosion. 0Cu, on the other hand, showed equally severe corrosive attack as demonstrated in the deformed only condition. The corrosion damage in 1Cu and 3Cu, however, still does not appear as bad as that in 0Cu.

Once again, there should be no reason for all the alloys not to show similar amounts of corrosion damage as all the alloys have equal amounts of martensite prior to ageing. Copper must therefore reduce the corrosion rates of these alloys in the deformed and aged condition. There is also some evidence of intergranular corrosion occurring in 0Cu after ageing which did not show up in Figure 4.20 (a) i.e. the solution treated and deformed only condition. Intergranular corrosion was also noticed, on a much smaller scale, in 1Cu and 3Cu although not as extreme as that seen for the solution treated and aged only condition (Figure 4.8 (c) and 4.9(c)). The higher degree of intergranular corrosion occurring in 0Cu may, once again, be due to the fact that this alloy contains 0.05 wt% carbon as opposed to 0.03 wt% in the other two alloys.

The sensitisation which occurs in the solution treated and aged condition is confined to the grain boundaries. In the solution treated, deformed and aged condition, however, there are more sites available for precipitates to form. Grain boundary precipitation is no longer dominant since prior deformation creates defect sites which are favoured locations for intragranular precipitation. The deformation-induced martensite has a high dislocation density providing ideal nucleation sites for chromium carbides or chromium carbo-nitrides. Furthermore, martensite is especially efficient at precipitating carbides because the solubility of carbon is lower in the martensite than in the austenite[66]. This means that most of the carbon in the martensite rapidly goes into the formation of carbides, giving a high density of fine carbides within the grain. Apart from the martensite, other ideal nucleation sites created during straining include deformation twin-stacking fault planes, twin-fault intersections, slip planes and regions of high dislocation density[67].

The precipitation of these chromium rich carbides or carbo-nitrides within the grain (intragranularly) after deformation and ageing results in fewer precipitates forming along the grain boundary as most of the available carbon has already been taken up by intragranular precipitation. This intragranular precipitation results in extensive intragranular corrosive attack (Figure 4.24) due to extensive chromium depletion within the grains. It was also reported by Briant *et al*[56] that martensite results in more rapid sensitisation for a given ageing time and temperature. This accounts for the consistently higher corrosion rates occurring in the deformed and aged condition than those in the aged only condition, for both ageing periods (0.5 and 3 hours) (Figure 4.23).

In summary, it does not seem that copper has an influence on the sensitisation of the martensite in these deformed alloys as the corrosion rate increase from the deformed condition to the deformed and aged (1/2 hour) condition appears to be consistent for all three alloys. Also, there was no further increase in corrosion rates with ageing time for any of the alloy suggesting that copper may not have any influence on the precipitation kinetics of the deformed alloys.

Consider the schematics illustrated in Figure 4.25. If the corrosion rate (C.R.) versus ageing time graph had shown trends which were not identical for each alloy, such as that shown in Figure 4.25(a), then one could say that copper has an influence on the precipitation kinetics. In the case of Figure 4.25(a) one could say that copper has a beneficial effect on reducing the precipitation kinetics of the deformed 1Cu and 3Cu since the curve for 0Cu (containing the least copper) showed an increase in corrosion rate with ageing time while the corrosion rates of the other two copper containing alloys remained the same with ageing time.

However, this was not the case as all alloys showed similar trends (Figure 4.25(b)). From this result, it can be concluded that copper does not affect the precipitation kinetics leading to sensitisation of these deformed alloys.

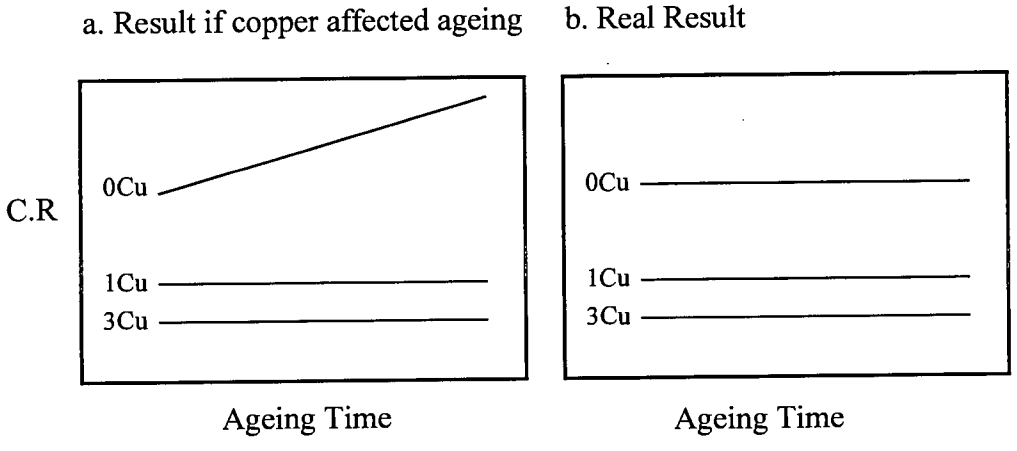

Figure 4.25 Schematic representation of how corrosion rate changes with ageing time depending on whether copper has an influence on ageing (a) or not (b).

However, 1Cu and 3Cu still show a consistently higher corrosion resistance (at each ageing time) than 0Cu for the deformed and aged conditions. This is evident from both (i) the lower corrosion rates of these alloys for the deformed and aged condition compared to 0Cu, as well as (ii) the less severe corrosive damage evident in the SEM micrographs of these alloys (Figure 4.24 (b) and (c)). Since all the alloys were in the same condition prior to ageing (i.e. solution treated and deformed to form equal martensite levels), it seems that the copper additions in 1Cu and 3Cu reduce the dissolution rates of these alloys in the deformed and aged condition.

4.6 POTENTIODYNAMIC SCANS

Potentiodynamic scans were carried out on all the alloys for all the above mentioned microstructural conditions. These scans were conducted in de-aerated 5 volume % sulphuric acid at 30°C. The scans are useful in that corrosion characteristics such as critical current density, passivation potential, passivity and transpassive behaviour can be assessed for each alloy in the various microstructural conditions. It was generally found that the trends observed for critical current densities corresponded with corrosion rate trends for each microstructural condition. This is illustrated in Figure 4.26 which compares potentiodynamic scans of 0Cu, 1Cu and 3Cu as well as the standard AISI 301 and 304L alloys in the solution treated condition.

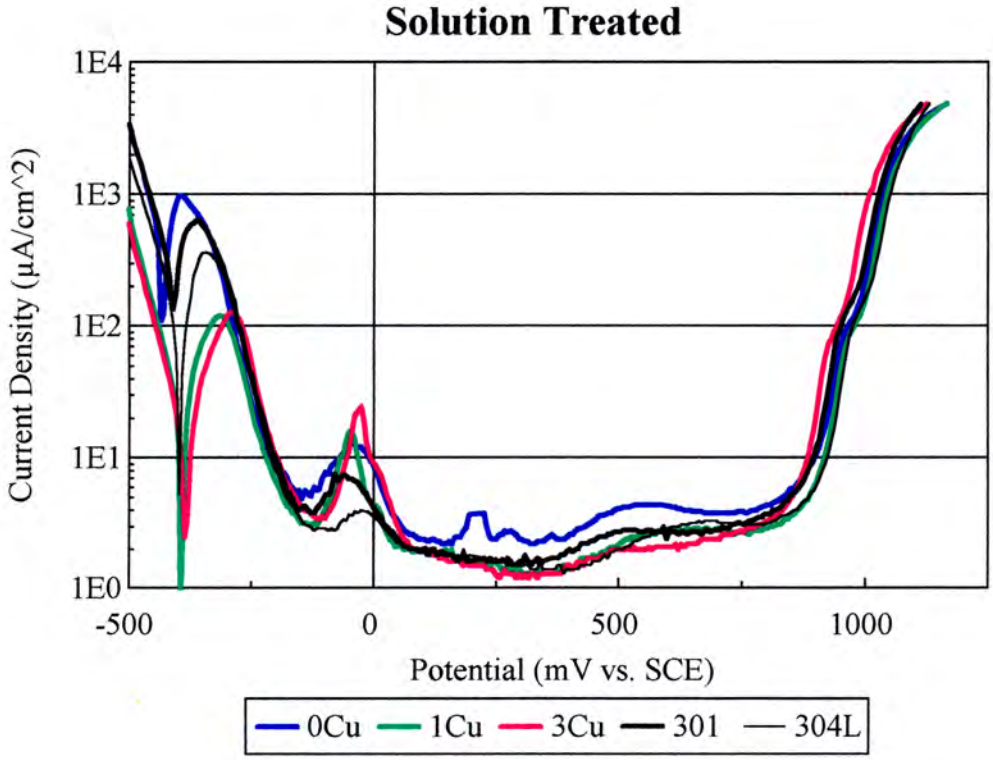

Figure 4.26 Potentiodynamic scans of the experimental and AISI 301 and 304L alloys (performed in de-aerated 5 volume % sulphuric acid at 30°C) in the solution treated condition.

0Cu shows the highest critical current density (point of maximum dissolution) which also corresponds to 0Cu's high corrosion rate in the solution treated condition. 1Cu and 3Cu display the lowest values of critical current density while the AISI 301 and 304L grades show intermediate values. In other words, the trend in critical current densities shown in Figure 4.26 can be compared with the trends in corrosion rates in Figure 4.12 for the solution treated condition. Figure 4.26 also shows that the passivation potential, E_{pp}, increases from 0Cu to 3Cu (i.e. with an increase in copper). This suggests that copper additions reduce the alloys ability to passivate.

The second anodic peak which is evident in all the scans between $-100mV_{SCE}$ and $0mV_{SCE}$ could be attributed to the anodic dissolution of metallic copper which was previously cathodically precipitated onto the surface of the specimen. This was discussed in more detail in Section 2.4 of the Literature Review. Although this second anodic peak increases with an increase in copper contained in the various stainless steels, the reasoning behind this phenomenon remains a contentious issue. 3Cu containing the most copper displays the highest current density at this peak while the 304L alloy, despite its low copper content (0.05wt%), still displays this positive current "hump", albeit the lowest.

0Cu's passive region showed the highest current densities than the other alloys in the solution treated condition while 1Cu and 3Cu showed the lowest passive current densities. This suggests that the passive film formed on 0Cu is unstable compared to the film formed on the copper-containing 1Cu and 3Cu alloys. No conclusions could be drawn regarding the transpassive behaviour of these alloys.

The passive current densities did not, however, change significantly with microstructural condition. The only microstructural condition which exhibited a noticeable change in passive current densities was that of the compressed (equivalent martensite levels) and aged condition. The potentiodynamic scans of the three alloys in this condition are shown in Figure 4.27 and are compared with the compressed only condition.

a.

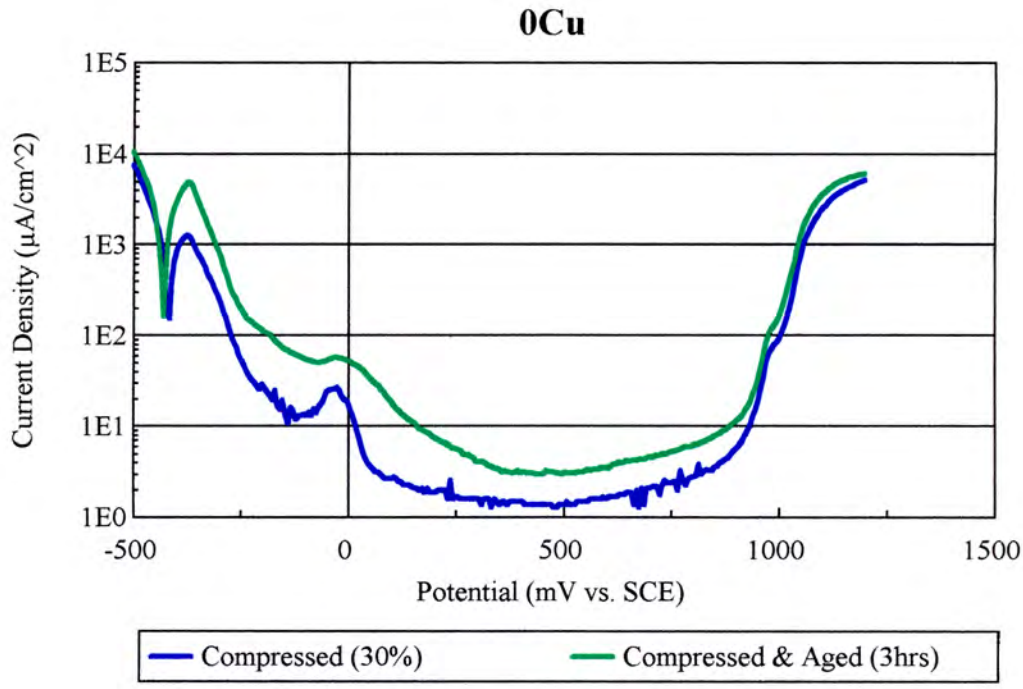
0Cu
1E5
1E4
1E3
1E2
1E1
1E0
Current Density (µA/cm^2)
-500
0
500
1000
1500
Potential (mV vs. SCE)
Compressed (30%)
Compressed & Aged (3hrs)

b.

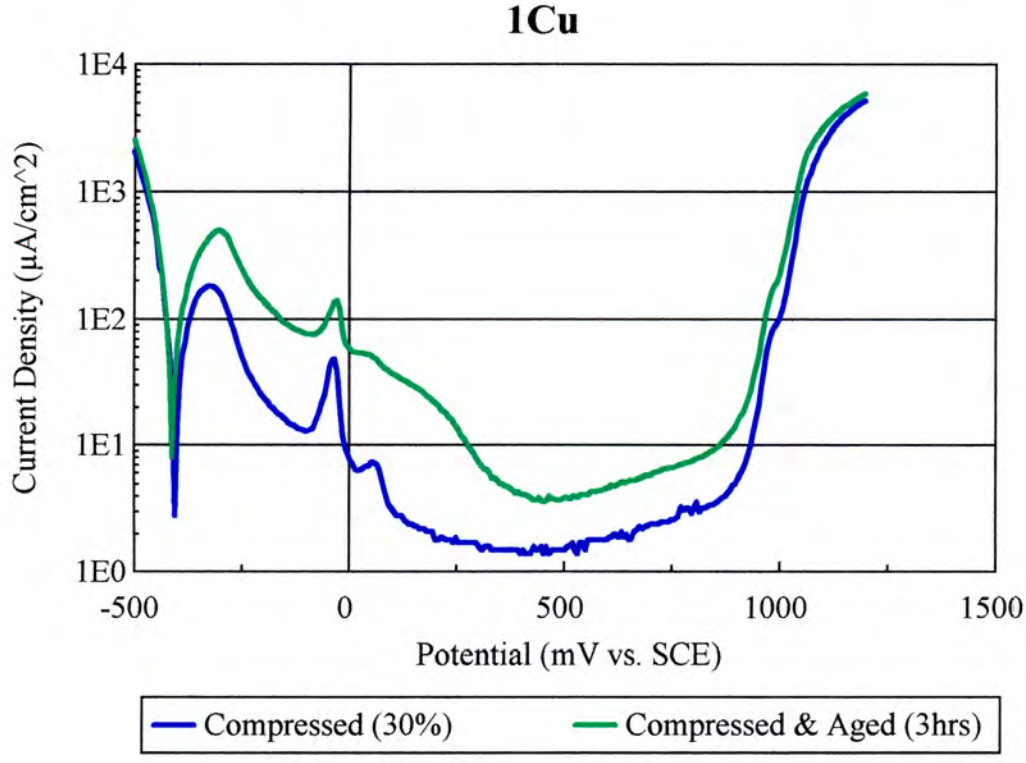
1Cu
1E4
1E3
1E2
1E1
1E0
Current Density (µA/cm^2)
-500
0
500
1000
1500
Potential (mV vs. SCE)
Compressed (30%)
Compressed & Aged (3hrs)

c.

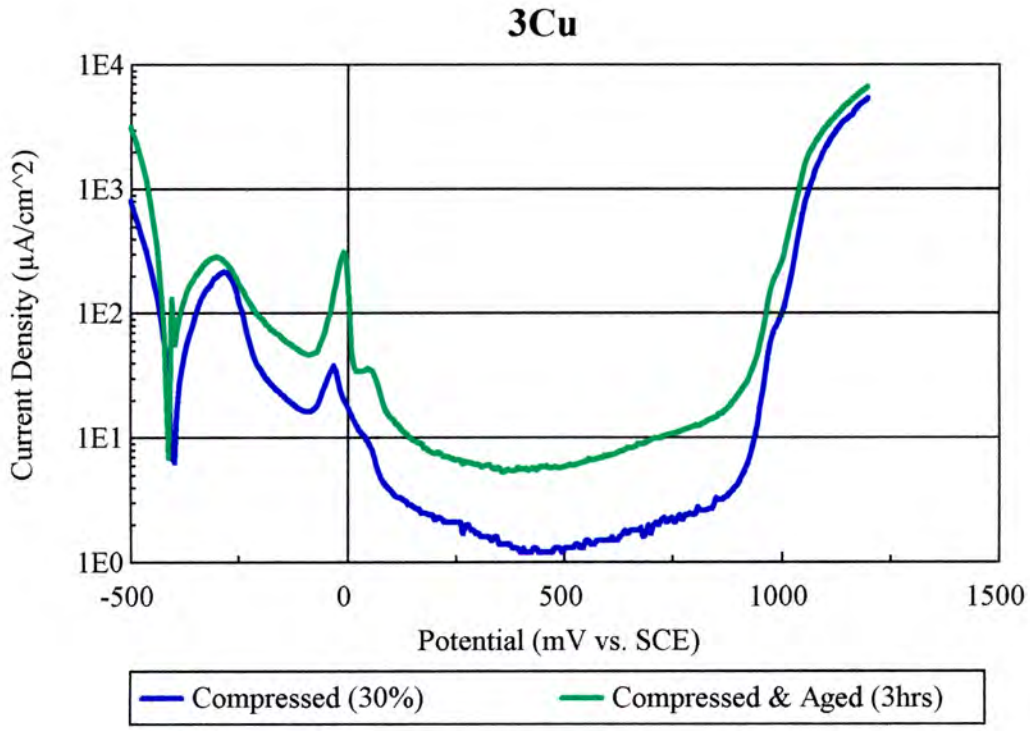

Figure 4.27 Potentiodynamic scans of 0Cu, 1Cu and 3Cu for both the compressed (controlled temperatures) and the compressed and aged conditions.

a. 0Cu

b. 1Cu

c. 3Cu

The increase in passive current density for the compressed and aged condition (for all the alloys) suggests that alloys in this condition do not form substantial protective passive layers. The high carbon content (which is not in solution) of the martensite leads to a high density of fine chromium carbides or carbo-nitrides being formed following ageing of the deformed microstructure. Since a large amount of chromium is taken up in the matrix during the formation of these intragranular precipitates, there is less chromium available for the formation of the protective chromium oxide passive film. Hence a film is formed which is less protective than that which is formed in the deformed only condition.

4.7 PITTING

As mentioned in Section 3.7, pitting tests posed a problem due to the difficulty in preventing crevices from forming (between the specimen and the mounting material) which lead to erroneous pitting results. Numerous mounting methods were tried but proved to be unsuccessful. The method described by Pawel *et al*[64,65] (Section 3.7) was finally used and examination of the specimen surfaces after cyclic pitting tests showed that there was no evidence of crevice corrosion. The results of these tests performed in a 500ppm de-aerated chloride solution at 30°C are shown in Figure 4.28 for the alloys in the solution treated condition.

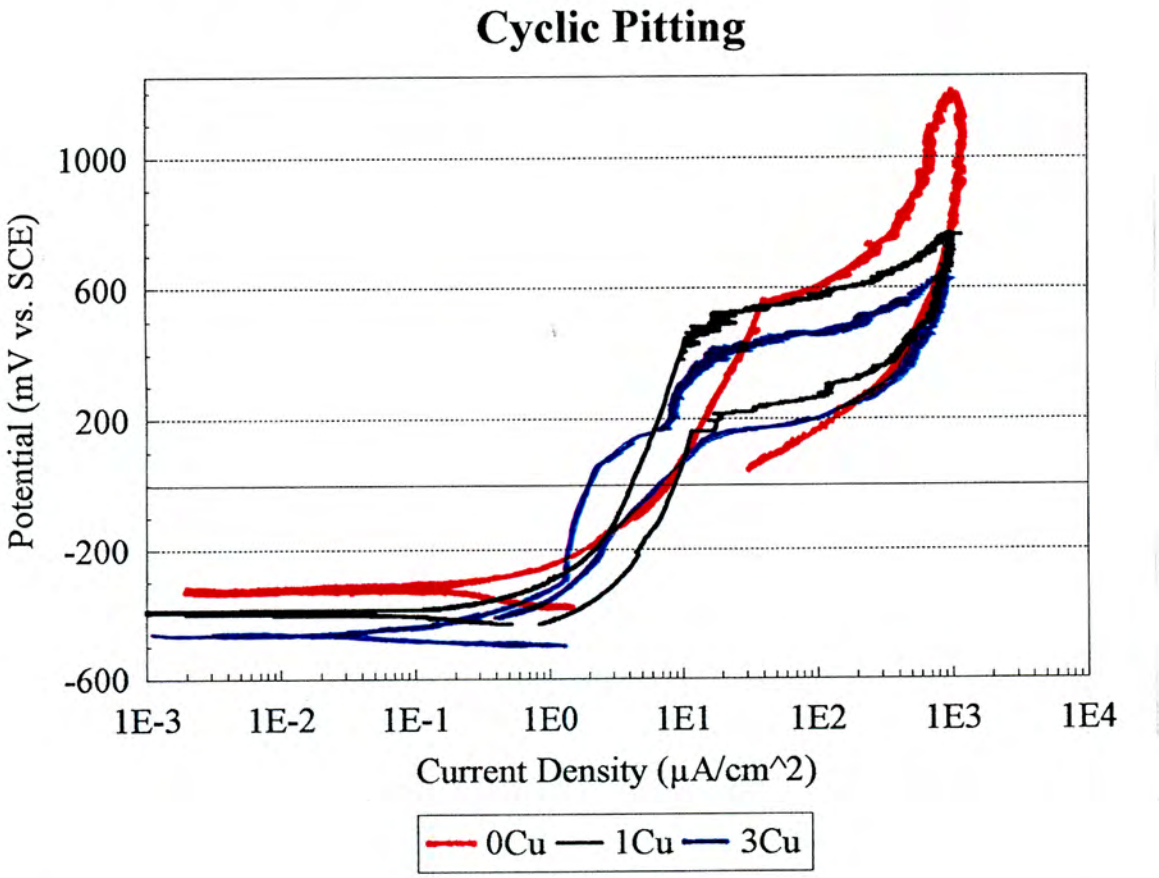

Figure 4.28 Cyclic pitting results for 0Cu, 1Cu and 3Cu (solution treated condition) tested in a 500ppm de-aerated chloride solution at 30°C

It appears from these results that the pitting potential, E_{pit}, increases slightly with a decrease in copper content which disagrees with work carried out by Murase[34] and Hann-Tuw *et al*[36]. The corrosion potential, E_{corr}, for 0Cu is highest (most noble) while that for 3Cu is lowest (most active). This trend was also observed during pit growth and at the maximum current density. Unfortunately, time constraints meant that these results were not reproduced and testing in different media for different microstructural conditions were also not pursued.

CHAPTER 5
SUMMARY

Based on the initial objectives of this work, the results obtained for corrosion tests carried out on three alloys containing nominal amounts of 5.4 wt% nickel, 0.25 wt% nitrogen and varying copper additions (0-3.3 wt%) can be summarised as follows:

For the solution treated only condition, the corrosion results of the alloys revealed that the virtually copper-free alloy (0Cu) exhibited poor corrosion behaviour relative to the copper-containing alloys, 1Cu and 3Cu. This could be attributed to either (i) the lack of copper in 0Cu or (ii) the slightly higher amount of residual martensite formed during metallographic preparation of this alloy. The latter is, however, assumed to be a less significant effect. The corrosion rates of all the alloys were generally lowest in the solution treated only condition compared to the other microstructural conditions.

The corrosion results of the alloys in the solution treated and aged condition showed similar corrosion rates to those in the solution treated only condition. These corrosion rates also unexpectedly did not increase with ageing time. This trend was observed for all alloys which suggests that copper does not have an influence on precipitation leading to sensitisation of these alloys. On the other hand, electron microscopy carried out after corrosion testing revealed that the degree of intergranular corrosion increased with an increase in ageing time for all the alloys and that this intergranular attack was most severe in 0Cu containing the least copper. It would therefore appear from the microscopy that copper does indeed influence the precipitation kinetics of these alloys during ageing. This was not, however, reflected as an increase in the corrosion rate values. Hence, it was suggested that the potentiodynamic polarisation tests conducted are not a suitable method for characterising and quantifying sensitisation. It was instead recommended that a technique known as the electrochemical potentiokinetic reactivation (EPR) technique be used to provide quantitative electrochemical measurements of sensitisation. Therefore, no clear conclusions could be drawn regarding the influence of copper on the ageing of these alloys following solution treatment.

For the solution treated and deformed (room temperature) condition, the corrosion results showed that for all the alloys, there was an increase in corrosion rates relative to the solution treated only condition. This is a result of the formation of deformation-induced martensite which is a high energy phase and is expected to corrode preferentially to austenite. XRD analysis revealed that 0Cu formed the most martensite while 3Cu formed the least. This confirms that copper increases the stability of austenite during deformation. The corrosion results also showed that 0Cu exhibited considerably higher corrosion rates than the other two copper-containing alloys. This could be attributed to either (i) the higher volume of high energy martensite in 0Cu or (ii) the lack of copper in 0Cu. The influence of copper on the dissolution rate of martensite could not be determined from these results due to the varying martensite levels in the three alloys.

Following solution treatment and deformation (to an equivalent 30% macro-strain), performed over a range of temperatures (to obtain equal martensite volumes of approximately 20%), 1Cu and 3Cu still showed a higher corrosion resistance than 0Cu. Since composition was the only variant amongst the alloys in this condition, it can be concluded that copper has a beneficial effect on reducing the corrosion rate in the deformed condition. The corrosion rates for 0Cu in the solution treated and deformed (controlled temperature) condition increased the most (relative to the solution treated only condition) and also showed the most severe corrosion damage in this condition. It could thus be concluded that the lack of copper in this alloy has a detrimental effect on increasing the dissolution rate of martensite.

For the solution treated, deformed (to form equal martensite volume fractions) and aged condition, the corrosion results showed that copper additions again appear to reduce the corrosion rates of these alloys. Following ageing, the corrosion rates of all the alloys increase relative to the solution treated and deformed (controlled temperature) condition. This is due to the sensitisation of martensite leading to severe intragranular corrosion. The amount of increase in corrosion rate (relative to the solution treated and deformed only condition) appears consistent for all alloys and the corrosion rates do not change significantly with an increase in ageing time. This suggests that copper does not influence the precipitation kinetics and the sensitisation of martensite during ageing.

In addition to the findings pertaining to the initial objectives of this study, the following conclusions could be drawn from this work:

5.1 The comparison of the AISI 301 and 304L alloys with the experimental alloys in the solution treated and aged condition showed that the 301 alloy behaved in much the same way as 0Cu. The 304L alloy, however, showed superior corrosion performance to 0Cu but inferior performance to 1Cu and 3Cu.

5.2 The corrosion rates of the alloys deformed (by compression) at different temperatures did not change significantly with martensite volume fraction. This result was unexpected, since martensite is a high energy phase which corrodes preferentially to austenite and it is expected that a higher volume of martensite would lead to higher dissolution rates.

5.3 1Cu and 3Cu (containing 1.23 and 3.34 wt% copper respectively) consistently showed the lowest corrosion rates relative to 0Cu (containing 0.07 wt% copper) for all the microstructural conditions.

5.4 Both 1Cu and 3Cu showed similar corrosion performance for all microstructural conditions, while a copper addition of 0.07 wt% markedly lowers the corrosion resistance of 0Cu. This suggests that there is a limit (in the vicinity of 3 wt%) to the amount of copper that can be added which will improve the corrosion performance of these alloys.

5.5 Potentiodynamic scans performed on all the alloys in the various microstructural conditions showed that the critical current density, I_{crit}, decreased with an increase in copper content thereby reducing the active range. The passivation potential, E_{pp}, moved to more noble directions as the copper content increased. The lower passive current densities for 1Cu and 3Cu indicates that these alloys form a more stable passive film in 5 volume % de-aerated sulphuric acid.

Since the initial motivation for this work stemmed from the phenomenon of delayed cracking after deep drawing and involved finding a way to optimise corrosion performance after the deep drawing of alloys with reduced nickel contents, copper has proven to be a beneficial alloying addition. Although the addition of copper leads to a reduction in tensile uniform elongation, it does not notably affect the deep drawability of the steel. Without copper additions, these alloys which suffer delayed cracking after deep drawing show drastically reduced corrosion performance after remedial attempts of post-forming stress relieving. Copper additions eliminate the need for this remedial action and have also proved to have a beneficial effect on reducing the dissolution rate of deformation-induced martensite. The characterisation of the corrosion behaviour of these copper containing alloys, as shown in this thesis, proves that these alloys look promising as substitutes for the conventional AISI 301 alloys presently used in forming applications.

REFERENCES

1. SIBANDA,M. (1994) **Evaluation of the Formability Properties of Nitrogen Alloyed Metastable Austenitic Stainless Steels**, MSc Thesis, Department of Materials Engineering, University of Cape Town

2. SIBANDA,M., VISMER,S.L. and KNUTSEN,R.D. (1994) **Consideration of Reduced Nickel containing Austenitic Stainless Steels for Forming Applications**, *Materials Letters*, 21, pp.203-207

3. TRUMAN,J.E. (1992) **Constitution and Properties of Stainless Steels**, *Materials Science and Technology - A Comprehensive Treatment*, Volume 7, Edited by R.W.Cahn, P.Haasen, and E.J.Kramer, VCH, Germany, pp.538,569

4. ROWLANDS,D.P. **The 'Secrets' of Stainless Steels**, Stainless Steel Information Series Nos.1 and 7, Published by the South African Stainless Steel Development Association (SASSDA)

5. PECKNER,D. and BERNSTEIN,I. (1977) **Handbook of Stainless Steels,** McGraw-Hill Inc., USA, pp.1.6-7,4.2,4.23,14.7,15.2,16.4-5,20.3,20.30

6. PICKERING,F.B. (1978) **Physical Metallurgy and the Design of Steels**, Applied Science Publishers Ltd., England, pp.248,251,227-229

7. VIKRAM RAO,M. (1973) **ASM Metals Handbook**, *Metallography, Structures and Phase Diagrams*, Volume 8, 8th Edition, p.291

8. CORTIE,M.B., MISSIO,L., BIGGS,T. and SHAW,M. (1992) **The Effect of Nitrogen Additions on a Metastable 17%Cr Austenitic Alloy Containing Mn, Ni and Cu**, *High Manganese Stainless Steels*, R.A.Lula (ed.), ASM International, pp.177-185

9. DUBRAWKA,E.G. and LOVEJOY,P.T. (1970) **Nickel substitutes and alternates for austenitic stainless steels**, Yearbook of the American Iron and Steel Institute, pp.131-150

10. CORTIE,M.B. (1994) **Copper as an Austenite Stabilising Addition to Stainless Steels,** Proc. 15th CMMI Congress, Johannesburg, SAIMM, vol.2, pp.165-172

11. SÁNCHEZ,R., BOTELLA,J., MARTOS,J. and FERNÁNDEZ (1993) **Properties of an austenitic stainless steel,** *Stainless Steel '93*, Associazione Italiana di Metallurgia, 2, pp.231-236

12. SEDRICKS,A.J. (1979) **Corrosion of Stainless Steels**, John Wiley and Sons, Inc., pp.3,49-56,70

13. LLEWELLYN,D.T. and MURRAY,J.D. (1964) **Cold-worked stainless steels**, *High Alloy Steels* Spec. Report no.86, The Iron and Steel Institute (London), pp.197-212

14. HUANG,C. and KAO,P. (1989) **Effects of cold rolling and annealing processes on texture and plastic anisotropy of copper-containing austenitic stainless steel sheets,** *ISIJ. International*, 29 (1), pp.64-73

15. RYOO,D.Y., LEE,Y.D., KIM,J.K. and HAN,S.Y. (1992) **Formability of type 304 stainless steels**, *Applications of Stainless Steel '92*, H.Nordberg and J.Björklund (eds.), Jernkontoret, Stockholm, pp.1078-1086

16. WARREN,D. (1960) **Corrosion and Weldability studies on chromium-manganese austenitic stainless steels,** *Corrosion-NACE,* 16, pp.101-112

17. STEPHENSON,E.T. (1983) **Effect of recycling on residuals, processing and properties of carbon and low-alloy steels,** *Metall. Trans. A,* 14, pp.343-353

18. KIKUCHI,M., KAJIHARA,M. and FRISK,K. (1988) **Solubility of nitrogen in austenitic stainless steels,** *High Nitrogen Steels,* Conference proceedings May 18-20 1988, Lille, France, eds. J.Foct and A.Hendry, publs. Institute of Metals, London, pp.63-74

19. BIGGS,T. (1993) **The Influence of Nitrogen on the Deformation Behaviour of a Modified AISI Type 200 Series Alloy,** Msc Thesis, Department of Materials Engineering, University of Cape Town

20. COLOMBIER,L. and HOCHMAN,J. (1967) **Stainless and Heat Resisting Steels,** Edward Arnold, London, p.101

21. FRANKS,R., BINDER,W.O. and THOMPSON,J. (1955) **Austenitic Cr-Mn-Ni Steels containing Nitrogen,** *Trans. Amer. Soc. Metals,* 47, pp.231-266

22. RAWERS,J.C., DUNNING,J.S., ASAI,G. and REED,R.P. (1992) **Characterisation of Stainless Steels Melted under High Nitrogen Pressure,** *Metall. Trans. A,* 23A, pp.2061-2068

23. SPEIDEL,M.O. (1989) **Properties and Applications of High Nitrogen Steels,** *High Nitrogen Steels,* Conference proceedings May 18-20 1988, Lille, France, eds. J.Foct and A.Hendry, publs. Institute of Metals, London, pp.92-96

24. MENZEL,J., STEIN,G. and DAHLMANN,P. (1989) **Massively Nitrogen-Alloyed Austenitic Bolt Materials for High Strength and High Temperature Applications,** *High Nitrogen Steels,* Conference proceedings May 18-20 1988, Lille, France, eds. J.Foct and A.Hendry, publs. Institute of Metals, London, p.147-150

25. KENDAL,A., TRUMAN,J.E. and LOMAX,K.B. (1989) **Properties of AISI 304 and AISI 316 stainless steel with addition of ~0.2% nitrogen,** *High Nitrogen Steels,* Conference Proceedings May 18-20 1988, Lille, France, eds. J.Foct and A.Hendry, publs. Institute of Metals, London, pp.405-413

26. PICKERING,F.B. (1989) **Some Beneficial Effects of Nitrogen in Steel,** *High Nitrogen Steels,* Conference Proceedings May 18-20 1988, Lille, France, eds. J.Foct and A.Hendry, publs. Institute of Metals, London, pp.10-31

27. BANOV,R.M. (1981) **Physical fundamentals of the structure and properties of nitrogen austenitic steels,** Bulgarian Academy of Sciences, Sofia

28. HONEYCOMBE,R.W.K. (1981) **Steels: Microstructure and Properties,** Edward Arnold, London, p.231

29. MARTINEZ,L.G., IMAKUMA,K. and PADHILA,A.F. (1992) **Influence of Niobium on Stacking-Fault Energy of all Austenite Stainless Steels,** *Steel Research,* 63 (5), pp.221-223

30. FUJIKURA,M., TAKADA,K. and ISHIDA,K. (1975) **Effect of Manganese and Nitrogen on the Mechanical Properties of Fe-18%Cr-10%Ni Stainless Steels,** *Trans. Iron Steel Inst. Jap.*, 15 (9), pp.464-469

31. RAWERS,J., BENNET,J., DOAN,R. and SIPLE,J. (1992) **Nitrogen solubility and nitride formation in Fe-Cr-Mn-Ni alloys,** *Acta metall. mater.*, 40 (6), pp.1195-1199

32. STEIN,G., MENZEL,J. and DORR,H. (1989) **Industrial Manufacture of Massively Nitrogen-Alloyed Steels,** *High Nitrogen Steels*, Conference proceedings May 18-20 1988, Lille, France, eds. J. Foct and A. Hendry, publs. Institute of Metals, London, p.32

33. FONTANA,M.G. and GREENE,N.D. (1978) **Corrosion Engineering**, Second Edition, McGraw-Hill, Singapore, p.342

34. MURASE,S. (1991) **The Influence of Copper Addition on the Corrosion Resistance of Stainless Steels**, MSc Thesis, University of the Witwatersrand, Johannesburg.

35. YAMAMOTO,A., ASHIURA,T. and KAMISAKA,E. (1985) **Corrosion Properties of copper- and niobium-added 19Cr Stainless Steel,** *Stainless Steels '84*, Conference proceedings September 3-4 1984, Göteborg, publs. Institute of Metals, London, pp.181-187

36. HANN-TUW LIN, WEN-TA TSAI, JU-TUNG LEE and CHI-SHANG HUANG (1992) **The Electrochemical and Corrosion Behaviour of Austenitic Stainless Steel Containing Copper,** *Corrosion Science*, 33, p.691

37. LIZLOVS,E.A. (1966) **Effects of Mo, Cu, Si and P on Anodic Behaviour of 17Cr Steels,** *Corrosion-NACE*, 22 (11), pp.297-308

38. JIANGNAN,Y., LICHANG,W. and WENHAO,S. (1992) **The Effect of Copper on the Anodic Dissolution Behaviour of Austenitic Stainless Steels in acidic Chloride Solution**, *Corrosion Science*, 33, p.851

39. OGURA,S., SUGIMOTO,K. and SAWADA,Y. (1976) **Effects of Cu, Mo, and C on the Corrosion of Deformed 18Cr-8Ni Stainless Steel in H_2SO_4/NaCl Solutions**, *Corrosion Science*, 16, p.323

40. MIYAHARA,K., SUGIHARA,R., SATOH,T. and HOSOI,H. (1991) **Effects of Alloying Elements of Manganese, Carbon and Nitrogen and Ageing Treatments on Corrosion Resistance of Fe-Cr-Mn Alloys**, *Proceedings of International Conference on Stainless Steels*, Chiba, ISIJ, pp.139-145

41. SEO,M., HULTQUIST,G., LEYGRAF,C. and SATO,N. (1986) **The Influence of Minor Alloying Elements (Nb, Ti and Cu) on the Corrosion Resistivity of Ferritic Stainless Steel in Sulphuric Acid Solution**, *Corrosion Science*, 26 (11), pp.949-960

42. MOSKOWITZ,A. (1967) **Effects of Residual Elements on Properties of Stainless Steels**, ASTM STP-418, American Society for Testing and Materials, Philadelphia, p.3

43. BANDY,R. and VAN ROOYEN,D. (1985) **Properties of Nitrogen-containing Stainless Steels Designed for High Resistance to Pitting,** *Corrosion-NACE*, 41 (4), pp.228-233

44. GUMPEL,P. and LADWEIN,T. (1989) **Effect of Nitrogen on Mechanical-Technological and Corrosion Properties of Stainless Steel,** *High Nitrogen Steels*, Conference proceedings May 18-20 1988, Lille, France, J.Foct and A.Hendry eds., publs. Institute of Metals, London, pp.272-279

45. TRUMAN,J.E. (1989) **Effects of Nitrogen Alloying on Corrosion Behaviour of High Alloy Steels,** *High Nitrogen Steels*, Conference proceedings May 18-20 1988, Lille, France, J.Foct and A.Hendry eds., publs. Institute of Metals, London, pp.225-239

46. TRUMAN,J.E., COLEMAN,M.J. and PIRT,K.R. (1977) **Note on the Influence of Nitrogen Content on the Resistance to Pitting Corrosion of Stainless Steels,** *Brit. Corr. J.*, 12, pp.236-238

47. SEDRIKS,A.J. (1985) **Metallurgical Aspects of Passivation of Stainless Steels,** *Stainless Steels '84*, Conference proceedings September 3-4 1984, Göteborg, publs. Institute of Metals, London, pp.125-133

48. MARSHALL,P. (1984) **Austenitic Stainless Steels-Microstructure and Mechanical Properties,** Elsevier Applied Science Publishers, pp.24,31-34,44,49,59

49. SIMMONS,J.W. (1995) **Mechanical Properties of Isothermally Aged High-Nitrogen Stainless Steel,** *Metallurgical and Materials Transactions A*, 26A, p.2085

50. JARGELIUS-PETTERSSON,R.F.A (1993) **Precipitation in Nitrogen-Alloyed Stainless Steel at 850°C,** *Scripta Metallurgica et Materialia*, 28, pp.1399-1403

51. BRIANT,C.L., MULFORD,R.A. and HALL,E.L. (1982) **Sensitisation of Austenitic Stainless Steels, I. Controlled Purity Alloys,** *Corrosion-NACE*, 38 (9), pp.468-477

52. MULFORD,R.A., HALL,E.L. and BRIANT,C.L. (1983) **Sensitisation of Stainless Steels, II. Commercial Purity Alloys,** *Corrosion-NACE*, 39 (4), pp.132-143

53. BENEKE,R. and SANDENBERGH,R.F. (1989) **The Influence of Nitrogen and Molybdenum on the Sensitisation Properties of Low-Carbon Austenitic Stainless Steel,** *Corrosion Science*, 29 (5), pp.543-555

54. MOZHI,T.A., CLARK,W.A.T., NISHIMOTO,K., JOHNSON,W.B. and MACDONALD,D.D. (1985) **The Effect of Nitrogen on the Sensitisation of AISI 304 Stainless Steel,** *Corrosion-NACE*, 41 (10), pp.555-559

55. BETRABET,H.S., NISHIMOTO,K., WILDE,B.E. and CLARK,W.A.T. (1987) **Electrochemical and Microstructural Investigation of Grain Boundary Precipitation in AISI 304 Stainless Steels Containing Nitrogen,** *Corrosion-NACE*, 43 (2), pp.77-84

56. BRIANT,C.L. and RITTER,A.M. (1980) **The Effect of Deformation Induced Martensite on the Sensitisation of Austenitic Stainless Steel,** *Metall. Trans.2A*, p.2009.

57. ASTM (1993) **Reference Test Method for making Potentiostatic and Potentiodynamic Anodic Polarisation Measurements,** Annual Book of Standards, Section 3, G5-87, p.87

58. STERN,M. and GEARY,A.L. (1957) **Electrochemical Polarisation,** *Journal of the Electrochemical Society*, 104 (1), p.56.

59. LeROY,R.L. (1975) **Evaluation of Corrosion Rates from Polarisation Measurements,** *Corrosion-NACE*, 31 (5), p.173.

60. CAPENDALE,A.E (1985) **The Influence of Water Composition on the Pitting Behaviour of a Stainless Steel**, Msc Thesis, Department of Materials Engineering, University of Cape Town

61. LIVITSANOS,C. and THOMSON,P. (1977) **Rapid Determination of the Deformation-Induced Martensite in Metastable Austenitic Stainless Steel**, *Journal of Materials Science*, 12, pp.2209-2213.

62. HALLIDAY,D. and RESNICK,R. (1981) **Fundamentals of Physics**, John Wiley and Sons, New York, p.764.

63. JATCZAK,C.F., LARSON,J.A. and SHIN,S.W. (1980) **Retained Austenite and its Measurement by X-ray Diffraction**, Information Manual SP-453 prepared by X-Ray Division of SAE Fatigue Design and Evaluation Committee, Society of Automotive Engineers Inc., Warrendale, pp.9-27.

64. PAWEL,S.J., STANSBURY,E.E. and LUNDIN,C.D. (1989) **Role of Nitrogen in the Pitting Resistance of Cast Duplex CF-Type Stainless Steels**, *Corrosion-NACE*, 45 (2), pp.125-133

65. LEE,I-S., STANSBURY,E.E. and PAWEL,S.J. (1989) **Technical Note: Determination of Pitting Susceptibility Using a New Sample Preparation Technique**, *Corrosion-NACE*, 45 (2), pp.134-135.

66. DARKEN,L.S. and GURRY,R.W. (1953) **Physical Chemistry of Metals**, McGraw-Hill, New York, p.417

67. ADVANI,A.H., MURR,L.E., ATTERIDGE,D.G., CHELAKARA,R. and BRUEMMER,S.M. (1991) **Deformation Effects on Intragranular Carbide Precipitation and Transgranular Chromium Depletion in Type 316 Stainless Steels**, *Corrosion-NACE*, 47 (12), pp.939-947